Sand 80-7013
Unlimited Release
UC-63a Distribution

Simulation and Simplified Design Studies of Photovoltaic Systems

D. L. Evans, W. A. Facinelli, and L. P. Koehler
Arizona State University

Prepared for Sandia National Laboratories under Contract No. 13-0313.

Prepared by Sandia National Laboratories, Albuquerque, New Mexico 87185 and Livermore, California 94550 for the United States Department of Energy under Contract DE-AC04-76DP00789

Printed September 1980

Sandia National Laboratories

SF 2900-Q(3-80)

Issued by Sandia Laboratories, operated for the United States Department of Energy by Sandia Corporation.

Printed in the United States of America

Available from
National Technical Information Service
U. S. Department of Commerce
5285 Port Royal Road
Springfield, VA 22161
Price: Printed Copy $8.00 ; Microfiche $3.00

Sandia Laboratories

Albuquerque, New Mexico
Livermore, California

date: December 3, 1980

to: Distribution

from: K. L. Biringer
Organization 4718

subject: Simulation and Simplified Design Studies of Photovoltaic Systems, SAND80-7013: ERRATA

Please enter the enclosed corrections to subject report:

page	line	
1-4	4	"°σ" should be replaced with "PV"
2-12	last	"optional" should be replaced with "optimal"
2-36	Fig. 2.7	Caption should read "Effect of Location and Weather Patterns"
3-14	last	"=0.88" should be ",α = 0.88"
3-36	Fig. 3.8	Change equation in figure to $\log_{10} Q_s = -0.640 + 0.732\ \overline{K_T}$
4-24	Fig. 4.3	Vertical Axis is "$\overline{H}/\overline{H}_{\text{long term}}$"; Horizontal Axis should have "$\overline{H}$" after ≤
5-14	2nd para. 1st line	Fig. 6" should be replaced with "Fig. 5.8"
5-15	Ref. 5.5	should be E.A. Hyman, "Phenomenological Cell Modeling: A Tool for Planning and Analyzing Battery Testing at the BEST Facility," Report RD77-1, Public Service Electric and Gas Company and PSE and G Research Corporation, Newark, NJ (1977).

SAND 80-7013
Unlimited Release

SIMULATION AND SIMPLIFIED DESIGN STUDIES OF PHOTOVOLTAIC SYSTEMS

D.L. Evans
W.A. Facinelli
L.P. Koehler

Mechanical Engineering Department
Arizona State University
Tempe, Arizona 85281

ABSTRACT

Results of TRNSYS simulations of photovoltaic systems with electrical storage are described. Studies of the sensitivity of system performance, in terms of the fraction of the electrical load supplied by the solar energy system, to variables such as array size, battery size, location, time of year, and load shape are reported.

An accurate simplified method for predicting array output of max-power photovoltaic systems is presented. A second simplified method, which estimates the overall performance of max-power systems, is developed. Finally, a preliminary technique for predicting clamped-voltage system performance is discussed.

ACKNOWLEDGEMENTS

The work embodied in this report entitled ''Simulation and Simplified Design Studies of Photovoltaic Systems'' was conducted by Arizona State University with Dr. D.L. Evans of the Mechanical Engineering Department serving as Principal Investigator.

Special thanks is due to Kent Biringer of Sandia Laboratories for his assistance, advice and comments.

The assistance of Renee Overbeck, Katty McIntosh, and Jeanette Heschke in preparing the manuscript is deeply appreciated.

TABLE OF CONTENTS

LIST OF SYMBOLS

Symbol	Definition
A	Array area
c	Daylength correction term [eq.(4.6)]
C_f	Correction factor to convert $K_e(\overline{T_c-T_a})/(\rho\alpha)$ for non-optimum tilts
$C_i (i=1,\cdots 6)$	Constants in equations used to define the I-V curve of cells or arrays [eqs. (5.1)]
C_s	Correction factor to convert average day insolation to good, mediocre or poor day insolation (see Fig. 4.4)
CV1, CV2	Symbols used to denote cells of different I-V curve shape (see page 5-2 and Table 5.1)
F	Battery fractional state of charge
F_B	If F_D is reached and if $F_B > F_D$, first priority is given to recharging the battery (from the array) to $F = F_B$
F_C	Maximum fractional state of charge permitted for the batteries
F_D	Minimum fractional state of charge permitted for the batteries
f_e	Fraction (or percent) of load that is met by a photovoltaic system
H	Daily total solar energy received on a horizontal surface. Includes direct and diffuse components of insolation
I	Electrical Current
I_c	Photovoltaic cell or array current
I_{mp}	Photovoltaic cell or array current at maximum power output
I_{sc}	Cell or array short circuit current
K_e	Thermal conductance for energy transfer as heat from the cells to the final heat sink (usually the atmosphere)
$\bar{K}_T$	Monthly average ratio of total radiation on a horizontal surface to radiation that would be received by this same surface if it were located above the atmosphere (the extraterrestrial radiation). This is sometimes referred to as a clearness number

L	Daily energy required by load
$\dot{L}$	Power required by the load
N_d	Number of days per month
n	Julian day of the year
P_{mp}	Photovoltaic cell or array maximum output power
Q	Actual battery state of charge
Q_{ae}	Daily electrical energy produced by a max-power tracked array
$Q_{ae,cv}$	Daily electrical energy produced by a battery clamped array
$Q_{ae,cv}^{*}$	Optimum electrical energy produced by a battery-clamped array. Produced when SR = SR^{*}
Q_e	Effective daily array electrical output energy, i.e., the actual array output multiplied by the ''straight through'' or power conditioning efficiency
$\dot{Q}_e$	Effective array power output (i.e., the array output power times the power conditioning efficiency, η_{pc})
$\dot{Q}_s$	Instantaneous insolation on tilted array
$Q_{s,i}$	Hourly insolation on tilted surface, [see eq. (3.3)]
$\dot{Q}_{sc}$	Instantaneous insolation reaching the cells
S	Electrical energy storage capacity. See page 2-7 for discussion of units used in this report
S_D	Energy stored in batteries which is ultimately delivered to the load
SR	Series ratio (ratio of number of solar cells in series to number of battery cells in series)
SR^{*}	The value of SR which gives maximum energy output for a particular month
s	Array tilt up from horizontal
s_M	Optimum s for maximum monthly energy collection (see Table 3.2)
T_a	Ambient dry bulb temperature
T_c	Cell temperature

T_M	Mean monthly temperature as compiled by the National Weather Service
T_{NOCT}	NOCT (Nominal operating cell temperature)
T_p	Time of day at which peak of sinusoidal load occurs
T_r	A reference temperature for cell efficiency (see η_r)
$T_{ri}(i=1,2)$	Constants in equations used to define the I-V curves of cells or arrays [eqs. (5.1)]
t	Time
t_D	Daylight daylength [see eq. (4.9)]
V	Voltage
V_b	Battery cell voltage
V_c	Photovoltaic cell or array voltage
V_{mp}	Cell or array voltage for maximum power output
V_o	Thermal voltage [eq. (5.1)]
V_{oc}	Cell or array open circuit voltage
XS	That portion of the daily effective array output energy which cannot be used immediately by the load
$\dot{XS}$	Instantaneous excess energy (i.e., the amount by which the array power exceeds the load demand)

GREEK SYMBOLS

α	Solar absorptance
β	Temperature coefficient for cell efficiency [see eq.(3.5)]
ε	Battery charging efficiency [see eq.(2.3)]
δ	Solar declination [see eq.(4.10)]
η	Instantaneous photovoltaic cell or array efficiency for conversion of incident solar radiation to electrical power
η_b	''Roundtrip'' storage efficiency
η_{pc}	''Straight through'' power conditioning efficiency
η_r	Photovoltaic array (or cell) reference efficiency at an array (or cell) temperature of T_r and insolation level of 1 kW/m^2
γ	Intensity coefficient for cell efficiency [see eq.(3.5)]
ϕ	Latitude
ρ	Solar reflectance (or transmittance) of optical components that may be placed between the array and the sun
σ	Standard deviation
τ	Solar transmittance
θ	An angle

SUBSCRIPTS

a	Array
e	Effective or electrical
i	Hourly value
n	Daily value
r	Reference value
s	Solar

SPECIAL SYMBOLS

$\overline{\quad}$	as, e.g., in $\overline{Q}_e$, means monthly average value
pos	symbol used before integral sign to indicate only positive values of the integral should be considered
(12)	as used, e.g., in $\overline{Q}_s(12)$ denotes midday (near solar noon) values

LIST OF TABLES

LIST OF FIGURES

1.0 INTRODUCTION

1.1 Background

Widespread adoption of photovoltaic (PV) systems for terrestrial use relies on several factors. The most important are system cost and system performance. These two are not inseparable, however, since performance dictates the price that can be paid for the system. For comparisons of PV systems with systems which use nonrenewable fuels, economic analyses require knowledge of fuel savings that would result should a PV system be used to meet part of the load. If PV systems are to be compared with other renewable energy alternatives, system sizing (i.e., performance calculations) must be done in order to compare the costs of each.

Detailed and sophisticated computer programs currently exist (Ref. 1.1, 1.2) which allow performance calculations to be made. These codes can be used to explore trade-offs and problem areas that may arise, but they typically require access to fairly large computing facilities and some sophistication of use. They obviously do not replace the need for construction and testing of hardware prototypes although they can greatly reduce the number of prototype systems that need to be built.

Such detailed programs also will not satisfy the eventual need for simplified design guidelines that will be necessary to effectively implement large scale use of PV systems. The codes do, however, serve as useful tools in the development of such design guidelines. This fact has already been demonstrated in the national solar thermal program where the development of the University of Wisconsin's TRNSYS (Ref. 1.3) simulation program has led to the f-Chart method of thermal system design (Ref. 1.4). Thus certain types of thermal systems (space heating and domestic

water heating) can now be reliably designed without resorting to computer calculations.

The terrestrial photovoltaic field has not yet reached that point of maturity where simplified design techniques are available. However, the rapid growth that this field is experiencing suggests that it is not too early to deal with such subjects.

1.2 This Study

The major thrust of the work documented in this report has been the investigation of the validity of certain simplified design procedures for photovoltaic system analysis. The goal has been to explore system sensitivities and to lay the groundwork for possible simplified design methods. This document is not, therefore, a design manual in the sense that it could be easily used for design purposes.

The systems addressed here are passively cooled and grid connected or have a non-photovoltaic back-up source. Both systems with and without dedicated battery storage are studied. Max-power tracked systems have received the most attention although inroads have been made in the clamped-voltage mode of operation.

Max-power tracked systems are easier to address in a simplified design procedure since the PV array can be uncoupled from the battery, power conditioning equipment, and the load. In the battery or voltage-clamped mode, the array voltage (and thus, power output) is determined by the battery and its interaction with the array and load.

Computer simulation has been used to guide the development and validation of the simplified techniques discussed here. Such simulations have also been used to uncover some fairly general design ''rules of thumb'' concerning battery sizing and to study

the sensitivity of the results to various system parameters and load behavior.

This report is divided into five (5) main parts. They are:

Chapter 2: System Simulation Studies

Chapter 3: Simplified Method for Predicting Array Output

Chapter 4: Simplified Method for Max-Power Tracked System Performance

Chapter 5: Simplified Method for Clamped-Voltage System Performance

Chapter 6: Discussion, Conclusions and Summary

1.3 Summary of this Study

This section briefly summarizes the results of this study. A slightly more detailed summary of the complete results can be found in Chapter 6.

- $\bar{Q}_e/\bar{L}$, the ratio of monthly average daily array output (multiplied by the power conversion efficiency) $\bar{Q}_e$, to the monthly average daily electrical load $\bar{L}$, and $S/\eta A$, the ratio of storage capacity (S) to effective array area (monthly average array efficiency times the array area, $\bar{\eta}A$) are good parameters for correlating f_e, the fraction of $\bar{L}$ supplied by solar, for various locations for similarly tilted arrays.

- When $\bar{Q}_e/\bar{L}$, is small, f_e differs from $\bar{Q}_e/\bar{L}$ only by the storage losses which can be small if much of the load occurs during daylight hours.

- When $\bar{Q}_e/\bar{L}$ is large, f_e can be significantly different from $\bar{Q}_e/\bar{L}$ due to storage losses and dumping (or not collecting) energy when storage is filled.

- Load shape is important in determining f_e for a given $\bar{Q}_e/\bar{L}$ and $S/\eta A$, for $S/\eta A < 50$ W-hrs/(%·m^2).

- $S/\eta A > 50$ W-hrs/(%·m^2) of storage is seldom warranted for most load shapes that might be considered for $^0\sigma$ applications.

- The knees of the f_e versus $S/\eta A$ curves are somewhat load shape and $\bar{Q}_e/\bar{L}$ dependent but typically occur in the region of $S/\eta A = 30$ W-hrs/(%·m^2).

- In addition to the obvious conclusion that locations of poor insolation require more array area to meet a given fraction of the load, the results of this study show that battery size should scale with the effective array area in order to yield the same system performance (i.e., f_e) in different locations.

- Predicted system performance does not appear to be strongly dependent on the frequency or magnitude of random fluctuations in the load.

- Predicted system performance does not appear to be strongly dependent on the battery model (at least for the three different battery models used) or on the range of battery state of charge. However, good representations of the charge and the discharge curves are necessary.

- The results of these simulation studies show that simplified design procedures should account for diurnal load shape, daylength (or time of year), and, to a lesser extent, location.

Simplified array output results:

- A method was developed whereby the monthly average array efficiency ($\bar{\eta}$) can be hand calculated from a minimum of information.

- This $\bar{\eta}$, when multiplied by the monthly average insolation on the array, gives the monthly average electrical output.

- The results are derived from long term (22 year) average behavior.

- The method was developed for passively cooled, max-power tracked systems.

- The results apply to either flat arrays (of various tilts) or 2-D tracked concentrating systems.

- Results were also derived which enable one to predict monthly average midday array temperature and electrical output.

- Statistics were compiled which permit an assessment of the expected departures from long term behavior.

Simplified Method for Max-Power Tracked System Performance:

- A simplified methodology was developed to predict the fraction of an electrical load that could be supplied by a passively cooled, flat array, PV system.

- The method was validated by comparison with computer simulation.

- The method accommodates various diurnal load shapes, daylengths, and climatic locations.

- The method is applicable to systems with and without dedicated storage.

- The method has potential for use with hand-held programmable calculators. It certainly can be used easily on small computers.

- The method makes use of Liu and Jordan (Ref. 1.5) type distributions of daily radiation on the horizontal to define a good, a mediocre, and a poor day to represent the monthly weather variations.

- Calculations are conducted for these three days and averaged to obtain a monthly value.

- Results for Albuquerque, NM, Madison, WI, and Medford, OR, show the method is within a standard deviation of 2.6% (absolute) of simulation results.

Clamped-Voltage Mode Results:

- Some representation for the solar cell I-V curve under various temperatures and insolation must be available in order to simulate or predict system performance.

- For a good choice of SR, the number of PV cells in series with each battery cell, the electrical output for clamped-voltage operation is only 2 to 3% below that for max-power tracking, if no power loss is considered for the max-power tracker.

- The optimum value of SR varies from month to month for a given location.

- A simplified design procedure akin to those described above appears to be infeasible.

- In preliminary comparisons, the results of a short computer program for predicting clamped-voltage array output vs. SR agree with those from TRNSYS simulations.

CHAPTER 1 REFERENCES

1.1 D.L. Evans, W.A. Facinelli, and R.T. Otterbein, ''Combined Photovoltaic/Thermal System Studies,'' Report SAND78-7031, Arizona State University, Tempe, AZ (1978).

1.2 E.R. Hoover, ''SOLCEL II: An improved Photovoltaic System Analysis Program,'' SAND79-1785, Sandia laboratories, Albuquerque, NM (1979).

1.3 S.A. Klein, W.A. Beckman, P.I. Cooper, N.A. Duffie, T.L. Freeman, J.C. Mitchell, D.M. Beekman, R.L. Oonk, P.J. Hughes, M.B. Eberlein, J.A. Duffie, W.E. Buckles, V.D. Karman, M.J. Pawelski, D.M. Utzinger, M.J. Brandemuehl, M.D. Arny, and J.C. Theilacker, TRNSYS — A Transient Simulation Program, Report 38, Solar Energy Laboratory, University of Wisconsin, Madison, WI (1979).

1.4 W.A. Beckman, S.A. Klein, and J.A. Duffie, Solar Heating Design, Wiley Interscience, New York, NY (1977).

2.0 SYSTEM SIMULATION STUDIES

This chapter discusses the computer simulation studies of photovoltaic electric systems that were done in order to assess the sensitivity of system performance results to various parameters. These studies then allowed the search for various correlations that might relate the important parameters to system performance, a first step in establishing simplified design procedures and ''rules of thumb.''

2.1 The System

The system modeled in these studies is illustrated in Fig. 2.1. It consists of a flat array ''photovoltaic collector,'' regulator, inverter, and battery storage. These units are used to supply whatever fraction of the electrical load they are capable of meeting. Whenever this fraction is less than one (1), the balance of the load is met by some back-up system whether it be a utility grid or a stand-alone auxiliary power source. If the load is totally met and storage cannot accept excess solar-generated electricity, the excess may be considered to be fed back to the back-up (e.g. if the back-up were a utility grid that would permit such operation) or ''dumped'' in some non-useful (i.e., non-useful to the electrical load) way. Hence, dumping would represent physically dissipating the energy as thermal energy in a resistive network, disconnecting all or part of the array in order to avoid the collection of the excess power, or moving off the max-power point.

In these simulations, the arrays were always assumed to be max-power tracked, i.e. the voltage on the array was continuously adjusted in order that the power out was the maximum possible. Deviations from this type of operation are discussed in Chapter 5.

2.1.1 The Simulation Program

All of the computer simulations reported in this chapter were performed using TRNSYS, a general simulation program for solar energy systems (Ref. 2.1) available from the University of Wisconsin. TRNSYS-compatible subroutines for the photovoltaic collector, regulator/inverter, and storage battery have been described previously (Ref. 2.2). Improved versions of these have been developed during the course of this study, along with an electrical subsystem which combines the above three components. The new versions were used in this study; they may be requested from the authors.

Time steps of 0.5 hour or less were used to avoid convergence problems. Monthly summaries of the results were from year-long simulations (8760 hours) were tabulated and analyzed.

2.1.2 The Solar and Meteorological Data Base

The data base used for these studies was the hourly Typical Meteorological Year (TMY) data (Ref. 2.3) in order to avoid the computation expenses involved in simulating multiple years of operation. The source of the solar information contained in the TMY data is the SOLMET data base (Ref. 2.4). This includes the standard year corrected total radiation on the horizontal and the direct normal (beam) radiation.

2.1.3 The Geographical Locations

Albuquerque, NM data were chosen to drive the initial and most extensive set of simulations. Since the weather in Albuquerque is consistently good from month to month, some simulations were also run using weather data for other locations representing a range of weather patterns. They are: Bismarck, ND; Madison, WI; Medford, OR; Phoenix, AZ; Santa Maria, CA; and Washington D.C./Sterling, VA. Of these locations, Madison, WI merits the title of most uniformly poor weather (although Washington/Sterling is competitive). Medford, OR, on the

other hand, spans the whole range of very poor (in the winter) to very good (in summer). For these reasons, Madison and Medford (along with Albuquerque) receive more attention in this report than other cities.

2.1.4 The Array

For these simulations the photovoltaic flat array was considered to consist of cells having an efficiency of 15% at 28°C. The array was south facing and tilted up from the horizontal at the local latitude angle (Ø). The encapsulant over the cells in the array was assumed to have a transmittance of 88%. With the assumed cell packing factor on the array of 1.0, the resulting array reference efficiency was 13.2% at 28°C.

For thermal considerations, the solar absorptance of the array was assumed to be 88% and the thermal loss coefficient was taken to be 20 kW/(m²·C) or 72 kJ/(hr·m²·C). The loss coefficient depends in a complicated way on wind speed and direction and on secondary flow patterns in the array field. Since these factors are difficult to determine, a constant thermal loss coefficient was used.

However, the correlations that are used in presenting the results of the simulations in this chapter make the results independent of most of these choices and therefore much more versatile than the above array description would indicate. This will become more apparent in Section 2.2.

2.1.5 Electrical Storage

The model for electrical storage used in these simulation studies is the modified-Shepherd Model for lead-acid batteries (Ref. 2.2). It is discussed in more detail in Section 2.3 where the sensitivity of the simulation results to the battery model is described.

In the results of Section 2.2, the batteries were permitted to function over the fractional state of charge range of $0.4 < F < 0.95$.

The sensitivity of the results to this range is also discussed in Section 2.3.

The battery charging strategy adopted for the results of this chapter gives first priority to recharging the battery to F = 0.6 with array output once the battery has reached its lowest permissible state of charge (F = 0.4); otherwise, first priority is given to satisfying the load. Compared to a strategy of always giving the load to be met first priority for array output, this gives a small reduction (~2%) of the solar fraction due to increased battery losses.

The battery is considered to be ''dedicated storage'' in that it was only charged by the array and never by the back-up or auxiliary power. This mode of operation may not represent the most economic mode of operation.

2.1.6 The Regulator/Inverter

The regulator and power conditioning equipment simulated in these studies gave a constant ''straight through'' efficiency (i.e., efficiency for converting d.c. array output power directly to a.c. power) of 81%. The assumption of a constant efficiency is not unreasonable since equipment of this type typically has very flat efficiency versus load curves over a wide part of the intended operating range. The actual efficiency is not critical since the results are presented here in a way that is independent of the value.

The regulator in the simulations includes a max-power tracker. Therefore, it must match power taken from the array at one voltage, with some or all of that power (if storage is involved) delivered to the battery at another voltage level. This is not presently a common method of operation in systems involving battery storage, but such operation is quite possible and may become common in future large systems (Ref. 2.5).

Results obtained for this max-power mode of operation may be useful in predicting results of battery-clamped operation (where the battery and photovoltaic array are wired directly in parallel). Chapter 5 discusses battery-clamped systems in more detail.

2.1.7 The Load

One of the difficult problems associated with developing simplified design procedures for photovoltaic systems is the wide diversity of electrical loads to which systems may be mated. Demand profiles or diurnal load shape can have a significant influence on system performance.

In the majority of the simulations described here, the diurnal load shape was assumed to consist of a cosine function of 24 hour period superposed on a constant background, as demonstrated in Fig. 2.2. The load shape was assumed to be repetitive from day to day. The daily total load or energy for Fig. 2.2 is given by

$$L = \int_0^{24} L(t)dt = 24L_0 \qquad (2.1)$$

Limited information (Ref. 2.6) suggests that for residential base load applications, an appropriate choice of parameters is $L_1/L_0 = 0.25$ and $T_p = 17$ (5 pm) (where T_p is the hour of maximum demand). These values were used as a baseline in the initial studies conducted under this program; the resulting load shape is referred to as the <u>baseline load</u>. The effect of load shape was then investigated by altering these parameters and redoing the simulation; these results are discussed in Section 2.2.4.

For applications such as residences and small commercial installations, the electrical demand is not continuous and ''smooth'' as shown in Fig. 2.2, although the monthly average daily profile may be. Particularly for systems with little or no storage, one might expect errors to arise in estimating the fraction of such ''noisy'' loads supplied by solar if the monthly average daily profile is used

each day in the simulation. This has been studied and is discussed in Section 2.2.5.

2.2 The Simulations

The results of the computer simulations of the photovoltaic systems described in Section 2.1 are discussed in this section with the exception of battery sensitivity studies, which are reported in Section 2.3. The results of all the studies are correlated in terms of the quantities:

f_e - the fraction (or percent) of the electrical load that is actually supplied directly by the solar system,

$\bar{Q}_e/\bar{L}$ - the ratio of the monthly average daily total solar electric availability to the monthly average daily total electrical load,

$S/\bar{\eta}\bar{A}$ - the ratio of storage size to the ''effective'' area of photovoltaic array.

The first of these, f_e, is a non-dimensional quantity that is similar to the solar fraction commonly used in the solar thermal field (Ref. 2.7). Knowledge of this parameter allows the designer to conduct an economic analysis, since he can predict his auxiliary energy savings and the resulting net present worth of these savings realized over a period of time.

The second combination, $\bar{Q}_e/\bar{L}$, is also non-dimensional. It differs from f_e since $\bar{Q}_e$ represents the array output $\bar{Q}_{ae}$, multiplied by the ''straight through'' efficiency for power conditioning, η_{pc}. However, not all of $\bar{Q}_e$ may actually be made available to the load since some may be irretrievably fed back to a utility, dumped or lost in storage. Only in the special case where the solar output is always less than the load should it be expected that $\bar{Q}_e/\bar{L}$ and f_e would be equal to one another. A designer, of course, has to know the magnitude of his load $\bar{L}$. With knowledge of

array output he can then select an array area that gives a desired $\bar{Q}_e/\bar{L}$. Chapter 3 presents a simplified method for predicting monthly average array operating efficiency and thus monthly average array output.

The third term, $S/\eta\bar{A}$, is a dimensional parameter that has been found by this study to be useful in ''collapsing'' data from many types of weather patterns. This should become apparent in the sections that follow.

Battery capacity, S, is often given in terms of amp-hrs where the battery is discharged over its useful capacity range at the S/10 rate (discharge current equal to the battery capacity divided by 10 hours). In some respects this is the least ambiguous method of stating capacity, but in other respects it is not explicit. Therefore, capacities have also been stated here in terms of energy (W-hrs), which are easier to use but less precise.

When amp-hr units are used in this study, they refer to the total capacity of all single cells (i.e., all nominal two volt cells) that make up the battery. If, for example, one is making use of a 12 volt, 100 amp-hour battery consisting of 6 cells in series, each cell has necessarily a capacity of 100 amp-hrs. Total capacity of all single cells would then by 6 x 100 or 600 amp-hrs., which is the number that should be used with the results presented here.

These same 6 cells could be connected in parallel to yield a 2 volt, 600 amp-hr battery which, for simulation of max-power tracked systems, would produce the same system performance as its 12 volt counterpart discussed above. However, in real systems, coordinating voltages among the array, the max-power tracker, and the battery is an important design consideration.

To convert amp-hr capacities to energy values, one needs only to multiply them by an appropriate voltage. Perhaps the best value would be the average between the voltage at the beginning and at the end of

an S/10 (S in amp-hrs) discharge rate. These voltages depend on the construction of the battery and on the range of fractional state of charge that is permitted during operation.

The fine points of this voltage choice have been sidestepped here by choosing the nominal voltage of 2.0 volts per cell as the appropriate voltage. Thus, the 12 volt, 100 amp-hr battery discussed above is assumed to represent 1200 W-hrs of storage, as does the 2 volt, 600 amp-hr battery. The results which follow demonstrate that system performance is not strongly enough dependent on $S/\bar{\eta}A$ to merit more precise interpretations of S.

The S that is used in the results that follow represents the effective capacity that is utilized in operation of the system. If a 500 amp-hr (1000 W-hr) cell is used but it is not permitted to discharge below a fractional state of charge of 0.5, this represents an effective S of 250 amp-hrs (500 W-hr), if full charge is permitted.

The $\bar{\eta}$ in $S/\bar{\eta}A$ is the monthly efficiency for converting solar energy into array output electrical energy. A simplified method for determining this is presented in Chapter 3. The A in $S/\bar{\eta}A$ represents the array area.

2.2.1 Baseline Load/Albuquerque/Equinox Months

Fig. 2.3 shows a map of system performance typical of the baseline load in Albuquerque, NM, in the months of March and September. Results for other months can vary from those shown in Fig. 2.3, primarily because of the change in the daily insolation profile created by changing daylengths. This effect is discussed in more detail in the next section.

In systems with relatively small arrays ($\bar{Q}_e/\bar{L} \sim 0.2$) the array output is always less than the immediate <u>baseline</u> demand. Consequently, the output is always used directly by the load and there

is no need for storage. System performance is then independent of the storage capacity.

As the array becomes larger (e.g., $\bar{Q}_e/\bar{L} = 0.6$), there are periods when the power output of the array exceeds the immediate requirement of the baseline load. With no storage available, this extra or excess (XS) energy must be dumped. As battery capacity is increased, however, some of the extra energy can be stored for use later when array output again satisfies less than the full load. Dumping decreases further with increased battery capacity until, with a storage capacity corresponding to about $S/\eta\bar{A} = 20$ amp-hrs/(%·m²) or 40 W-hrs/(%·m²), dumping is eliminated, and no further improvement in performance can be achieved with increased storage.

As the array becomes larger yet (e.g., $\bar{Q}_e/\bar{L} = 1.0$) its output increases, but virtually all of the increased production occurs during periods in which the full baseline load already is satisfied by a smaller array. Without storage, almost all of the increased output is merely dumped and does not significantly improve performance. The addition of storage, however, again permits the extra midday array output to be used in the afternoon and nighttime when the system otherwise would be incapable of satisfying the load. As in the case of $\bar{Q}_e/\bar{L} = 0.6$, a storage capacity exists for which dumping is minimized and any additional storage is not effectively utilized.

When the array size increases further, the monthly average daily output exceeds the daily load ($\bar{Q}_e/\bar{L} = 1.2$). Without storage, little improvement in performance is noted. With sufficient battery capacity [typically 25 amp-hrs/(%·m²) or 50 W-hrs/(%·m²)] the system satisfies nearly the entire load, with excess array output being dumped. These larger storage sizes are what might be termed ''intermediate size storage'' in that they are depleted by several consecutive days of poor insolation and are replenished during the next good insolation period. The temptation of speaking of ''number of hours'' of storage will be avoided until the effect of geographic location is discussed in Section 2.2.3.

Fig. 2.4 illustrates the use of the battery. The small diagrams superposed on this figure are frequency distributions of the battery state of charge. For example, these show that small batteries [$\bar{S}/\eta\bar{A}$ ~ 20 W-hrs/(%·m²)] cover their entire permitted range of state of charge, since they typically charge completely during the day and then fully discharge overnight. For $\bar{Q}_e/\bar{L}$ = 0.6, photovoltaic array output is insufficient to fill a large capacity battery [$\bar{S}/\eta\bar{A}$ > 40 W-hrs/(%·m²)]. As a result, the state of charge is at or near its minimum permitted value most of the time. If this minimum happens to be near zero (i.e., if the battery were allowed to be fully discharged), such operation would not favor long battery lifetimes. This situation reverses for large arrays (e.g., $\bar{Q}_e/\bar{L}$ ~ 1.2) and large batteries. Here the array output maintains the batteries at full charge most of the time since there is more than enough energy to meet the average daily load. Such operation would favor long battery lifetime.

Note that a fixed $\bar{S}/\eta\bar{A}$ does not infer the same battery capacity at $\bar{Q}_e/\bar{L}$ = 0.6 as it does at $\bar{Q}_e/\bar{L}$ = 1.2. For the same load, it takes twice the array size for a $\bar{Q}_e/\bar{L}$ = 1.2 as it does for a $\bar{Q}_e/\bar{L}$ = 0.6. Equal $\bar{S}/\eta\bar{A}$ thus requires twice the battery capacity for $\bar{Q}_e/\bar{L}$ = 1.2 as for $\bar{Q}_e/\bar{L}$ = 0.6.

2.2.2 Baseline Load/Albuquerque/Seasonal Variations

Fig. 2.5 demonstrates the seasonal variation in system performance. The figure considers four months in Albuquerque: March, June, September, and December. The effects of monthly average insolation differences again have been removed from the figure by comparing behavior at constant $\bar{Q}_e/\bar{L}$ ratios. The figure indicates that, when little storage is provided, significantly better performance is achieved in summer. With additional storage, seasonal variations are minimized.

The major factor contributing to the seasonal variation shown is daylength. In winter months, a shorter daylength requires a greater

peak array output in order to attain the same total output. The steeper noontime peak in array production is more poorly matched to the given load profile. Hence, more energy is directed to storage in winter months and, if insufficient storage exists, more energy is dumped. Thus, at the lower values of storage in Fig. 2.5 the December curve shows the worst performance. March and September exhibit improved behavior while June, with the longest daylength, generates an output most closely matched to the load profile and consequently has the best performance.

Fig. 2.6 demonstrates the above results through the use of typical load and output curves for June and December. The more peaked December array output profile is clearly illustrated.

2.2.3 Baseline Load/Effect of Location or Weather Patterns

Fig. 2.7 exhibits the variation in system performance typical of the months of March and September for seven cities for $\bar{Q}_e/\bar{L} = 0.6$. Similar results are observed for other values of $\bar{Q}_e/\bar{L}$. Monthly average daily total radiation differences between the locations have been effectively removed by considering constant array output to load ratios (i.e., fixed $\bar{Q}_e/\bar{L}$ ratios). Differences in daylength due to latitude differences in these equinox months are less than ten minutes for the range of latitudes considered. The major contributing factor is thus the difference in local weather traits, e.g., the speed and frequency of storm fronts in a given area, the occurrence of morning or afternoon fog or cloudiness, etc. According to Fig. 2.7 this effect is comparatively minor even in systems with no storage at all, when comparisons are made at a given $\bar{Q}_e/\bar{L}$.

Fig. 2.8 demonstrates the combined effects of seasonal and weather differences. It shows performance during the year, again for seven cities, of systems equipped with two different storage capacities. The small storage cases portray clearly the periodicity which leads to daylength as an explanation for seasonal differences in performance. The larger storage cases once again demonstrate the

effect of storage in diminishing losses caused by poor matching of the load to the array output.

Both Figs. 2.7 and 2.8 demonstrate the value of using $S/\eta\bar{A}$ along with $\bar{Q}_e/\bar{L}$ as correlation parameters. No other combination of variables has been found to serve as well in collapsing the data from such an assortment of climates into nearly single curves of fixed $\bar{Q}_e/\bar{L}$.

If the dimensionless group $S/\eta\bar{A}\bar{Q}_S$ were used in place of the dimensional group $S/\eta\bar{A}$, the curves for different locations would not collapse as well onto a nearly single curve. For example, if the horizontal axis of Fig. 2.7 were changed to $S/\eta\bar{A}\bar{Q}_S$, any data point for Madison would be moved farther to the right of a corresponding point for Albuquerque of equal $S/\eta\bar{A}$, since $\bar{Q}_S$ would be less for Madison than for Albuquerque. Obviously, neither $S/\eta\bar{A}$ nor $S/\eta\bar{A}\bar{Q}_S$ have any effect on the vertical axis or at very large S, but each has different effects between these two extremes.

Admittedly, $\eta\bar{A}\bar{Q}_S$ is intuitively more appropriate to use in the denominator of the storage parameter. For example, doubling the insolation and halving the array efficiency does not change the system performance, yet this would double the parameter $S/\eta\bar{A}$ and thus have the appearance of increasing f_e.

The most important point to be made regarding to the use of $S/\eta\bar{A}$ is that the results presented here are for ''similarly tilted arrays.''[1] For the same array configuration and ''similar'' tilts, geographically dependent insolation variations are such that $S/\eta\bar{A}$ happens to be useful in collapsing data.

---

[1] ''Similarly tilted arrays'' means that array tilts in different locations either are optimally tilted for maximum energy collection in each location or are equal increments away from these optional tilts

Thus, for comparing monthly results for two different locations, say for ''similar'' tilts of $(\phi + \theta)$ where θ is independent of location, $S/\eta A$ is a useful parameter. It is not as useful for comparing monthly system performance results for array tilts of $(\phi + \theta_1)$ with results for tilts of $(\phi + \theta_2)$ if θ_1 is appreciably different from θ_2. Then $S/\eta A\bar{Q}_S$ would be more useful. One can, however, introduce a modified A for a given location by multiplying it by the ratio of the insolation on the tilt $(\phi + \theta_1)$ to the insolation on the tilt $(\phi + \theta_2)$.

As an example, consider the same arrays operated in June in both Madison and in Albuquerque, neglecting for the moment the difference between the monthly operating efficiencies due to climate and tilt differences. If the tilt of the array in Madison is $(\phi + 27 = 70°)$ and that in Albuquerque $(\phi - 13 = 20°)$, one has to correct $S/\eta A$ in one of the two cities so as to obtain ''similar'' tilts in both locations before system comparisons can be made. Suppose the Madison results are chosen for correction. Then a modified area A' needs to be calculated that would account for a change in tilt from $(\phi + 27 = 70°)$ to $(\phi - 13 = 30°)$ in Madison $(\phi = 43°)$. Thus,

$$A'_{Mad} = A_{Mad}\ \bar{Q}_S(\text{for } 30° \text{ tilt})/\bar{Q}_S(\text{for } 70° \text{ tilt}) \qquad (2.2)$$

$$= A_{Mad}\ (1.5)$$

where 1.5 represents the June ratio for insolation on the two tilts. (Sources of this information will be discussed in Chapter 3.) Now $S_{Alb}/\eta A_{Alb}$ can be compared with $S_{Mad}/\eta A'_{Mad}$ since adjustments to similar tilts has been made (i.e., to tilts of $(\phi - 13)$).

The usefulness of $S/\eta A$ might appear questionable, but it should be remembered that usually only optimum or nearly optimum tilts are considered in design. In such applications, $S/\eta A$ is a much more convenient parameter than $S/\eta A\bar{Q}_S$. Its use forms the basis for some ''rules of thumb'' to be discussed in Chapter 6.

A significant result of this section is that for a given load, $\bar{L}$, a location which requires n times as much array area in order to attain the same $\bar{Q}_e/\bar{L}$ ratio as another location, also needs essentially n times as much battery capacity, ignoring array efficiency differences, in order to provide a comparable solar fraction, f_e. It is certainly no surprise that, for example, one needs more array area in Madison, WI than in Albuquerque, NM to meet a given load. However, it is not widely known that the ratio of battery capacity to array area is the same in both locations for comparable performance.

Also, since different amounts of array may be required to operate at a given $\bar{Q}_e/\bar{L}$ at different times of the year (due to the insolation behavior and tilt), a fixed $S/\eta A$ may yield different amounts of storage through the year. Table 2.1 demonstrates this point for three different locations. Here the storage has been expressed as ''hours of storage'' or the time it would take to deplete the storage if it were discharged from full charge at the average daily demand L_0. Expressed in this fashion, the storage is independent of the actual load size.

Presumably a designer would design (i.e., choose the array size, array tilt and battery size) for the month with the least favorable insolation to load ratio. He would then calculate the $\bar{Q}_e/\bar{L}$ and $\bar{S}/\eta A$ that his design would yield during the remaining months so that yearly performance could be estimated. Once storage size and array size are selected, only $\bar{\eta}$ in $S/\bar{\eta}A$ would vary from month to month. However, considering the relative insensitivity of f_e to $S/\eta A$ (see Fig. 2.3), the variations in $\bar{\eta}$ could be ignored with little loss in accuracy.

2.2.4 Variation of Load Shape/Albuquerque/Equinox Months

Fig 2.9 exhibits the effects on system performance of variations in the load characteristics. These calculations were made for Albuqueruqe, NM and are typical of March or September behavior. The

effects are shown as a function of storage capacity for two different $\bar{Q}_e/\bar{L}$'s. The values $T_p = 0$ (a peak demand at midnight) and $T_p = 12$ (a peak demand at noon) demonstrate the full effect of the phase of the load. $T_p = 0$ represents a demand exactly out of phase with the array output, while $T_p = 12$ describes a demand precisely in phase with the array. System behavior for cases of a constant load throughout the day (in which T_p has no meaning) is described here by $L_1/L_0 = 0$.

With limited storage, the matching of demand to array output is clearly important. The peak output of south facing arrays usually occurs at noon. Thus, when the minimum demand occurs at noon (as it does when $T_p = 0$), a greater portion of the output must be dumped and poorer system performance results. Conversely, when the maximum demand occurs at noon ($T_p = 12$) a larger part of the array production is used directly, thereby minimizing the quantity of energy which is dumped and yielding improved system performance.

Larger L_1/L_0 ratios merely amplify the effect. An increase in L_1/L_0 from 0.25 to 0.50 results in improved performance in the case of $T_p = 12$, while the same change causes reduced performance in the case of $T_p = 0$.

With increased storage, less of the array output which exceeds the immediate demand needs to be dumped and in all cases, performance improves with increased storage. At large storage capacities [e.g., $S/\eta A$ 25 amp-hrs/(%·m²) or 50 W-hrs/(%·m²)] no dumping occurs, and system performance differs only slightly due to battery inefficiencies applied to differing quantities of energy flowing through storage.

Fig. 2.9 thus demonstrates that the amplitude and the phase of the load can significantly affect system performance. However, this figure also shows that for reasonable load shapes, more than 25 amp-hrs/(%·m²) or 50 W-hrs/(%·m²) of battery storage is not useful in improving system performance. This may be a useful ''rule of thumb'' in preliminary design applications.

2.2.5 Effect of Random Fluctuations in the Load

In addition to rather continuous or monthly average diurnal variations, other largely random fluctuations in load are likely to occur as various electrical devices switch on and off during a day. It is reasonable to expect that such fluctuations will have the greatest effect on performance (i.e., on the solar fraction, f_e) for systems with no storage since there will be no means of buffering the array output. Also, it can be shown that the effect of such fluctuations will be maximized when the array output power is nearly equal to the electrical demand. For the baseline load used here, this occurs for solar system sizes for which $\bar{Q}_e/\bar{L} \sim 0.4$. Simulations are described here which explore the effect of fluctuation amplitude and frequency on system performance for systems with no storage.

One motivation for these studies was an apparent problem in predicting the actual energy flows in utility connected systems where sell-back of excess array generated power is permitted. If ratios of price-to-sell to price-to-buy (commonly called the sell-back ratio) are different from one (1.0) it would appear that short term fluctuations, although they may produce no net power flows between the utility and the load, may produce a net monetary flow. If simulations were done using time periods longer than the periods typcial of the fluctuations, it would then seem that proper economic analyses could not be accomplished since only net energy transfers could be obtained. These net energy flows would not reveal anything about the actual bidirectional monetary flows.

The studies reported in this section were done by superposing on the baseline load at each time step a ''noise'' component picked from a set of random numbers normally distributed about zero. The standard deviation of the random number set (expressed as a fraction of L_0) was used to characterize the magnitude of the fluctuations. In the cases where a large negative fluctuation would have produced a negative load, the load was set to zero. Variation of the simulation time step effectively changed the duration or period of the fluctuations. Both

the power flows to the utility (when there was excess solar power) and from the utility were integrated as was the solar generated power going directly to the load.

Fig. 2.10 shows a simple energy flow diagram for reference. Since under max-power tracking, the array output is fixed for given location, orientation, and weather, any change in the solar-generated power that is fed back to the utility produces a change in the amount of solar-generated power that goes directly to the load. For a fixed load, this then produces a change in the solar fraction, f_e. Thus, changes in the bidirectional power flows to and from the utility due to fluctuations, produce changes in f_e. Once f_e is known, proper economic analysis can be made.

Table 2.2 shows that monthly system performance is remarkably insensitive to such random fluctuations, even for standard deviations, σ, as large as 50% of the mean demand. The results shown are for Albuquerque January TMY data, but similar calculations for Medford, OR show comparable results.

In Table 2.2 the change in f_e due to changing Δt at $\sigma = 0$ represents the numerical errors of the type encountered in any finite time-step calculation procedure of the type involved in TRNSYS. However, the problem of fluctuations elucidated above is best considered by examining the changes produced by increasing σ at a fixed Δt. Although there is little effect of σ on the monthly results, performance on individual days can be and are substantially affected.

These somewhat surprising results are explained by considering Fig. 2.11 which shows a typical daily interaction between array output and load. The region labeled XS corresponds to the energy output of the array which, in the absence of storage, must be fed back to the utility. Only those fluctuations from the average load which result in a change in XS can cause a change in system performance. Thus, fluctuations during non-daylight hours have no impact whatsoever on performance. Also, only the largest of negative fluctuations affects

performance during the early morning and late afternoon. In the period around noon, negative deviations from the average load result in increased dumping and thereby tend to decrease performance. However, positive deviations during this period are at least partially satisfied by the excess midday output of the array. This decreases the amount of energy dumped and tends to improve system performance. The net result over the period of a month is that the adverse effect of negative midday fluctuations is nearly compensated for by the favorable effect of positive fluctuations.

If the fluctuations become large enough (e.g., σ = 200% in Table 2.2), the negative fluctuations degrade performance much more than positive fluctuations improve it. This leads to a sizable reduction in the solar fraction, f_e.

Load shape and size obviously play a role in system performance in the presence of fluctuations. For example, a load that tracked, on the average, the array power output (both in size and shape) would suffer in performance during periods of negative fluctuations but would never realize any improvements during positive fluctuations. No systematic investigation of load shape has been carried out here.

2.3 Battery Model Sensitivity

2.3.1 Choice of Battery Model

Section 2.2 presents results correlated in a way that permits conclusions to be drawn concerning the sensitivity of f_e to factors such as array size, battery storage capacity, and various system efficiencies. This section describes the results of battery sensitivity studies using three models of a lead-acid storage battery, and basically concludes that the results are nearly insensitive to the choice of battery model.

Details of battery modeling have been discussed in a previous report (Ref. 2.2). The key relationship for such a model is the

formula relating battery voltage to its current and stage of charge, i.e., $V_b = V_b(I,F)$. This function is shown graphically in Fig. 2.12 for a single lead-acid cell for the Shepherd (Ref. 2.8), Hyman[2] (Ref. 2.9), and GE (Ref. 2.6) models, the three versions tested in these simulations. The term ''battery'' refers to a collection of lead-acid cells connected in series and in parallel.

The major inefficiency in using a storage battery is due to the higher voltages encountered when charging than when discharging, so that more power is necessary for charging than is available during subsequent discharge. As shown in Fig. 2.12, this difference in voltage is about the same for the Shepherd and Hyman models, and they should yield very similar simulation results. The voltage difference between charge and discharge is less for the GE model than for the other two, and hence use of the GE model should give more efficient battery performance.

Since the inefficiency depends on both the typical charge and discharge rates at which the battery is operated, a valid sensitivity analysis of the battery models requires doing simulations in which the battery experiences an assortment of charge and discharge currents.

The battery currents in max-power systems vary at least as much as in comparable clamped-voltage systems. Hence, the sensitivity results reported here were obtained using only the former mode of operation. In the max-power mode, it can be shown that the current into or out of each battery cell is independent of the series/parallel wiring of individual cells to form the battery.

In general, a small battery (small S) will see higher currents than will a large one (large S). The charge and discharge rates also depend upon the sizes of the photovoltaic array and the load, relative to the battery size. Therefore the sensitivity studies of this section include simulations having different combinations of battery,

---

[2]Also referred to as the modified-Shepherd Model

solar cell array, and load sizes. Table 2.3 lists the eight combinations of component sizes used and the results of the simulations for the three battery models in terms of solar fraction, f_e, for equinox months. The differences in performance (from one model to another) are less than an incremental 2%.

In two of the cases, reasons are apparent for the close agreement among the models in their estimation of system performance. In Case 6, the battery is large relative to both the array and load, which means that it operates at low charge/dischrage rates. The voltage difference in each battery model is small for small currents, and thus one would expect that all three models will give nearly the same system performance.

On the other hand, the battery cells in systems with relatively small storage capacity will see large currents, leading to greater storage inefficiencies. But the small capacity limits how much of the array output can be stored and how much of the load can then be supplied by the batteries, so they contribute little to the overall system performance. This is the situation in Case 3.

The combinations of components for which the performance is most difficult to anticipate are those in which the battery size is a good match to the array and load sizes, i.e., Cases 4 and 5. In these circumstances it is hard to predict how the results using the different battery models will compare, but as indicated in Table 2.3, the differences in performance are negligible for these cases as well as for Cases 1 to 3 and 6 to 8.

Besides giving essentially the same results, the simulations using each of the three models require nearly the same amounts of computer time. However, the Shepherd and Hyman models are generally superior because they can be easily modified when better data on lead-acid batteries becomes available or when other kinds of batteries need to be modeled. Furthermore, the Hyman model realistically represents the voltage as a continuous function of the current at any

given state of charge, whereas the Shepherd model has a discontinuity at $I = 0$. For these reasons, the Hyman model was used in the simulations reported earlier in this chapter.

2.3.2 Energy Losses in the Battery

Other losses, in addition to those associated with the difference between the charge and discharge voltage curves, must be considered in an accurate battery model. In the lead-acid type of cell, these include electrolysis of water which occurs during an occasional ''equalizing'' charge and various chemical losses. (For a complete discussion of energy dissipation in a battery see Refs. 2.9 or 2.10.)

These minor losses are most conveniently accommodated in a battery model by lumping them into a ''charging efficiency factor.'' This parameter multiplies the charging current to yield the actual rate of change of battery state of charge (Ref. 2.2), i.e., when $I > 0$,

$$dQ/dt = I \cdot \varepsilon \tag{2.3}$$

The value of ε to be used in simulations depends upon the manner in which the real electric system is operated, e.g., how often an equalizing charge is applied. The simulations under discussion in this chapter have $\varepsilon = 0.95$, a value which is typical of actual battery operation (Ref. 2.10).

The effect of the ''voltage difference'' losses and charging losses on system performance is exhibited in Fig. 2.13. The lowest set of curves are for the Hyman battery model with $\varepsilon = 0.95$. In these cases both kinds of losses occur. The middle set of curves are again for the Hyman model, but with $\varepsilon = 1.0$. The difference between the two curves thus represents the charging losses.

The uppermost set of curves in Fig. 2.13 are from simulations using a model of an ideal lossless battery. (This is the ''Mode 1''

battery model with $\varepsilon = 1.0$, Ref. 2.2.) The upper gap is thus due to the ''voltage difference'' losses.

These storage ''voltage difference'' losses are clearly more important than are the charging losses, particularly for the cases with the larger $\bar{Q}_e/\bar{L}$, and bring about a significant degradation in overall system performance. These results imply that: (1) accurate modeling of photovoltaic systems with storage batteries requires a good representation of $V_b = V_b(I,F)$, and (2) the choice of the value of ε, at least within the range of 0.95 to 1.0, is only of minor importance.

2.3.3 Range of State of Charge

The appearance of the Hyman model's charge/discharge curves in Fig. 2.12 suggests that battery (and, hence, system) performance may depend upon where the battery tends to operate in its state of charge range. That is, ''voltage difference'' losses will be less when the battery charges and discharges near the middle range of F, compared with its operating at either high or low values of F. This section compares the results of simulations having different state of charge limits on the battery (F_C, F_B, and F_D) which restrict it to different ranges of state of charge.

In the systems discussed in Sections 2.1 and 2.2, the battery was inherently restricted to operate between $F_D = 0.4$ and $F_C = 0.95$ with $F_B = 0.6$. Battery losses and therefore system performance would be somewhat different if lower values of F_D and F_C were used, although the frequency distributions shown in Fig. 2.4 would remain essentially unchanged. This was confirmed by rerunning the simulations with $F_D = 0.05$, $F_C = 0.6$, and $F_B = 0.25$. Battery losses and overall system performance are compared in Table 2.4 and Fig. 2.14. Results in Fig. 2.14, when viewed in light of the state of charge histograms, clearly reveal the following trends:

(1) When F is usually low [$\bar{Q}_e/\bar{L} = 0.6$, $S/\bar{\eta A} = 50$ W-hrs/(%·m²)], the 0.40 to 0.95 range gives more efficient battery performance.

(2) When F is usually high [$\bar{Q}_e/\bar{L} = 1.2$, $S/\bar{\eta A} = 50$ W-hrs/(%·m²)], the 0.05 to 0.60 range gives more efficient battery performance.

These results are consistent with the spacing between the charge and discharge curves in the Hyman model at various battery states of charge. Yet, the differences between the two sets of simulations, both in terms of the battery losses (Table 2.4) and solar fraction (Fig. 2.13) are small.

The system performance results depicted in Fig. 2.14 differ primarily because of additional dumping of excess array output in the $0.05 < F < 0.60$ cases. In these simulations, a lower permitted voltage limit kept the battery from discharging over the entire allowed range of $\Delta F = 0.55$; i.e., no constant voltage, taper discharge was permitted. No such limitation existed in the $0.40 < F < 0.95$ cases as a constant voltage, taper charge was permitted at an upper voltage limit. Thus, the simulations with F confined to a lower range have an effective battery capacity less than in those with a higher range of F. With less storage capacity, more dumping occurs and the system performance is poorer.

Since these simulations were done, a more sophisticated regulator/inverter model has been developed which permits a tapered discharge at constant voltage. Simulations with $0.05 < F < 0.60$ incorporating this scheme would have an effective battery capacity larger than the set of simulations with the same range of F described above. This would lead to results which agree even more closely with those from the $0.40 < F < 0.95$ simulations.

CHAPTER 2 REFERENCES

2.1 S.A. Klein, W.A. Beckman, P.I. Cooper, N.A. Duffie, T.L. Freeman, J.C. Mithcell, D.M. Beekman, R.L. Oonk, P.J. Hughes, M.B. Eberlein, J.A. Duffie, W.E. Buckles, V.D. Karman, M.J. Pawelski, D.M. Utyinger, M.J. Brandemuehl, M.D. Arny, and J.C. Theilacker, TRNSYS —A Transient Simulation Program, Report 38, Solar Energy Laboratory, University of Wisconsin, Madison (1979).

2.2 D.L. Evans, W.A. Facinelli, and R.T. Otterbein, ''Combined Photovoltaic/Thermal System Studies,'' Report SAND78-7031, Arizona State University, Tempe, AZ (1978).

2.3 I.J. Hall, R.R. Prairie, H.E. Anderson, and E.C. Boes, ''Generation of a Typical Meteorological Year,'' Proc. 1978 Annual Meet. Amer. Sec. of ISES, Denver, CO (1978).

2.4 ''SOLMET User's Manual, Hourly Surface Radiation — Surface Meteorological Observations,'' National Oceanic and Atmospheric Administration, Environmental Data Service, Asheville, NC (1979).

2.5 L.L. Bucciarelli, B.L. Grossman, E.F. Lyon, and N.E. Rasmussen, ''The Energy Balance Associated with the Use of a Maximum Power Tracker in a 100-KW-Peak Power System,'' Proc. Fourteenth IEEE PV Specialists' Conference, San Diego, CA (1980).

2.6 ''Conceptual Design and Systems Analysis of Photovoltaic Systems,'' Report No. ALO-3686-14, General Electric Co., Space Division, Philadelphia, PA (1977).

2.7 W.A. Beckman, S.A. Klein, and J.A. Duffie, Solar Heating Design, Wiley Interscience, New York, NY (1977).

2.8 C.M. Shepherd, ''Design of Primary and Secondary Cells II. An Equation Describing Battery Discharge,'' J. Electrochem. Soc., 112, 657 (1965).

2.9 E.A. Hyman, ''Phenomenological Cell Modeling: A Tool for Planning and Analyzing Battery Testing at the BEST Facility,'' Report RD77-1, Public Service Electric and Gas Company and PSE and G Research Corporation, Newark, NJ (1977).

2.10 G.W. Vinal, Storage Batteries, John Wiley and Sons, New York, NY (1955).

Table 2.1

Hours of Storage for Discharging at L_o

for Various Times of the Year at Three Locations

For all Locations and Times, $f_e \approx 55\%$

Month	Q_e/L	$S/\bar{\eta}A$ $\frac{W\text{-hrs.}}{(\%\cdot m^2)}$	Albuquerque (Hours)	Madison (Hours)	Medford (Hours)
March	.6	30	9.8	12.7	14.4
June	.6	30	8.7	12.1	9.7
Sept.	.6	30	9.8	13.6	11.5
Dec.	.6	30	11.9	29.5	47.0

These Hours of Storage numbers are based on supplying a power equal to the average load, L_o. To determine the hours of storage based on average solar system output power (i.e. $\bar{Q}_e/24$), divide these numbers by 0.6.

Table 2.2

Utility Sellback Results
Albuquerque TMY, January
Random Load (of std. dev. σ) Superposed on Baseline Load
Δt = Time Step in Hours

Qe/L	XS (% of L)	σ (% of L_0)	f_e (%)			
			Δt = 0.05	Δt = 0.10	Δt = 0.50	Δt = 1.0
40%	9.0	0	31.01	31.03	30.98	30.69
		10	31.01	31.02	31.04	30.51
		20	30.76	30.77	30.91	30.21
		30	30.31	30.33	30.60	29.75
		40	29.64	29.66	30.03	28.93
		50	28.78	28.80	29.25	27.86
		200	N/A	16.43	16.94	15.60
60%	24.9	0	34.94	34.96	34.87	34.42
		10	34.99	35.01	34.93	34.30
		20	34.81	34.85	34.84	34.02
		30	34.50	34.55	34.59	33.57
		40	34.04	34.11	34.16	32.91
		50	33.44	33.52	33.61	32.14
100%	61.3	0	38.74	38.77	38.63	37.97
		10	38.82	38.86	38.77	37.80
		20	38.67	38.73	38.73	37.54
		30	38.42	38.53	38.59	34.19
		40	38.06	38.22	38.32	36.65
		50	37.59	37.80	37.97	36.02
		200	N/A	28.93	29.99	27.26

Table 2.3

Effect of Battery Model

Albuquerque TMY, Equinox Months, Baseline Load

Case #		1	2	3	4	5	6	7	8
Battery		Small	Large	Small	Small	Large	Large	Small	Large
Array		Small	Small	Large	Small	Large	Small	Large	Large
Load		Large	Large	Large	Small	Large	Small	Small	Small
$\bar{Q}_e/\bar{L}$		0.4	0.4	0.8	0.8	0.8	0.8	1.2	1.2
$S/\bar{\eta}A$ (Wh/%·m^2)		38.1	63.5	12.7	38.1	38.1	63.5	12.7	38.1
f_e(%)	GE	39.6	39.6	60.2	76.7	76.7	77.0	72.2	97.6
	Hyman	39.4	39.6	59.0	75.3	75.3	76.1	71.5	97.6
	Shepherd	39.4	39.4	59.3	74.8	74.8	75.3	71.5	97.4

Table 2.4

Storage Losses as a Percentage of Load

Albuquerque TMY, Equinox Months, Baseline Load

Range of State of Charge \ $S/\overline{nA}$ (W-hrs/(%m^2))	$\bar{Q}_e/\bar{L}$ = 0.6					$\bar{Q}_e/\bar{L}$ = 1.2				
	12.7	25.4	38.1	50.8	63.5	12.7	25.4	38.1	50.8	63.5
.05 < F < .60	3.0	5.5	5.6	5.5	5.5	7.2	9.9	8.5	7.5	6.9
.40 < F < .95	3.4	5.1	5.0	4.9	4.8	6.5	9.8	8.6	7.7	7.1

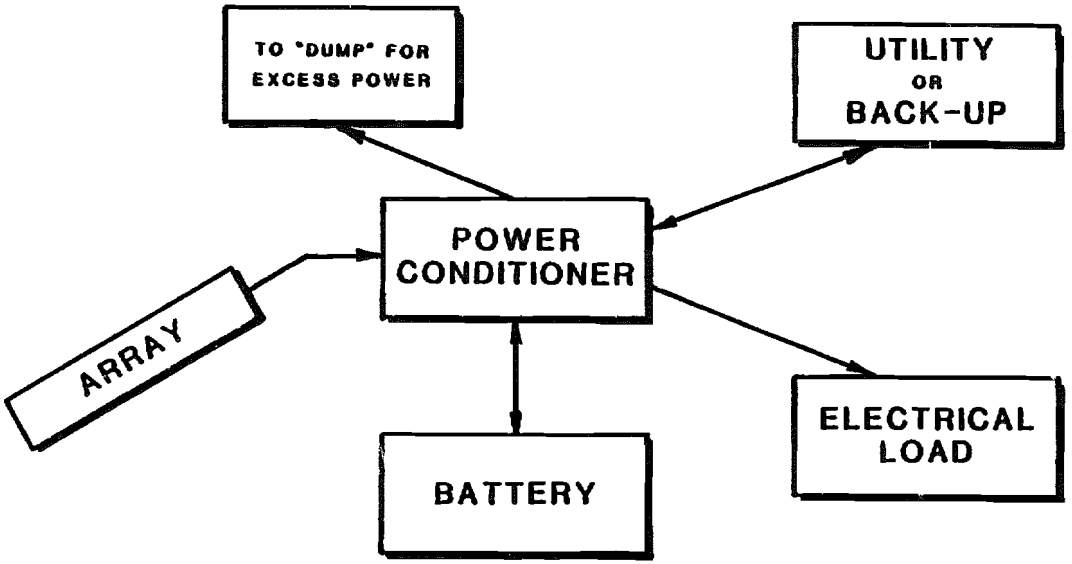

Figure 2.1 Schematic of Photovoltaic Electric System

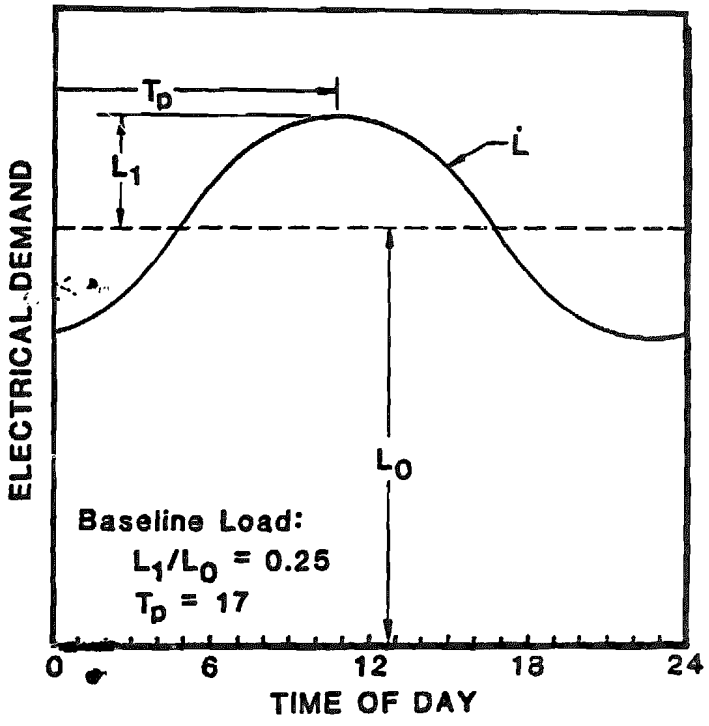

Figure 2.2 Diurnal Load Shape

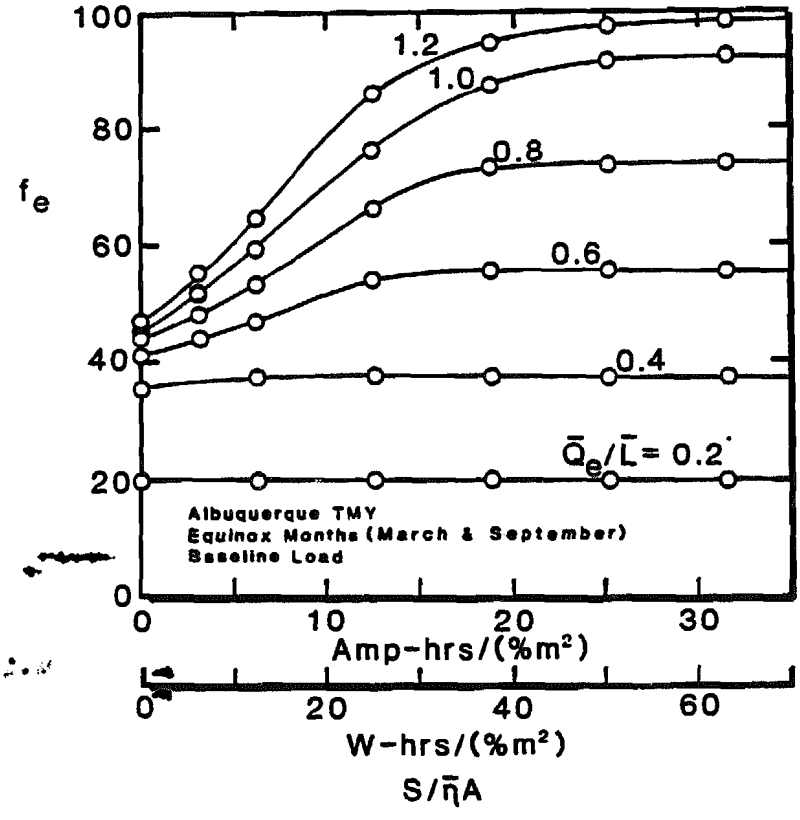

Figure 2.3 System Performance Predictions of TRNSYS Simulations

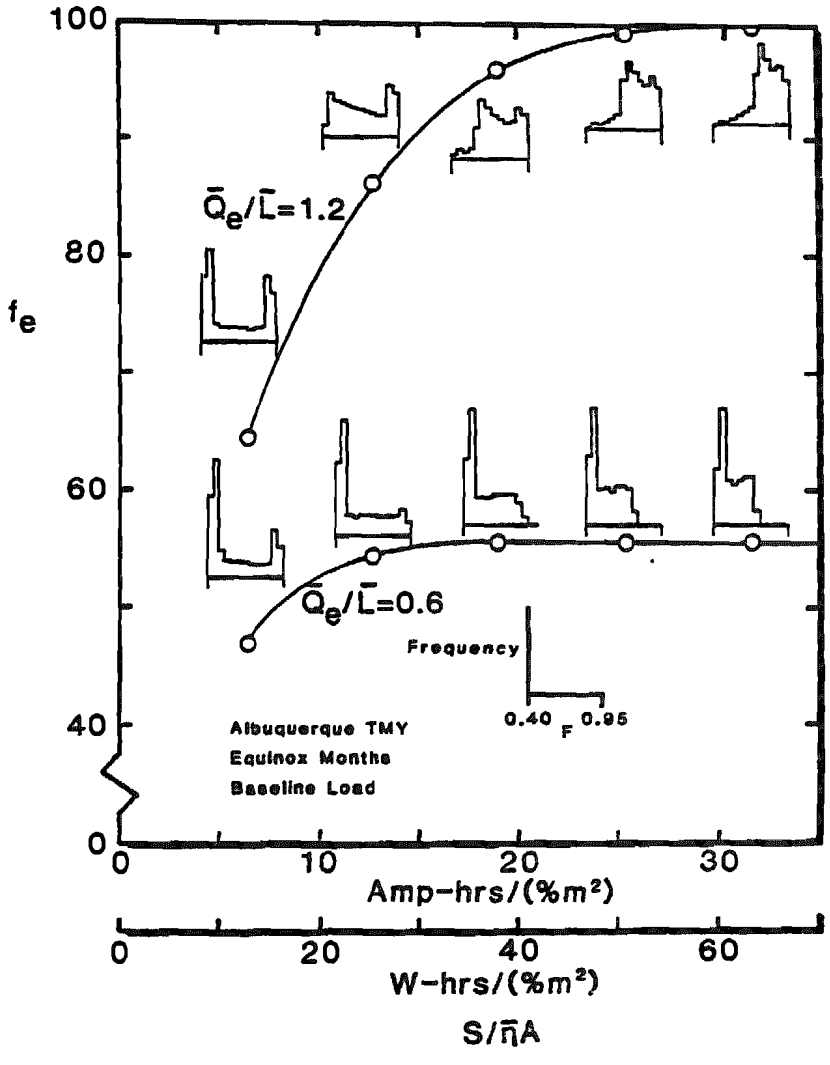

Figure 2.4 Storage Battery Utilization for Various Size Systems F = Fractional State of Charge of Battery.

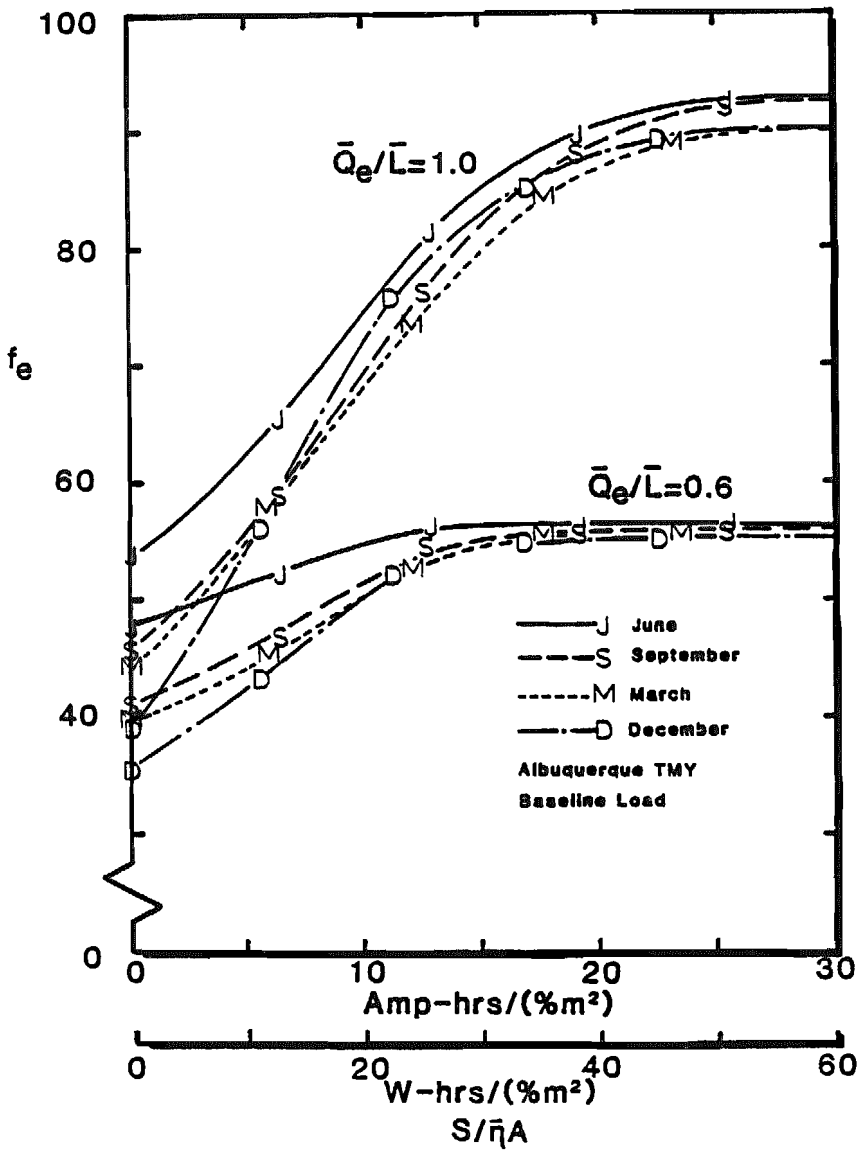

Figure 2.5 Seasonal Variation in System Performance.

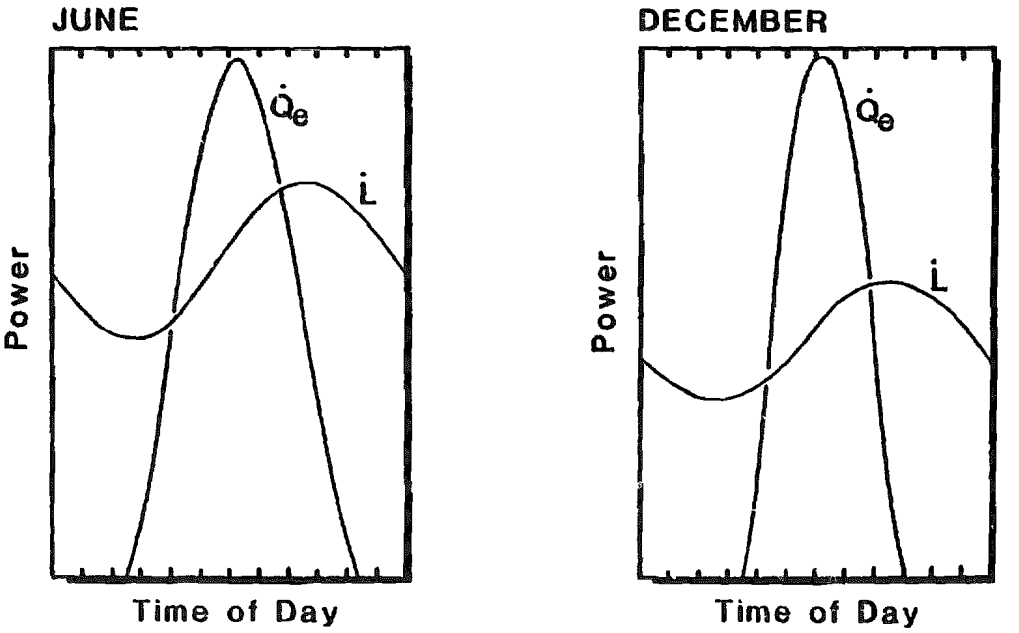

Figure 2.6. Seasonal Differences Between Daily Load Shape and Insolation Profiles for the Same $\bar{Q}_e/\bar{L}$. Curves are Normalized to the Maximum $\dot{Q}_e$ Each Month.

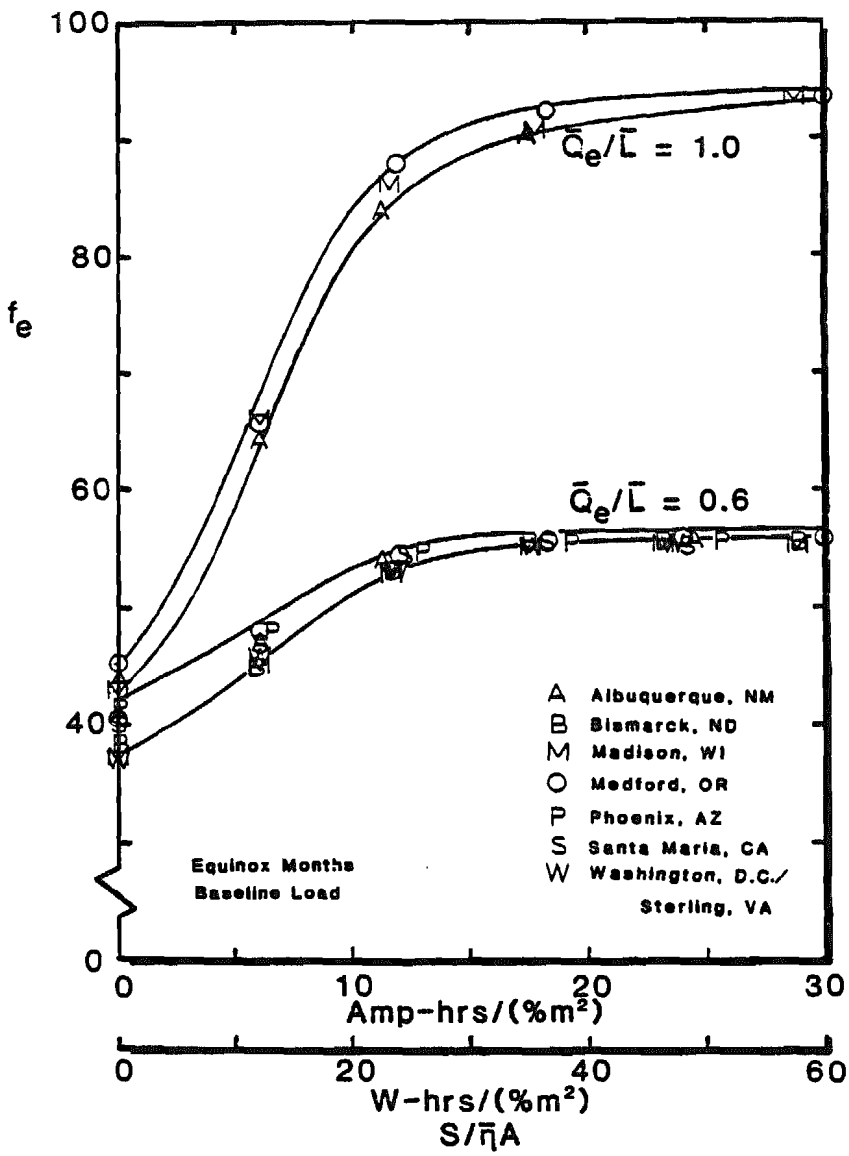

Figure 2.7 Effect of Location on Weather Patterns.

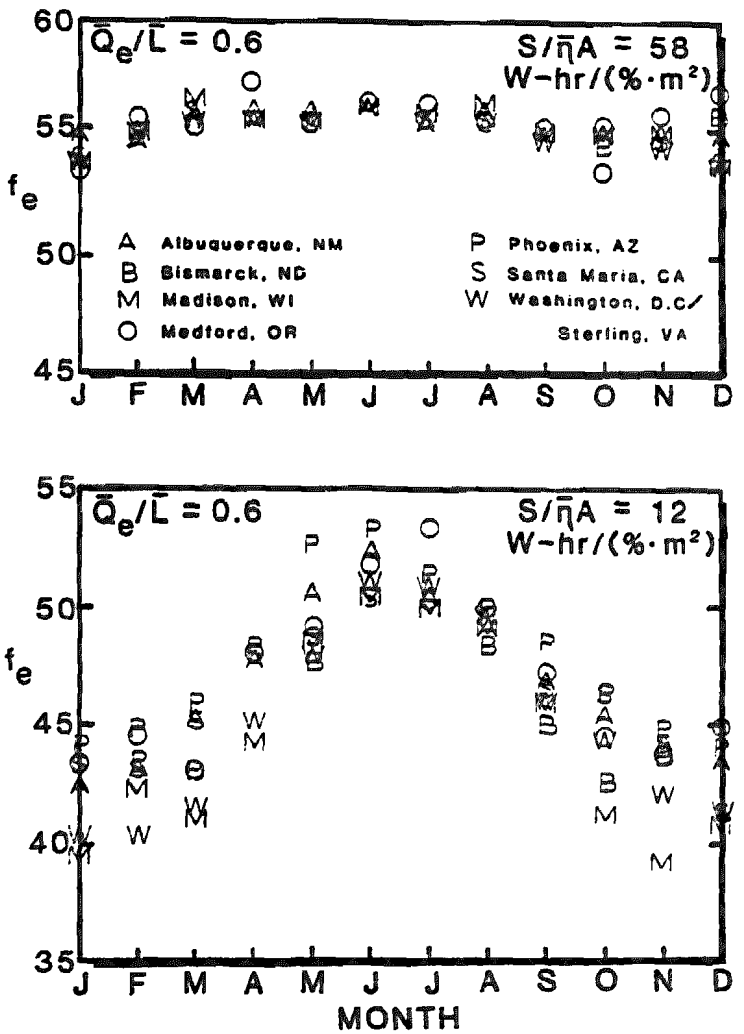

Figure 2.8 Combined Effect of Seasonal Variations and Local Weather Patterns.

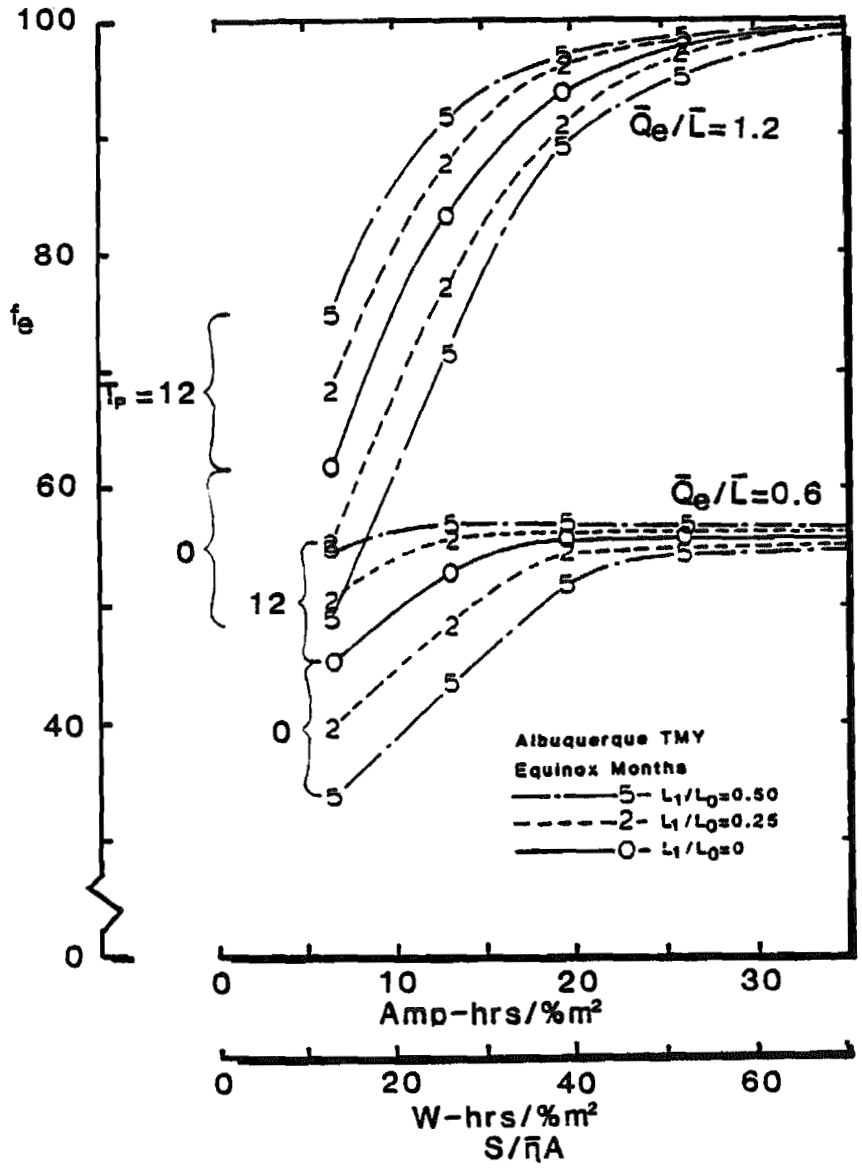

Figure 2.9 Effect of Load Shape on System Performance.

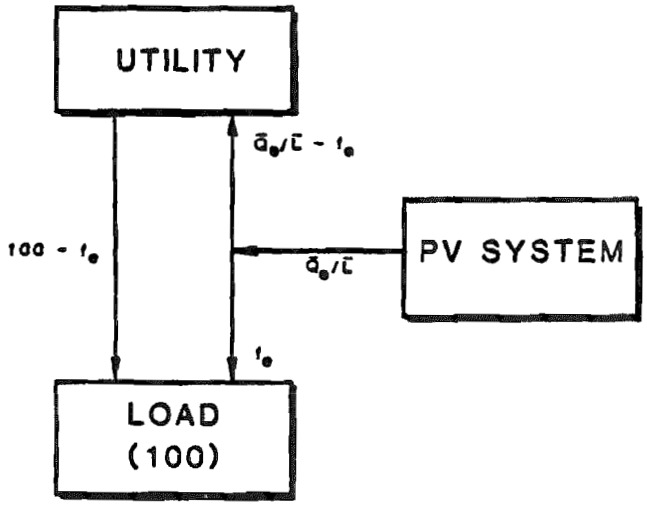

Figure 2.10 Energy Flow Diagram for Utility-Feedback.

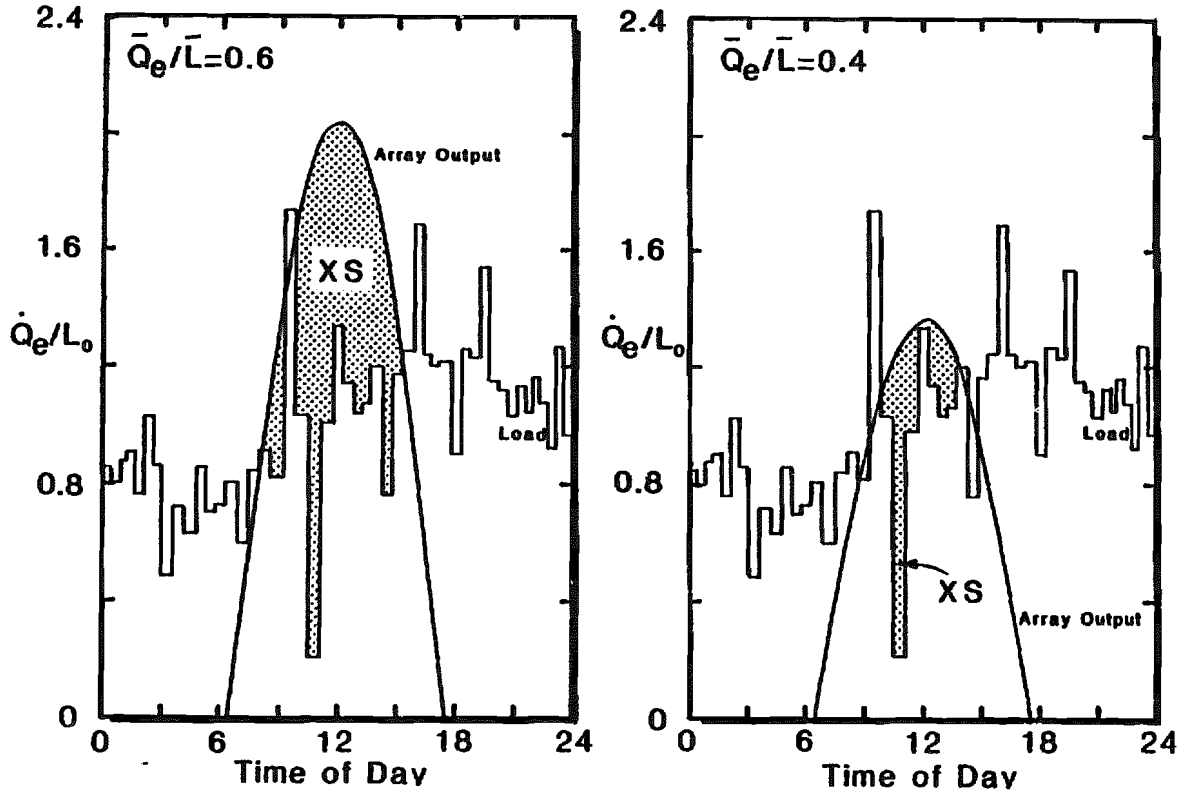

Figure 2.11 Typical Daily Interactions Between Array Output and Fluctuating Load for $\bar{Q}_e/\bar{L}$ = 0.6 and $\bar{Q}_e/\bar{L}$ = 0.4.

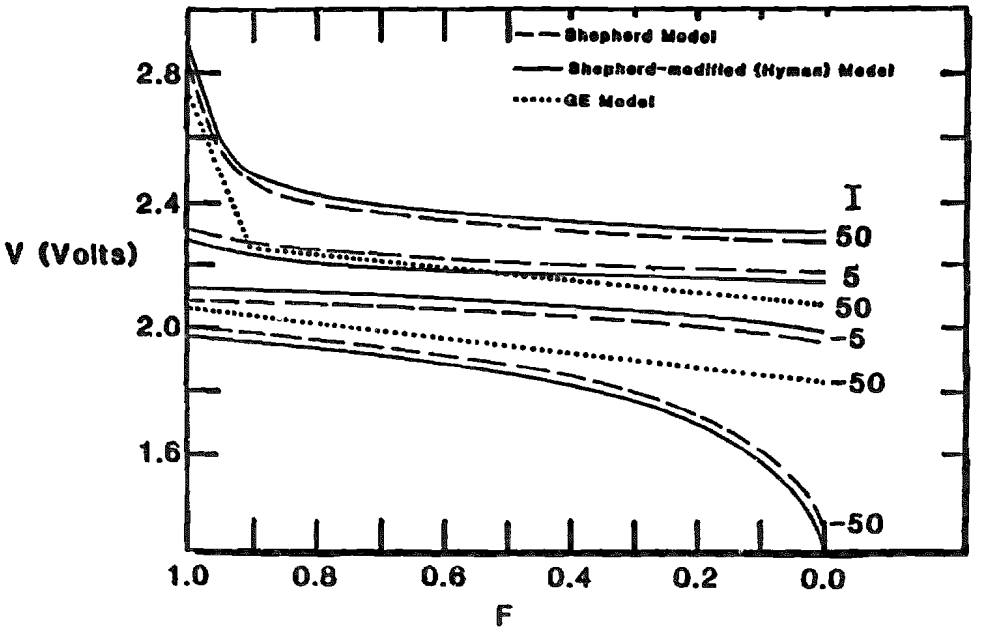

Figure 2.12 Charge (I > 0) and Discharge (I < 0) Characteristics of Three Models for a Lead-Acid Battery Cell of 250 Amp-hr Capacity.

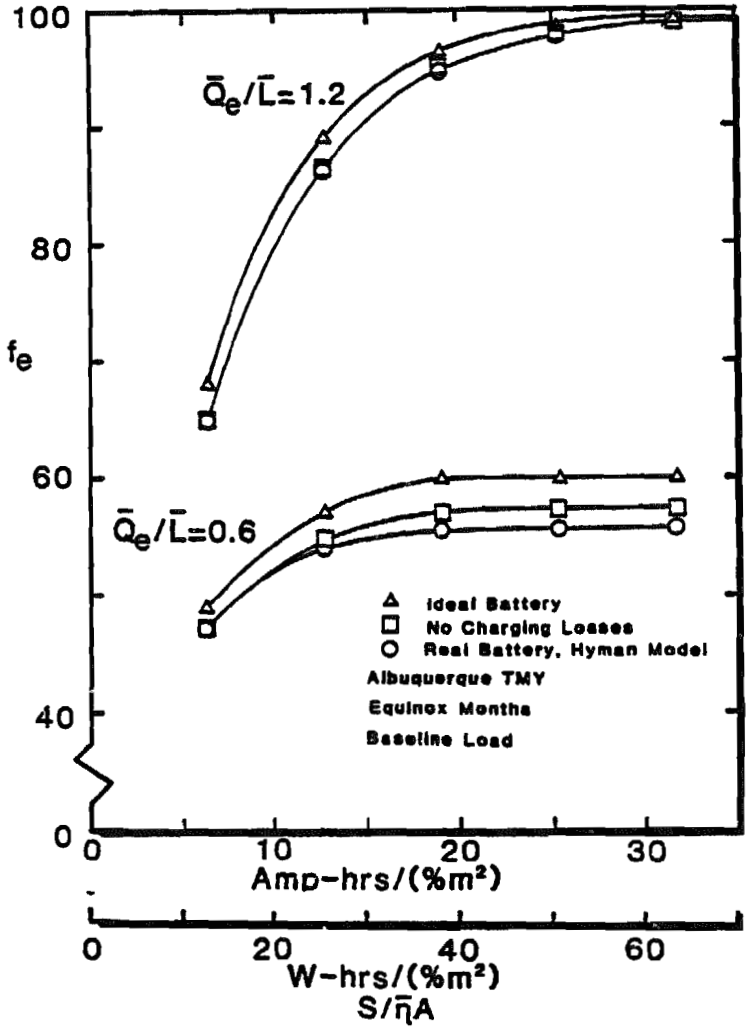

Figure 2.13 Effect of Battery "Voltage Difference" and Charging Losses on System Performance.

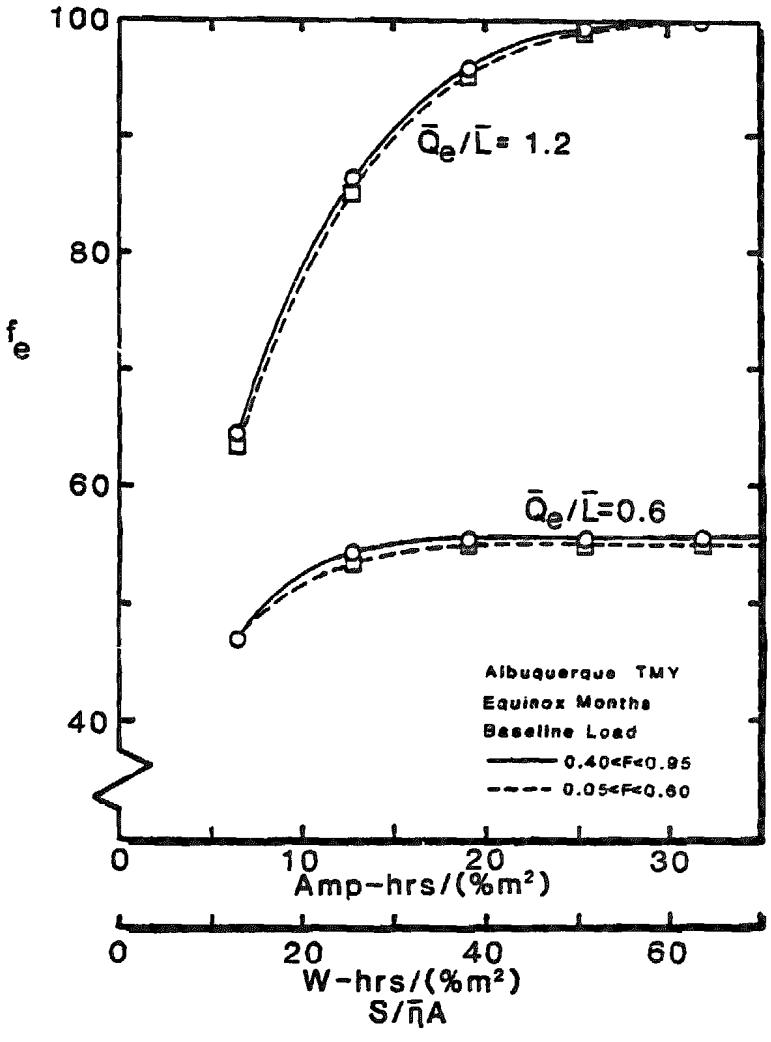

Figure 2.14 Effect of Different Ranges of Battery State of Charge.

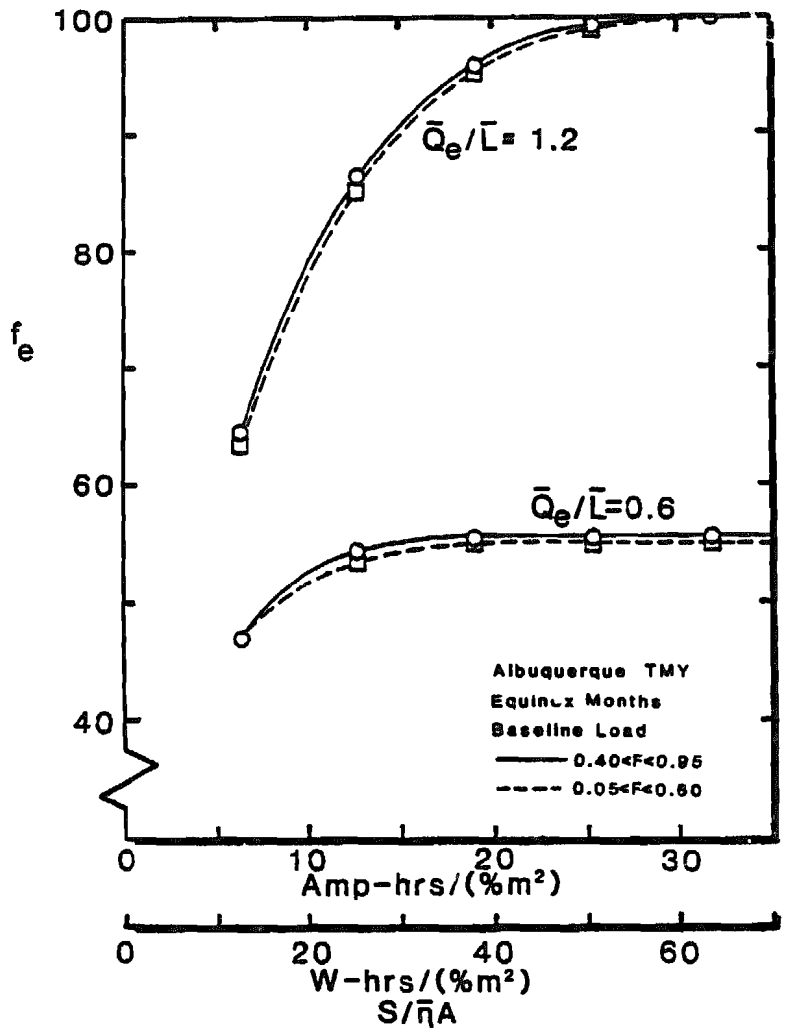

Figure 2.14 Effect of Different Ranges of Battery State of Charge.

3.0 PREDICTING ARRAY OUTPUT

3.1 The Assumptions

In photovoltaic system design it is necessary to predict the output of a given solar cell array under various conditions. As shown in Chapter 2, if the output is small enough and coincides timewise with the load to be met, the solar contribution to the load can often be easily estimated from the calculated array output. If the output is large and/or does not coincide timewise with the load, then predicting the solar contribution to the load is not as easy since not all of the array output may be used. However, in this case, the calculation of array output is desirable since it may play an important role in correlating system performance results.

The present chapter is devoted to a simplified procedure for calculating array output starting with a minimum of input information. The time periods of interest are monthly intervals since there exists a rather good data base on weather and insolation for such periods.

The analysis and results that follow strictly apply to only passively cooled arrays since these types of systems are most strongly tied to ambient weather conditions. The results may, with care, be useful for actively cooled arrays where the heat sink for the thermal energy deposited in the array is ultimately the ambient outdoor weather although this has not been studied extensively. The results definitely do not apply to combined systems that make use of the thermal energy, since in such systems, cell temperature is often determined by non-weather related conditions.

It is also assumed here that the solar cell arrays are max-power tracked; i.e., the voltage imposed on the array is always such that the electrical power produced is a maximum. This assumption is not quite as restrictive as it first appears since it can be shown (Ref. 3.2) that, under the proper conditions, other modes of operation

can produce nearly the same amount of energy as max-power tracked arrays do over some common period of time. For example, arrays that operate in a battery clamped mode (i.e., the battery voltage determines the array voltage) may operate on a nearly comparable basis with max-power tracked systems if the ratio of solar cells to battery cells is properly chosen (see Chapter 5).

The approach adopted here is to find a mean monthly array efficiency that when multiplied by the mean monthly solar irradiation of the array, yields essentially the same electrical energy production as the integration of the instantaneous outputs over the month. This latter quantity can be obtained by use of a sophisticated computer simulation program, but this in itself is not regarded as a simplified technique. It is used here only as an artifice in the determination of the mean monthly array efficiency.

The mean monthly solar irradiation on the array has, of course, been the subject of much work, particularly in the solar thermal field. There are several accepted methods for estimating its value; these will be referenced later in this chapter.

3.2 The Analysis

In terms of the instantaneous solar irradiation, $\dot{Q}_s(t)$ on a photovoltaic array, the monthly average daily array electrical output energy, $\bar{Q}_{ae}$, is given by

$$\bar{Q}_{ae} = A \int \eta \ \dot{Q}_s(t) \ dt/N_d \qquad (3.1)$$

where η is the instantaneous array efficiency and the integration is carried out over monthly periods. $\bar{Q}_e$, the electrical energy potentially available to the load introduced in Chapter 2, is related to $\bar{Q}_{ae}$ by:

$$\bar{Q}_e = \eta_{pc} \bar{Q}_{ae} \qquad (3.2)$$

where η_{pc} is the ''straight through'' power conditioning efficiency of the system.

Instantaneous insolation data required in eq. (2.1) is very seldom available. Many times hourly data are the best which are available; i.e. instantaneous insolation data integrated over one hour time intervals. If the insolation for hour i, defined as $Q_{s,i}$, is given by

$$\bar{Q}_{s,i} = \int_i \dot{Q}_s \, dt \tag{3.3}$$

where the integration is over the i^{th} hour, then eq. (3.1) can be approximated by

$$\bar{Q}_{ae} = A \sum \eta_i \, Q_{s,i} / N_d \tag{3.4}$$

Here the summation goes over all hourly intervals in the month and η_i is the ''hourly'' efficiency. Equation (3.4) is an approximation to eq. (3.1) since it is impossible to reconstruct the instantaneous insolation from the hourly insolation. Hence, it is impossible to tell what fraction of each hour was characterized by ''high'' insolation (and thus lower efficiency due to the higher temperature of the array) and what part by ''low'' insolation (and thus a lower efficiency). Although this has not been explored in detail, the difference between eqs. (3.1) and (3.4) should be small for low concentration ratio collectors (e.g. flat plate arrays). This difference undoubtedly increases with concentration.

The array efficiencies η and η_i, for max-power operation, are functions of array (and cell) design, cell temperature and array irradiation. Array design is typically characterized by stating a reference efficiency η_r, for the array when the cell temperature is at a reference T_r (often 28C), and array illumination is at some reference level $Q_{s,r}$ (often assumed to be 1 kW/m² or one sun). For the purposes of this work η_i will be assumed to be related to

cell temperature, $T_{c,i}$, and array insolation, $Q_{s,i}$ (in kW/m²), through (Ref. 3.1)

$$\eta_i = \eta_r [1 - \beta (T_{c,i} - T_r) + \gamma \log_{10} Q_{s,i}] \quad (3.5)$$

Here β and γ are primarily cell material dependent coefficients that relate most closely to the open circuit voltage behavior of the cells (and thus to the max-power voltage). Equation (3.5) generally ignores the dependence of the max-power current on cell temperature, an effect which is often small. Most often this equation is seen without the last term ($\gamma = 0$) (e.g. Ref. 3.2) although it can be important in low insolation locations. In high irradiation situations, such as in concentrator systems, where series resistance effects become important, the insolation dependent term in eq. (2.4) does not provide the proper behavior especially above the irradiation levels that produce the maximum efficiency (Ref. 3.3).

Thus, to the accuracy that most insolation data are known, the monthly average daily array electrical energy production for max-power operation is given by

$$\bar{Q}_{ae} = A \sum \eta_i Q_{s,i}/N_d$$

$$= A \sum \eta_r [1 - \beta (T_{c,i} - T_r) + \gamma \log_{10} Q_{s,i}] Q_{s,i}/N_d \quad (3.6)$$

where the summations go over all the hours of the month. Adding and subtracting the hourly ambient (dry bulb) temperature $T_{a,i}$, and the mean monthly temperature T_M, to the terms in parentheses and recollecting yields:

$$\bar{Q}_{ae} = (\eta_r A/N_d)[\sum Q_{s,i} - \beta \sum (T_{c,i} - T_{a,i}) Q_{s,i}$$

$$- \beta \sum (T_{a,i} - T_M) Q_{s,i} - \beta (T_M - T_r) \sum Q_{s,i}$$

$$+ \gamma \sum Q_{s,i} \log_{10} Q_{s,i}] \quad (3.7)$$

The use of eq. (3.6) in any simplified design procedure is, of course, inappropriate because of the occurrence of the hourly quantities, $T_{a,i}$, $T_{c,i}$, and $Q_{s,i}$. From a simplified standpoint, it would be preferable to calculate Q_{ae} from:

$$\bar{Q}_{ae} = \bar{\eta} A \Sigma Q_{s,i}/N_d \tag{3.8}$$

where $\bar{\eta}$ is a monthly average conversion efficiency and the summation is just the monthly average daily insolation on the array. This latter quantity can be estimated from procedures commonly used in solar thermal related work.

An expression similar to eq. (3.5) can be used to represent $\bar{\eta}$:

$$\begin{aligned}\bar{\eta} &= \overline{\eta_r [1 - \beta(T_c - T_r) + \gamma \log_{10} Q_s]} \\ &= \eta_r \overline{[1 - \beta(T_c - T_r) + \gamma \log_{10} Q_s]} \\ &= \eta_r [1 - \beta\overline{(T_c - T_r)} + \gamma \overline{\log_{10} Q_s}]\end{aligned} \tag{3.9}$$

where the terms now lacking an i subscript are left to be defined. With this, eq. (3.8) becomes

$$Q_{ae} = \eta_r A [1 - \beta \overline{(T_c - T_r)} + \gamma \overline{\log_{10} Q_s}] \Sigma Q_{s,i}/N_d \tag{3.10}$$

Adding and subtracting T_a and the mean monthly temperature T_M to eq. (3.10) yields

$$\begin{aligned}Q_{ae} = (\eta_r A/N_d)[&\Sigma Q_{s,i} - \beta \overline{(T_c - T_a)} \Sigma Q_{s,i} - \beta \overline{(T_a - T_M)} \Sigma Q_{s,i} \\ &- \beta (T_M - T_r) \Sigma Q_{s,i} + \gamma \log_{10} Q_s \Sigma Q_{s,i}]\end{aligned} \tag{3.11}$$

where it has been noted that

$$\overline{(T_M - T_r)} = (T_M - T_r) \tag{3.12}$$

Comparison of eqs. (3.7) and (3.11) shows that they yield the same result for Q_{ae} if[1]

$$\overline{(T_c - T_a)} \sum Q_{s,i} = \sum (T_{c,i} - T_{a,i})\, Q_{s,i} \tag{3.13}$$

$$\overline{(T_a - T_M)} \sum Q_{s,i} = \sum (T_{a,i} - T_M)\, Q_{s,i} \tag{3.14}$$

$$\overline{\log_{10} Q_s} \sum Q_{s,i} = \sum Q_{s,i} \log_{10} Q_{s,i} \tag{3.15}$$

These three equations serve to define the quantities $\overline{(T_c - T_a)}$, $\overline{(T_a - T_M)}$, and $\overline{\log_{10} Q_s}$.

3.2.1 The Term $\overline{(T_c - T_a)}$

Intuitively, $\overline{(T_c - T_a)}$ that appears in eq. (3.13) represents the monthly average difference between the cell temperature and the ambient temperature during daylight hours. The $(T_{c,i} - T_{a,i})$ term, to which it is related, should be driven by the relationship between the insolation on the array and the thermal losses from the array to the environment. Indeed, an hourly energy balance on an array yields (see Fig. 3.1).

$$K_e\, (T_{c,i} - T_{a,i}) = Q_{s,i}\, \alpha\rho - Q_{s,i}\, \eta_i \rho \tag{3.16}$$

where the left hand side represents the thermal losses from the cells to the surroundings, the first term on the right hand side represents the energy absorbed from the solar irradiation and the second term on the right hand side is the electrical energy produced by the array. K_e is the thermal conductance (per aperture area) for heat transfer from the cells to the surroundings (Ref. 3.4) and is a complicated function of array design, ambient temperature, local wind conditions,

---

[1]The choices made in eqs. (3.13), (3.14) and (3.15) are not unique but they seem to be natural in that they will allow reasonable physical interpretation

and geometry. Since a designer usually has little information on which extensive calculations can be based, it will be assumed that an adequate average value of K_e can be defined.

Fortunately, η_i is usually small in comparison to α in eq. (3.16); therefore, the second term on the right hand side will be neglected in the analysis that follows. An iterative procedure for correcting for non-negligible η_i will be shown later.

Thus, eq. (3.16) yields

$$(T_{c,i} - T_{a,i}) = \alpha\rho\, Q_{s,i}/K_e \tag{3.17}$$

Using this in eq. (3.13) yields

$$\overline{(T_c - T_a)} = \Sigma\, [Q_{s,i}{}^2 \alpha\rho\, /K_e]/\Sigma\, Q_{s,i} \tag{3.18}$$

or

$$K_e\, (T_c - \overline{T_a})/\alpha\rho = \Sigma\, Q_{s,i}{}^2/\, \Sigma\, Q_{s,i} \tag{3.19}$$

The quantity $K_e(T_c - T_a)/(\alpha\rho)$ was computed monthly using eq. (3.19) for seven widely varying climatic locations in the United States for which SOLMET (Ref. 3.5) data were available. The locations and number of years of data used are shown in Table 3.1.

The SOLMET data used consisted of the hourly standard year corrected total radiation on the horizontal (TH) and the direct normal (DN) or beam radiation. For flat arrays, optimum tilts chosen for each month were used. Each hour the DN contribution to the TH was removed from the latter in order to recover the diffuse component on the horizontal (DH). DH was then adjusted to yield diffuse radiation on the tilt (DT) by multiplying DH by $(1 + \cos s)/2$, which assumes a uniform sky. DT was then combined with the ground reflected radiation (a ground reflectance of 0.2 was used) and the appropriate DN component on the tilt to yield total radiation (TT) on the tilt.

The quantity $K_e\overline{(T_c - T_a)}/(\alpha\rho)$ was also calculated for concentrating collectors assuming they were capable of two-dimensional

(2-D) tracking. For this type of tracking, $Q_{s,i}$ was just the DN radiation from the SOLMET data.

For each location, a long term average $K_e\overline{(T_c - T_a)}/(\alpha\rho)$ was then computed for each month from the multiple years of data. Various correlations relating these quantities to other long term average weather and solar data were attempted. The simplest and most effective correlation that was discovered is shown in Fig. 3.2, which relates long term $K_e\overline{(T_c - T_a)}/(\alpha\rho)$ to the long term average $\bar{K}_T$, the ratio of TH to the value of TH in the absence of the atmosphere (the extraterrestrial radiation) (Ref. 3.6). Long term $\bar{K}_T$'s were also obtained from the SOLMET data. Each data point shown in Fig. 3.2 represents the average of at least 16 years of SOLMET data and in most cases, 22 years.

Presumably a good correlation of $K_e\overline{(T_c - T_a)}/(\alpha\rho)$ with the ratio of TT to the extraterrestrial radiation on the tilt would also exist. However, if any radiation data exist for a site, it is usually either TH or the ratio $\bar{K}_T$. Therefore, it is much more convenient from a designer's standpoint to use $\bar{K}_T$ than any other ratio.

TH by itself is not a good correlation parameter since it involves daylength. For example, in the summer months when the days are long, a region of cloudy weather and relatively low average hourly insolation might have as much average daily radiation as a less cloudy period in the winter (shorter days) having higher average hourly insolation. The cell temperature rise above ambient [to which $\overline{(T_c - T_a)}$ is related] would be larger in the winter than in the summer for this hypothetical example. Dividing the total radiation by the extraterrestrial radiation, as is done in obtaining $\bar{K}_T$, normalizes out the daylength and allows a more direct comparison of average hourly insolation.

Although only the data for monthly optimum tilted flat arrays are shown in Fig. 3.1, there is little detectable difference in the data

for 2-D tracked concentrators as long as K_e is the thermal conductance based on the aperture area and not the cell or absorber area. Again, this analysis assumes $Q_{s,i}$ is uniformly distributed in time over the hour i. Such would be the case for steady cloud cover. Broken and scattered clouds could cause significant deviations in areas of low $\bar{K}_T$.

That there is little if any difference between the flat array data and the data for concentrators is not too surprising since the quantity $\Sigma Q_{s,i}^2/\Sigma Q_{s,i}$ most heavily weights high insolation periods. Thus, the high incidence angle morning and evening periods for flat plates which are characterized by low irradiation are not important in determining the average monthly efficiency.

The solid line shown in Fig.3.2 is the best fit straight line characterizing the data. It can, with good accuracy, be used to represent the long term behavior of $K_e\overline{(T_c - T_a)}/(\alpha\rho)$. However, a designer often would like to know what variations might be expected from the long term averages. Therefore, two deviations have been considered here. First, the scatter that could be anticipated in the monthly $\bar{K}_T$ at a particular location about the long term average $\bar{K}_T$ for that same month and same location is shown in Fig. 3.3. All months have been included here, independent of the relative size of $\bar{K}_T$. The distribution of the individual monthly $\bar{K}_T$'s about the long term average $\bar{K}_T$ is nearly Gaussian with a standard deviation, σ, of 0.042. If one considered only the months and locations of high $\bar{K}_T$ this distribution would be characterized by a somewhat smaller standard deviation. Likewise, lower $\bar{K}_T$'s would be characterized by somewhat larger standard deviations.

Second, the scatter that would be represented about the straight line shown in Fig. 3.3 if data from every month and every location were shown, is represented in Fig. 3.4. Here A_o and A_1 take on the values of the appropriate coefficients shown in the linear equations on Fig. 3.2. Again, the distribution is nearly Gaussian with a standard deviation as shown (typically 0.043 kW/m^2).

While a designer using flat plates may choose an optimum tilt to maximize energy production for some one month of the year, it may be neither desirable nor necessary to adjust the tilt each month. However, even though the tilt may be non-optimum during many months, a designer may still need to predict array output. Therefore, calculations have been made to determine $K_e\overline{(T_c - T_a)}/(\alpha\rho)$ for non-optimum tilts. The results of these calculations were expressed as a correction factor, C_f, that when multiplied by the $K_e\overline{(T_c - T_a)}/(\alpha\rho)$ for the optimum tilt yields the $K_e\overline{(T_c - T_a)}/(\alpha\rho)$ for non-optimum tilt. Such a multiplicitive factor is possible since, as discussed previously, $K_e\overline{(T_c - T_a)}/(\alpha\rho)$ is most strongly influenced by high insolatin values that occur near midday. Thus, one would expect C_f to be dependent (nearly) on the cosine of the absolute value of the difference between the actual tilt (s) and the monthly optimum tilt (s_M) (both tilts are assumed to be up from horizontal and the arrays are assumed to be south facing).

The optimum tilts were found to be almost totally latitude (ϕ) dependent. They can be calculated from the information found in Table 3.2.

Fig. 3.5 shows data on the correction factor C_f as a function of $(s_M - s)$. The data there are for summer and winter months for Albuquerque, NM and Madison, WI. These two locations have $\bar{K}_T$'s that are at the high and low ends, respectively, of the typical range of $\bar{K}_T$'s found in most locations. Although the data in Fig. 3.5 show a nearly cosine dependence on $(s_M - s)$, the quadratic equation given there fits the data somewhat better.

For some types of design information it may be desirable to be able to predict $\overline{(T_c - T_a)}$ at midday or solar noon. This was evaluated by restricting the summations in eq. (3.19) to just the two hour period centered about solar noon each day. The same cities and years considered previously were used. Figures 3.6a and 3.6b show the long term results as a function of the long term $\bar{K}_T$ as defined previously. Unlike the results shown in Fig. 3.2, there is now a

distinct difference between optimally tilted flat plate results (Fig. 3.6a) and 2-D tracking results (Fig. 3.6b).

3.2.2 The Term $\overline{(T_a - T_M)}$

Next consider the term $\overline{(T_a - T_M)}$ defined by eq. (3.14). This term, in essence, is a measure of the difference between the average temperature during high insolation hours of the day and the mean monthly temperature. Manipulation of eq. (3.4) yields

$$\overline{(T_a - T_M)} = \Sigma\, T_{a,i}\, Q_{s,i} / \Sigma\, Q_{s,i} - T_M \tag{3.20}$$

Typically, daily minimum temperatures are reached between 4 and 5 a.m. and maximum temperatures are reached between 4 and 5 p.m. Therefore, temperatures around 10 to 11 a.m. are usually close to the daily mean temperature. One would expect, then, that $\overline{(T_a - T_M)}$ would be only slightly larger than zero. This indeed is the case as is shown in Fig. 3.7. Here the Typical Meteorological Year (TMY) (Ref. 3.7) data for the seven sites noted previously (see Table 3.1), were used in order to save computation expenses.

For the purposes of this simplified design methodology it is sufficiently accurate to take

$$\overline{(T_a - T_M)} = 3\ C \tag{3.21}$$

3.2.3 The Term $\overline{\log_{10} Q_s}$

Next, eq. (3.16) can be manipulated to give

$$\overline{\log_{10} Q_s} = \Sigma\, Q_{s,i} \log_{10} Q_{s,i} / \Sigma\, Q_{s,i} \tag{3.22}$$

which now serves to define $\overline{\log_{10} Q_s}$. As was done for the term $K_e \overline{(T_c - T_a)}/(\alpha\rho)$, a value of $\overline{\log_{10} Q_s}$ was calculated each month for the locations and number of years shown in Table 3.1. The long term

monthly average values of $\overline{\log_{10} Q_s}$ vs. the long term monthly $\bar{K}_T$ are shown in Fig. 3.8. Also given is a best fit linear equation representing the data displayed and the standard deviation, σ, of all the data (all months for all seven sites) about the linear fit.

The results shown in Fig. 3.8 are for optimally tilted flat arrays although there is little discernible difference for 2-D tracking surfaces. Non-optimumally tilted flat plates pose a problem, however.

Examination of eq. (3.22) shows that values of $Q_{s,i}$ near 0.368 kW/m² most heavily weight the result for $\overline{\log_{10} Q_s}$ since $Q_{s,i} \log_{10} Q_{s,i}$ is a maximum at that value. For flat arrays, such insolation levels occur at time intervals away from solar noon that depend upon latitude, time of year, and radiation patterns. These complications have so far precluded the establishment of a simple correction factor which could convert the results of Fig. 3.8 into more useful results for non-optimum tilts.

3.3 The Use of the Procedure

The task of calculating the monthly electrical energy output from max-power tracked photovoltaic arrays has been reduced to evaluating the terms that appear in the following equations:

$$\bar{\eta} = \eta_r \left[1 - \beta \overline{(T_c - T_a)} - \beta \overline{(T_a - T_M)} - \beta (T_M - T_r) + \gamma \log_{10} Q_s\right] \qquad (3.23a)$$

$$Q_{ae} = \bar{\eta} A \Sigma Q_{s,i}/N_d = \bar{\eta} A \bar{Q}_s \qquad (3.23b)$$

In order to use these equations, a designer must supply:

a) η_r, T_r – these are determined by the array design and should be obtained from the array manufacturer. (See Section 6.5)

b) β, γ - properties that are primarily dependent on the cell composition. These should be obtained, where possible, from the cell manufacturer's data. Values for silicon cells should be close to $\beta = 0.005C^{-1}$, $\gamma = 0.12$. (See Section 6.5)

c) α - This should be obtained, if possible from the manfacturer. Absorptance data for cells are difficult to find; values used in the literature range from 0.8 to 0.96 (Ref. 3.8 through 3.13). Lack of knowledge of the exact value of this parameter can be somewhat compensated for by knowing NOCT as discussed in Section 3.4, below.

d) ρ - this will be determined by the optical elements that may be present between the array and the sun. For flat plates, $\rho = 1$; for concentrators, $\rho < 1$.

e) T_M - the monthly mean temperature can be obtained from weather station data if such a station exists in the vicinity of the installation site. If weather data are taken at all, values of T_M are usually available. Ref. 3.14 contains values for 171 locations in the U.S. and Canada. Ref. 3.15 contains data for 261 sites in the U.S. and Canada. If data on daylight temperatures are available, these should be used for the $(T_a - T_M) + T_M$ that appears in eq. (3.23a).

f) $\bar{K}_T$ - this ratio can be obtained from Ref. 3.14 for 171 locations or Ref. 3.15 for 261 locations

in the U.S. and Canada. For other locations where total radiation data on the horizontal exist, $\bar{K}_T$ can be obtained by dividing it by the extraterrestrial radiation, this latter quantity being an easily calculable amount (See Ref. 3.16).

g) K_e - this depends on the thermal design of the array, the wind speed, wind direction and to a lesser extent on the temperatures of both the array and the ambient. Thus, this parameter is determined by both the array design and the local microclimate. For flat arrays, K_e can be estimated from Nominal Operating Cell Temperature (NOCT) results if they are available. This is discussed in Section 3.4.

h) $\overline{(T_c - T_a)}$ - is obtained from Fig. 3.2, with knowledge of K_e, ρ, and α.

i) $\overline{(T_a - T_M)}$ - = 3°C

j) $\overline{\log_{10} Q_s}$ - is determined from Fig. 3.8.

k) $\Sigma Q_{s,i}/N_d$ - can be determined from procedures established in the solar thermal field (see Ref. 3.14, 3.16) or from tables or charts that exist (Refs. 3.15, 3.16). Further discussion can be found in Section 3.4.

The following example is provided to illustrate the use of this simplified method. Consider a max-power tracked flat array facing south, tilted up from horizontal at the local latitude (s=Ø) in Albuquerque, N.M. Assume K_e = 0.02 kW/(m² C) = 0.88, ρ = 1.0,

$\eta_r = 0.15$ (15%), $T_r = 0C$, $\beta = 0.005C^{-1}$, and $\gamma = 0$. The comparison of the simplified technique with hourly simulation will be made for the TMY month of January ($\bar{K}_T = 0.614$, $T_M = 1.1$ C.) Thus, from Fig. 3.2 for the optimum tilt during a month when $\bar{K}_T = 0.614$,

$$K_e \overline{(T_c - T_a)}/(\alpha\rho)_{opt} = 0.73 \text{ kW/m}^2 \tag{3.24}$$

From Table 3.2, the optimum tilt for January in Albuquerque (latitude, $\phi = 35.05°$) is $s_m = \phi + 29 = 64°$. Therefore,

$$(s_m - s) = 64 - 35.05 = 29°, \tag{3.25}$$

which gives a correction factor from Fig. 3.5 of

$$C_f = 0.90. \tag{3.26}$$

For this non-optimum tilt

$$K_e \overline{(T_c - T_a)}/(\alpha\rho) = 0.90\ (0.73)$$

$$= 0.66 \text{ kW/m}^2 \tag{3.27}$$

For the assumed K_e, ρ, and α

$$\overline{(T_c - T_a)} = (0.66)(0.88)/0.02 = 29°C \tag{3.28}$$

Then eq. (3.23a) yields

$$\bar{\eta} = 0.15\ [1 - 0.005\ (29) - 0.005\ (3) - 0.005\ (1.1-0)]$$

$$= .125 = 12.5\% \tag{3.29}$$

The above result strictly applies only when there is a balance between the solar energy absorbed by the array and the thermal losses to the surroundings; electrical output from the array has been neglected.

For many purposes this efficiency is sufficiently accurate, particularly when compared with the uncertainties that are usually involved in knowing or calculating $\Sigma Q_{s,i}$ for use in eq. (3.23b). However, when a more accurate $\bar{\eta}$ is required, an iterative procedure can be invoked in the following way. First, the above $\bar{\eta}$ (now referred to as $\bar{\eta}_1$ is used as a first approximation to η_i in eq. (3.16). Equation (3.19) then becomes:

$$K_e \overline{(T_c - T_a)}/\rho(\alpha - \bar{\eta}_1) = \Sigma Q_{s,i}^2/\Sigma Q_{s,i} \qquad (3.30)$$

Equation (3.28) becomes

$$\overline{(T_c - T_a)} = 0.66 \quad (0.88 - .125)/0.02 = 25°C \qquad (3.31)$$

and eq. (3.23a) yields:

$$\bar{\eta} = 0.15 \quad [1 - 0.005(25) - 0.005(3) - 0.005(1.1-0)]$$

$$= 0.128 = 12.8\% \qquad (3.32)$$

Increased accuracy gained by further iteration in this manner is usually never warranted.

Simulation using the hourly January TMY data as outlined in Ref. 3.2 yields a monthly average efficiency of 12.6%. Also, using the simplified procedure, twelve monthly calculations weighted with monthly average insolation were used to obtain a yearly efficiency of 11.4%. Hourly simulation showed a yearly efficiency of 11.3%. A month by month comparison is shown in Table 3.3a.

The versatility of the procedure is shown by other results in Table 3.3 for (a) a poorly tilted array in Medford, OR, and (b) a 2-D tracking concentrator in Madison, WI. TMY data were used for these locations. Although monthly discrepancies as large as 5% (relative) may occur, yearly efficiencies are, typically, exceptionally close.

3.4 Problems with the Procedure

One of the largest problems with the simplified method developed in this Chapter is that in order to convert the monthly average efficiencies, $\bar{\eta}$, into electrical energy production, a designer must be able to calculate the monthly solar irradiation of the array. although methods have been developed to do this from a minimum of information, none of the ways is entirely satisfactory.

However, this is not a problem that is unique to this procedure but instead is one that plagues all solar design efforts, including those that make use of hourly simulation. Many of the data bases (Ref. 3.6, 3.14) make use of existing long term data of very questionable quality. Some more recent works (Ref. 3.17, 3.18) make use of data that, in various ways, have been rehabilitated from this same original data base. Although the rehabilitated data are probably superior to the original set, there are still uncertainties about the accuracy.

Figures 3.9, 3.10, 3.11, 3.12, 3.13, 3.14, and 3.15 compare the SOLMET data base derived $\bar{K}_T$'s for all months for the seven sites used at length in this study with the $\bar{K}_T$'s from the early Liu and Jordan work (Ref. 3.6). Generally, good agreement exists for summer months but during the winter the Liu and Jordan values are consistently above the SOLMET average values.

Generally, a designer should use the most accurate data that is available to him. If <u>good</u> measurements are available, they should be used with the realization that they usually represent only short term trends. If a photovoltaic system is to be installed in one of the SOLMET sites, the SOLMET data base is probably the best choice.

Figures 3.16 and 3.17 were prepared for use in preliminary design work or in areas where little or questionable insolation data exist. These are based on SOLMET data for the seven sites used in this work.

These show that there is some correlation between the long term monthly average daily total radiation on the monthly optimum tilt vs $\bar{K}_T$ (Fig. 3.16) and the long term monthly average daily direct normal radiation vs $\bar{K}_T$ (Fig. 3.17). Due to the significant amounts of scatter of these data, these should be used only as last resorts. Daylength differences are of the most significant contributors to this scatter.

Less scatter is inherent in such plots if insolation is averaged for some given hourly period of the day. For example, Figs. 3.18 and 3.19 show long term hourly insolation data averaged during the two hour period around solar noon for the seven SOLMET sites. The data are correlated with the long term average monthly $\bar{K}_T$. Fig. 3.18 displays average midday intensity of the total radiation on the optimum tilt, while Fig. 3.19 is for the midday direct normal intensity. These data are used in the clamped-voltage mode of system operation discussed in Chapter 5.

Another problem confronting the designer is the choice of K_e, the thermal conductance for heat rejection from the cells. As mentioned in the previous section, this problem is compounded since it involves both the array design and the local weather conditions. For flat arrays a link between these two variables is provided by the Nominal Operating Cell Temperature (NOCT) (Ref. 3.19) if the application under study uses the array mounted in a configuration similar to that specified in the NOCT testing. Figure 3.20 shows that an energy balance requires:

$$K_e\ (T_{NOCT} - T_{a,NOCT}) = \alpha Q_{s,r} \quad (kW/m^2) \tag{3.33}$$

where

$Q_{s,r}$ = 1.0 or 0.8 kW/m² (See Table 3.4).

Thus

$$K_e/\alpha = Q_{s,r}/(T_{NOCT} - T_{a,NOCT}) \quad (kW/m^2 \cdot C) \tag{3.34}$$

Traditionally, $T_{a,NOCT} = 20°C$. If monthly wind speeds during daylight hours average near 1 m/s and temperatures average near 20C (the test conditions for NOCT measurements) in the area where an array is to be located, then it would be reasonable to use this ratio in conjunction with Fig. 3.2 to obtain a monthly $\overline{(T_c - T_a)}$. This obviously solves the problem of requiring independent information on α. However, Fig. 3.21 has been prepared to simplify the calculation of $\overline{(T_c - T_a)}$ for such conditions. A designer simply multiplies the ordinate of this figure by $(T_{NOCT} - T_{a,NOCT})$ and by C_f to get $\overline{(T_c - T_a)}$ for his application.

If wind speeds differ from 1 m/s or temperatures differ from 20C, the correction term ΔT shown in Fig. 3.22 can be added to the standard NOCT value of an array to correct it for local conditions. For example, if wind speeds average about 1.5 m/s and ambient temperatures about 32C the NOCT to be used in eq.(3.34) or with Fig. 3.21 should be 3C smaller than the standard NOCT value.

Several uncertainties should be kept in mind when choosing a representative K_e for either flat plates or concentrators. These include uncertainties involved in the prediction of the thermal resistance of the array itself during the design stage (cell placement, thermal contact resistance, voids, cover material, etc.), wind direction, and secondary flow effects created by elements making up the array field.

For concentrators, K_e is often expressed on an absorber area or heat sink area basis. For use in the procedure presented here, K_e has to be based on the aperture area. The concentrator example in Table 3.3 has been specified to have a K_e of 0.01 $kW/(m^2 \cdot C)$ based on aperture area but would have a K_e of 0.2 $kW/(m^2 \cdot C)$ based on absorber area (concentration ratio or aperture to absorber area ratio of 20).

CHAPTER 3 REFERENCES

3.1 ''Photovoltaic Systems Concept Study,'' Report ALO-2748-1, Spectrolab, Inc., Sylmar, CA (1977).

3.2 D.L. Evans and L.W. Florschuetz, ''Cost Studies on Terrestrial Photovoltaic Power Systems with Sunlight Concentration,'' Solar Energy 19, 255 (1977).

3.3 ''Terrestrial Photovoltaic Power Systems with Sunlight Concentration'', Report #ERC-R-77006, Arizona State University, Tempe, AZ (1977).

3.4 L.W. Florschuetz, ''On Heat Rejection from Terrestrial Solar Cell Arrays with Sunlight Concentration,'' Proc. Eleventh IEEE PV Specialists' Conference, Scottsdale, AZ (1975).

3.5 ''SOLMET User's Manual, Hourly Surface Radiation — Surface Meteorological Observations,'' National Oceanic and Atmospheric Administration Environmental Data Service, Asheville, NC (1979).

3.6 B.Y.H. Lin and R.C. Jordan, ''The Long-Term Average Performance of Flat-Plate Solar-Energy Collectors,'' Solar Energy 2, 53 (1963).

3.7 I.J. Hall, R.R. Prairie, H.E. Anderson, and E.C. Boes, ''Generation of a Typical Meteorological Year,'' Proc. 1978 Annual Meet. Amer. Sec. of ISES, Denver, CO (1978).

3.8 R.A. Arndt, J.F. Allison, J.G. Haynos and A. Meulenberg, Jr., ''Optical Properties of the Comsat Non-Reflective Cell,'' Proc. Eleventh IEEE PV Specialists' Conference, Scottsdale, AZ (1975).

3.9 C.R. Baraona and H.W. Brandhorst, ''V-Grooved Silicon Solar Cells,'' Proc. Eleventh IEEE PV Specialists' Conference, Scottsdale, AZ (1975).

3.10 F. Restrepo and C.E. Backus, ''On Black Solar Cells or the Tetrahedral Texturing of a Silicon Surface,'' IEEE Transactions on Electron Devices ED-23, 1193 (1976).

3.11 L.W. Florschuetz, ''Extension of the Hottel-Whillier Model to the Analysis of Combined Photovoltaic/Thermal Flat Plate Collectors,'' Solar Energy 22, 361 (1979). Also see Proc. Sharing the Sun Joint Conference, U.S. and Canadian Sections of International Solar Energy Society, Vol. 6, pg. 79, Winnipeg, (1976).

3.12 L.W. Florschuetz, ''On Heat Rejection from Terrestrial Solar Cell Arrays with Sunlight Concentration,'' Proc. Eleventh IEEE PV Specialists' Conference, Scottsdale, AZ (1975).

3.13 ''Terrestrial Photovoltaic Power Systems with Sunlight Concentration,'' Proc. Eleventh IEEE PV Specialists' Conference, Scottsdale, AZ (1975).

3.14 W.A. Beckman, S.A. Klein, and J.A. duffie, Solar Heating Design, Wiley Interscience, New York, NY (1977).

3.15 S.A. Klein, W.A. Beckman and J.A. Duffie, ''Monthly Average Solar Radiation on Inclined Surfaces for 261 North American Cities'' Report #44, Solar Energy Laboratory, University of Wisconsin, Madison (1978).

3.16 J.A. Duffie and W.A. Beckman, Solar Energy Thermal Processes, John Wiley and Sons, New York, NY (1974).

3.17 W.H. Hoecker, G.F. Cotton and W.A. Hass, ''Solar Radiation and Climate Data for Quasi-Homogeneous Climate Regions of the United States'' Report #ERC ARL-77, Air Resources Laboratories, National Oceanic and Atmospheric Administration, Silver Springs (1979).

3.18 E.C. Boes, H.A. Anderson, I.J. Hall, R.R. Prairie, R.T. Stromberg, ''Availability of Direct, Total and Diffuse Solar Radiation to Fixed and Tracking Collectors in the U.S.A.'' Report #SAND77-0885 (with Addendum), Sandia Laboratories, Albuquerque (1977).

3.19 J.W. Stultz and L.C. Wen, ''Low-Cost Silicon Solar Array Project,'' Report #5101-31, Jet Propulsion Laboratory, Pasadena (1977).

Table 3.1

SOLMET Sites and Years of Data
Used in this Study

Site	Years
Albuquerque, NM	22
Bismarck, ND	22
Madison, WI	22
Medford, OR	22
Phoenix, AZ	22
Santa Maria, CA	16
Washington D.C./Sterling, VA	21

Table 3.2

-Optimum Tilts-

Tilt Angle (s_M) between the Plane of the Flat Array and Horizontal* for Maximum Monthly Average $K_e(\overline{T_c}-\overline{T_a})/(\alpha\rho)$

Month	s_M(Degrees)†
1	ϕ + 29
2	ϕ + 18
3	ϕ + 3
4	ϕ - 10
5	ϕ - 22
6	ϕ - 25
7	ϕ - 24
8	ϕ - 10
9	ϕ - 2
10	ϕ + 10
11	ϕ + 23
12	ϕ + 30

*Array is assumed to be South Facing
†ϕ is Latitude (Degrees)

Table 3.3a

Comparison of
Simplified Procedure for Predicting Array Output
with Hourly Simulation

Location	Albuquerque
Collector	Flat Plate
Concentration Ratio	1
Tilt (Degrees)	35
K_e kW/(m²·C)	0.02
α	0.88
ρ	1
η_r (%)	15
T_r (C)	0
β (C^{-1})	0.005
γ	0

Month	TMY $\bar{K}_T$	TMY T_M (C)	η_{est}† (%)	$\bar{\eta}_{simul}$* (%)
1	0.614	2	12.8	12.6
2	0.654	4	12.4	12.2
3	0.664	7	12.0	11.9
4	0.727	13	11.4	11.3
5	0.739	19	11.1	10.9
6	0.732	23	10.8	10.7
7	0.701	26	10.7	10.4
8	0.707	25	10.6	10.5
9	0.697	20	11.0	10.8
10	0.713	15	11.3	12.2
11	0.679	7	12.2	12.2
12	0.645	3	12.6	12.6
yr.			11.5	11.3

† Estimated by Chapter 3 simplified methods

* Simulated by hourly computer calculations

Table 3.3b

Comparison of
Simplified Procedure for Predicting Array Output
with Hourly Simulation

Location	Madison
Collector	2-D Tracked
Concentration Ratio	20
Tilt (Degrees)	-
K_e kW/(m^2·C)	0.01
α	0.88
ρ	0.88
η_r(%)	15
T_r(C)	C
β(C^{-1})	0.005
γ	0

Month	TMY $\bar{K}_T$	TMY T_M (C)	$\bar{\eta}_{est}$ † (%)	$\bar{\eta}_{simul}$ * (%)
1	0.448	-8	12.4	12.8
2.	0.497	-6	12.0	12.3
3	0.524	-2	11.8	11.4
4	0465	9	11.0	10.8
5	0.494	15	10.4	10.2
6	0.514	20	9.9	10.2
7	0.542	22	9.6	9.8
8	0.558	20	9.7	10.1
9	0.525	17	10.1	10.4
10	0.461	10	10.9	10.8
11	0.393	2	11.9	11.6
12	0.364	-4	12.5	12.2
yr.			11.2	10.8

† Estimated by Chapter 3 simplified methods

* Simulated by hourly computer calculations

Table 3.3c

Comparison of
Simplified Procedure for Predicting Array Output
with Hourly Simulation

Location	Medford
Collector	Flat Plate
Concentration Ratio	1
Tilt (Degrees)	10
K_e kW/(m^2·C)	0.02
α	0.88
ρ	1.0
η_r (%)	15
T_r(C)	0
β(C^{-1})	0.005
γ	0

Month	TMY $\bar{K}_T$	TMY T_M (C)	$\bar{\eta}_{est}$† (%)	$\bar{\eta}_{simul}$* (%)
1	0.331	4	13.7	13.8
2	0.423	5	13.3	13.8
3	0.484	8	12.7	13.1
4	0.532	10	12.3	12.3
5	0.590	13	11.8	11.8
6	0.639	19	11.2	11.1
7	0.715	23	10.7	11.3
8	0.679	22	11.0	11.4
9	0.623	19	11.5	11.7
10	0.513	13	12.3	12.3
11	0.385	7	13.3	13.3
12	0.262	2	14.1	13.9
yr.			11.9	11.7

† Estimated by Chapter 3 simplified methods

* Simulated by hourly computer calculations

Table 3.4

Essence of the NOCT Test Requirements (Ref. 3.19)†

Insolation†	=	0.8 or 1.0 kW/m^2
Ambient Air Temperature	=	20^{o} C
Wind Average Velocity	=	1 m/s, "not predominantly parallel to the array"
Mounting	-	Tilted so that it is normal to the sun ($\pm 5^{o}$) at solar noon with the bottom edge of the array two feet or more above the local ground level.
Electrical Configuration	-	Open Circuit Condition

†Two values of insolation are currently used for NOCT specification. Early work used 0.8 kW/m^2 recommended in Ref. 3.19. Recent work has tended to use 1.0 kW/m^2.

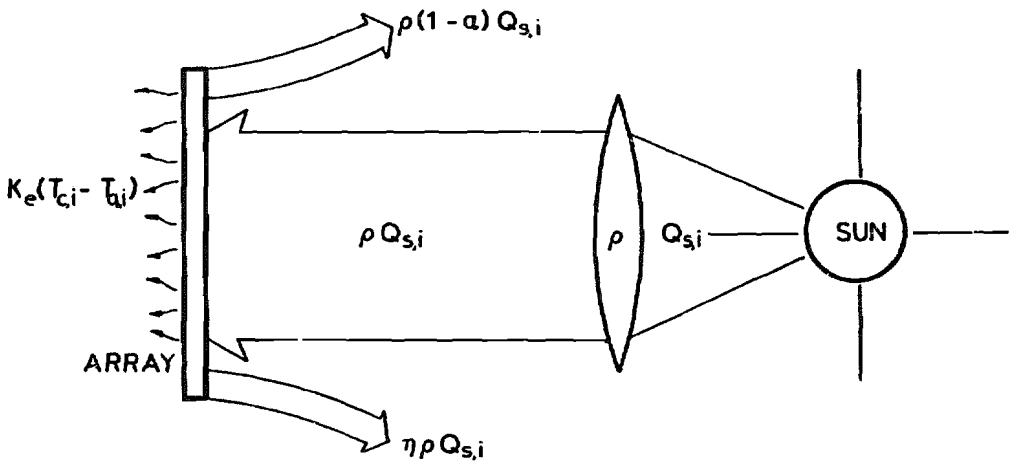

Figure 3.1 Energy Balance Schematic for an Array

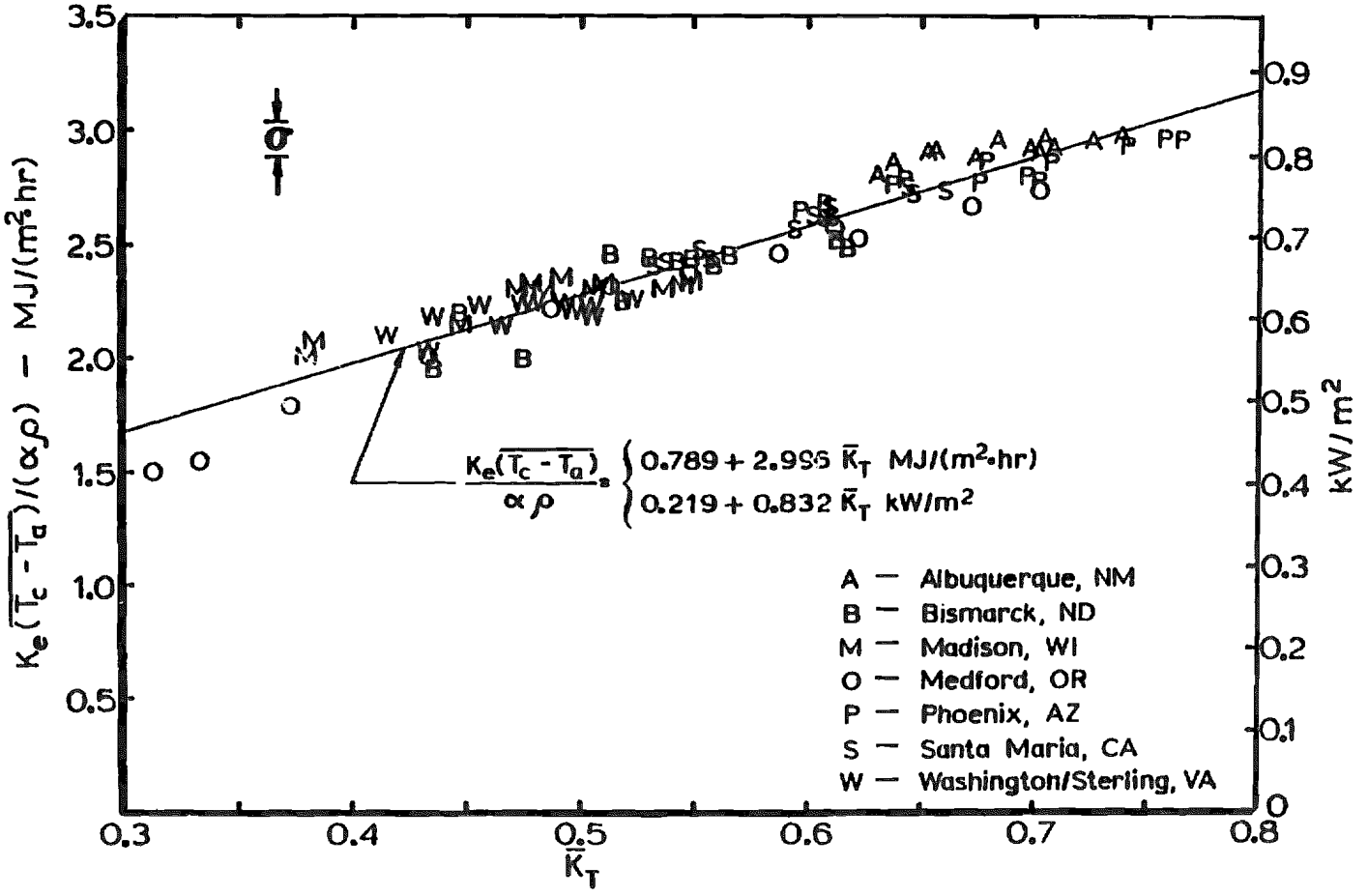

Figure 3.2 Long Term Monthly Results for $K_e\overline{(T_c - T_a)}/(\rho\alpha)$ vs. $\bar{K}_T$.

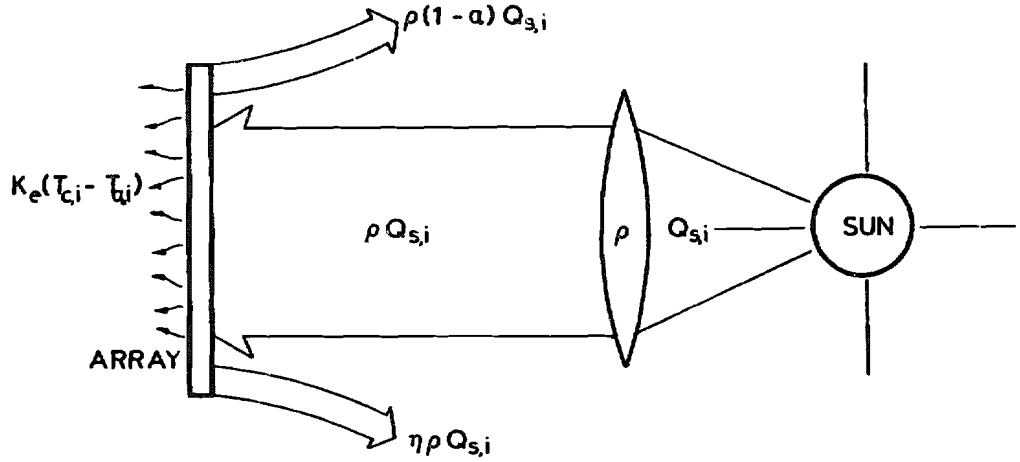

Figure 3.1 Energy Balance Schematic for an Array

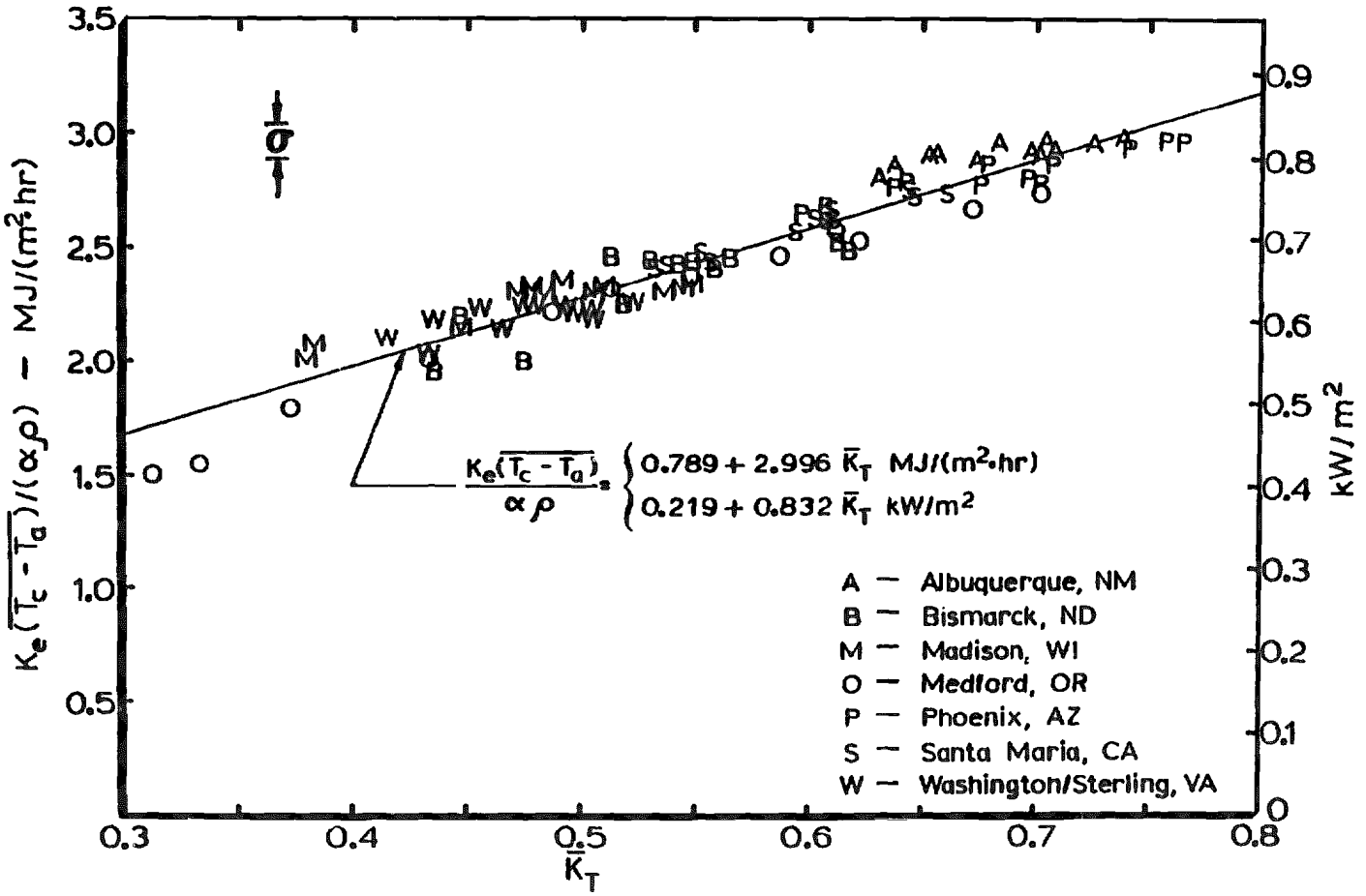

Figure 3.2 Long Term Monthly Results for $K_e(\overline{T_c - T_a})/(\rho\alpha)$ vs. $\bar{K}_T$.

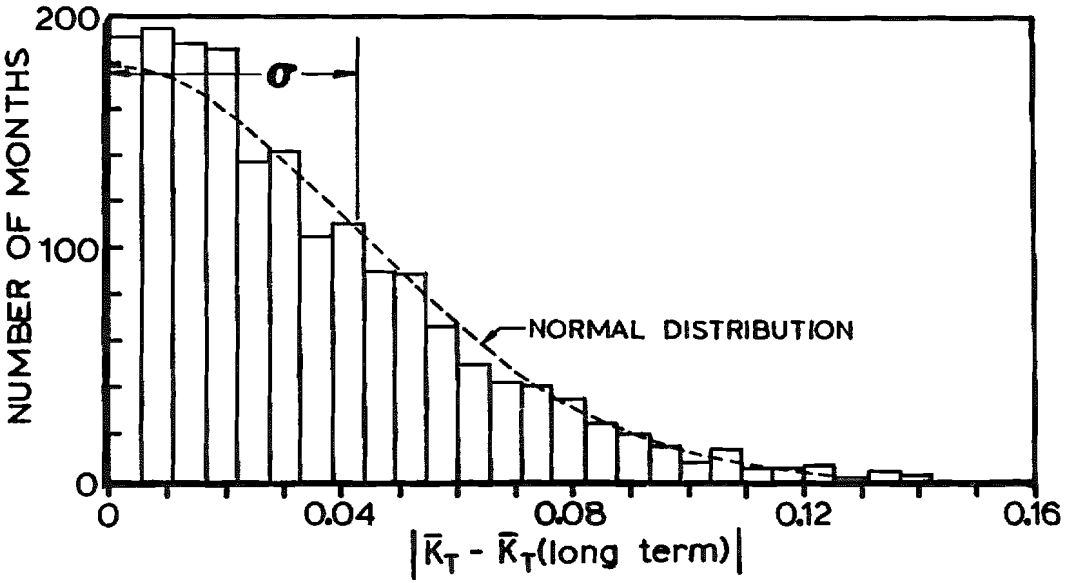

Figure 3.3 Distribution of Individual Monthly $\bar{K}_T$ about the Long Term $\bar{K}_T$ for the Same Month and Location. The Seven Cities Listed in Fig. 3.2 were Used.

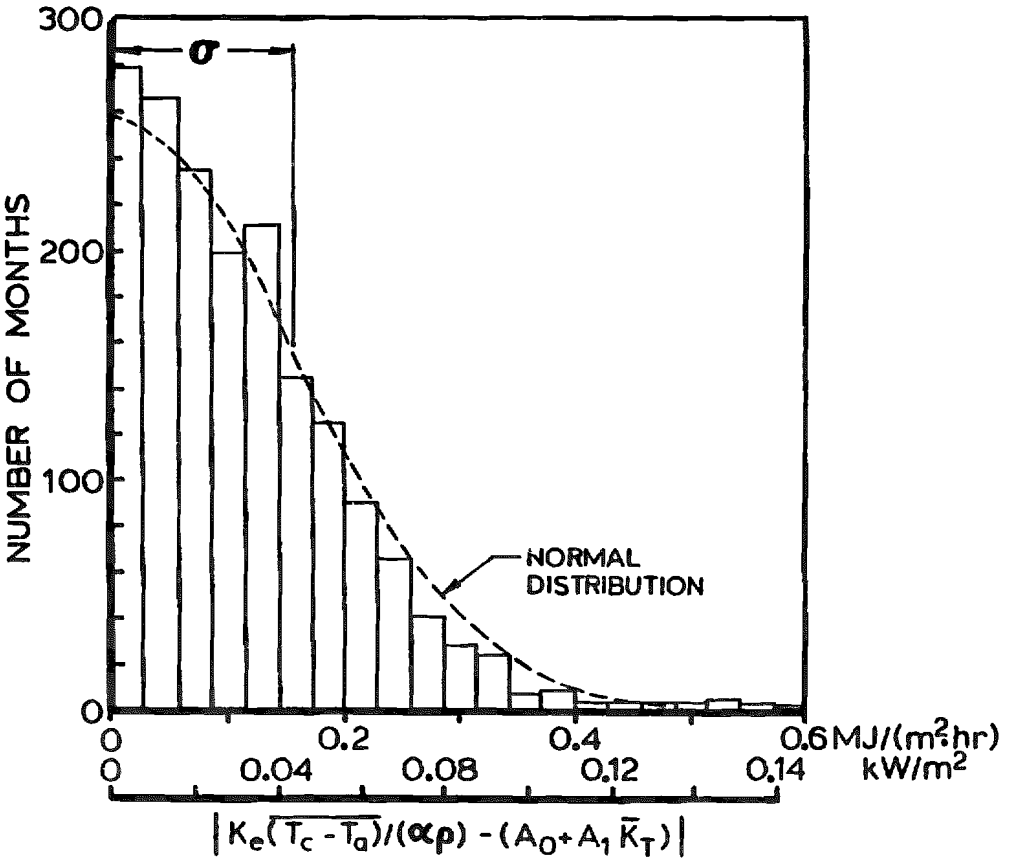

Figure 3.4 Distribution of Individual Monthly $K_e(\overline{T_c} - \overline{T_a})/(\rho\alpha)$ about the Straight Line Fit Shown in Fig. 3.2.

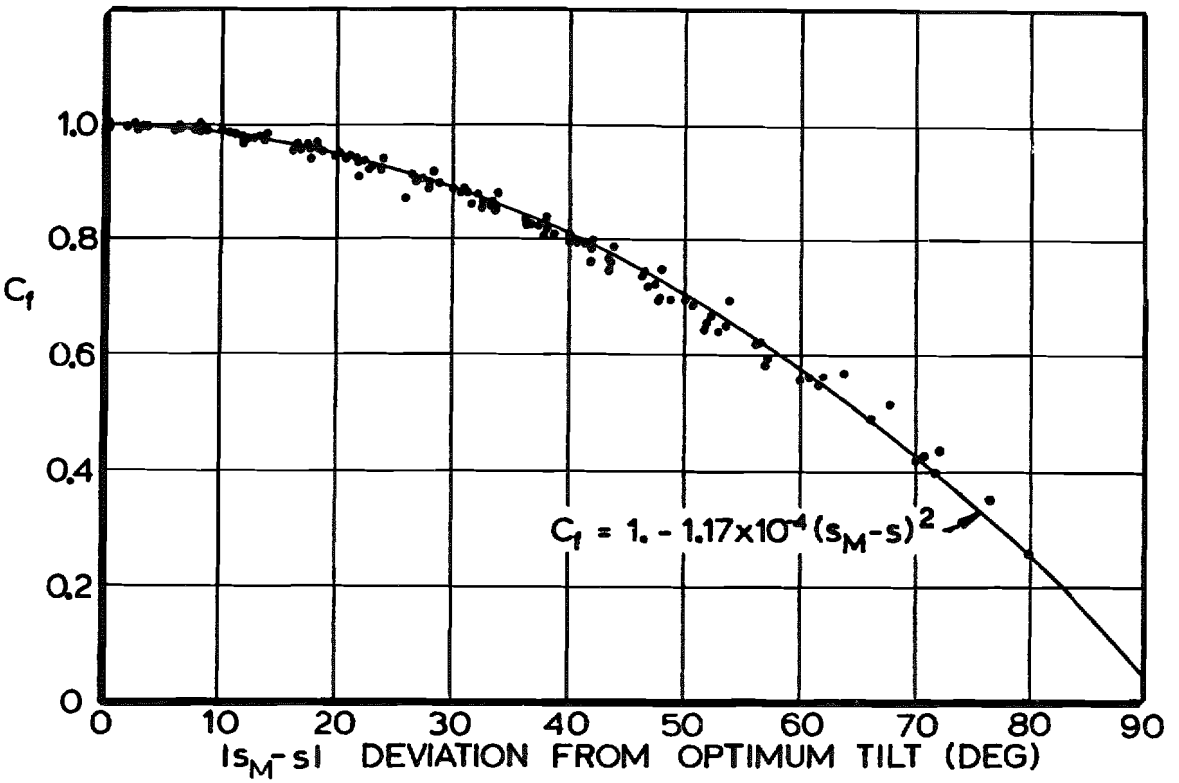

Figure 3.5 Correction Factor for Converting to Non-Optimum Tilts

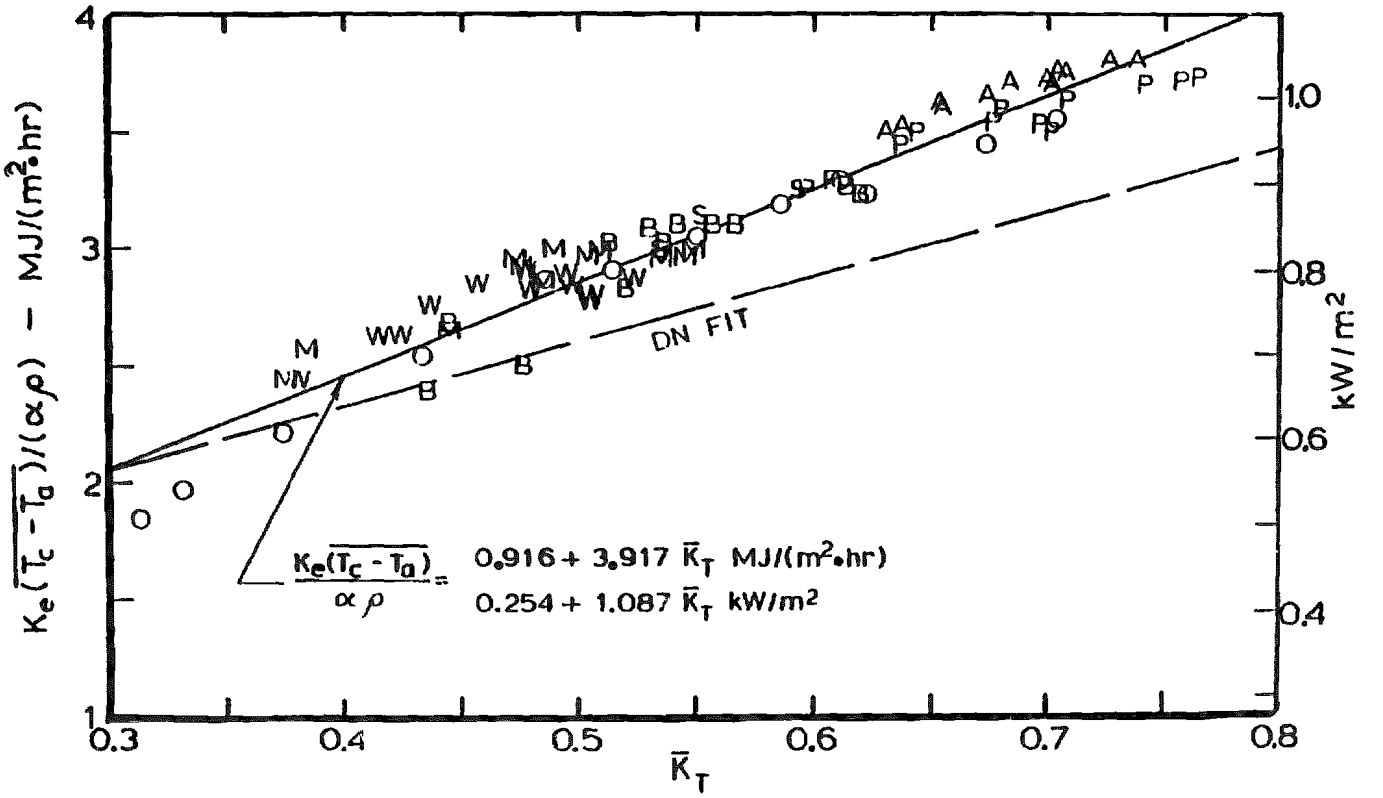

Figure 3.6a Midday Values of $K_e(\overline{T_c - T_a})/(\rho\alpha)$ vs. Long Term Monthly $\bar{K}_T$. These Data are for Total Radiation on the Optimum Tilt. Adjustment to Non-optimum Tilts can be Made by a Cosine Correction. The Direct Normal Data (DN) are Shown in Figure 3.6b. See Fig. 3.2 for Legend.

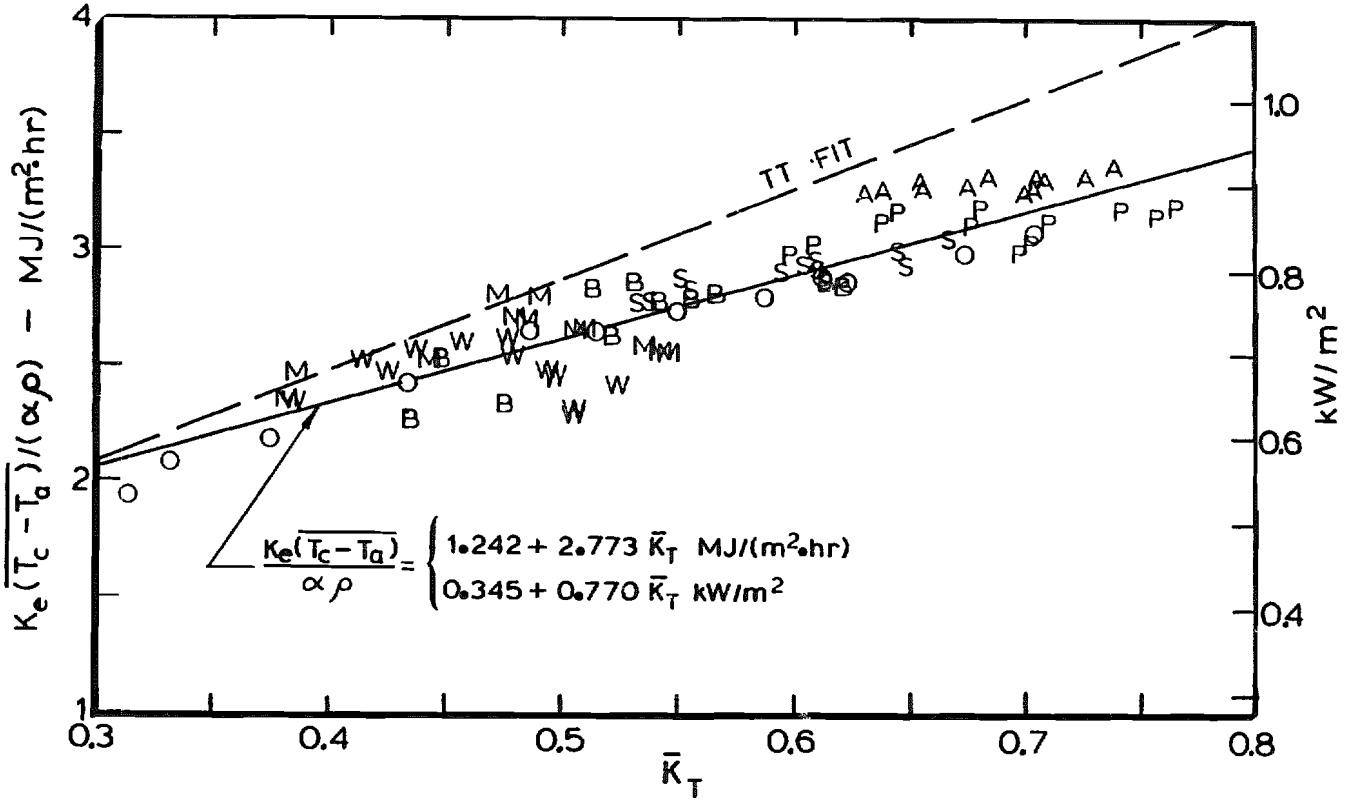

Figure 3.6b Midday Values of $K_e\overline{(T_c - T_a)}/(\rho\alpha)$ vs. Long Term Monthly $\bar{K}_T$. These Data are for Direct Normal Radiation. The Total Radiation on the Tilt (TT) Data are Shown in Fig. 3.6a. See Fig. 3.2 for Legend.

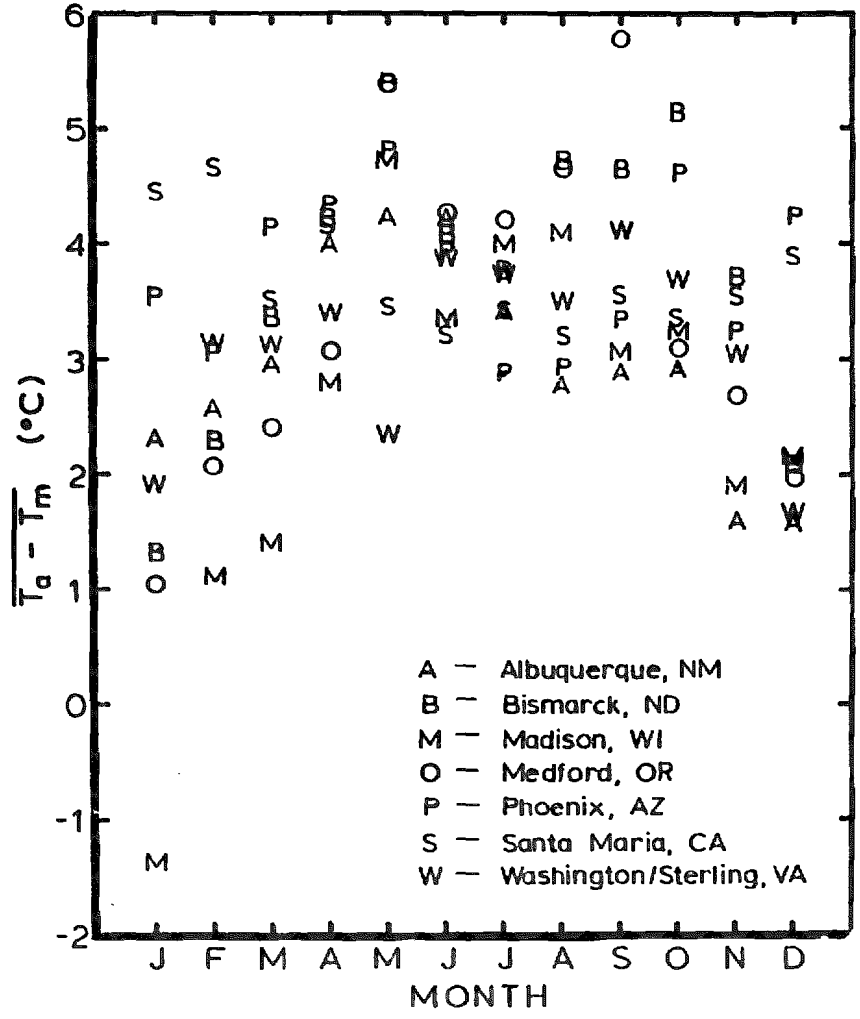

Figure 3.7 TMY Monthly Results for $\overline{(T_a - T_M)}$ for Seven Cities.

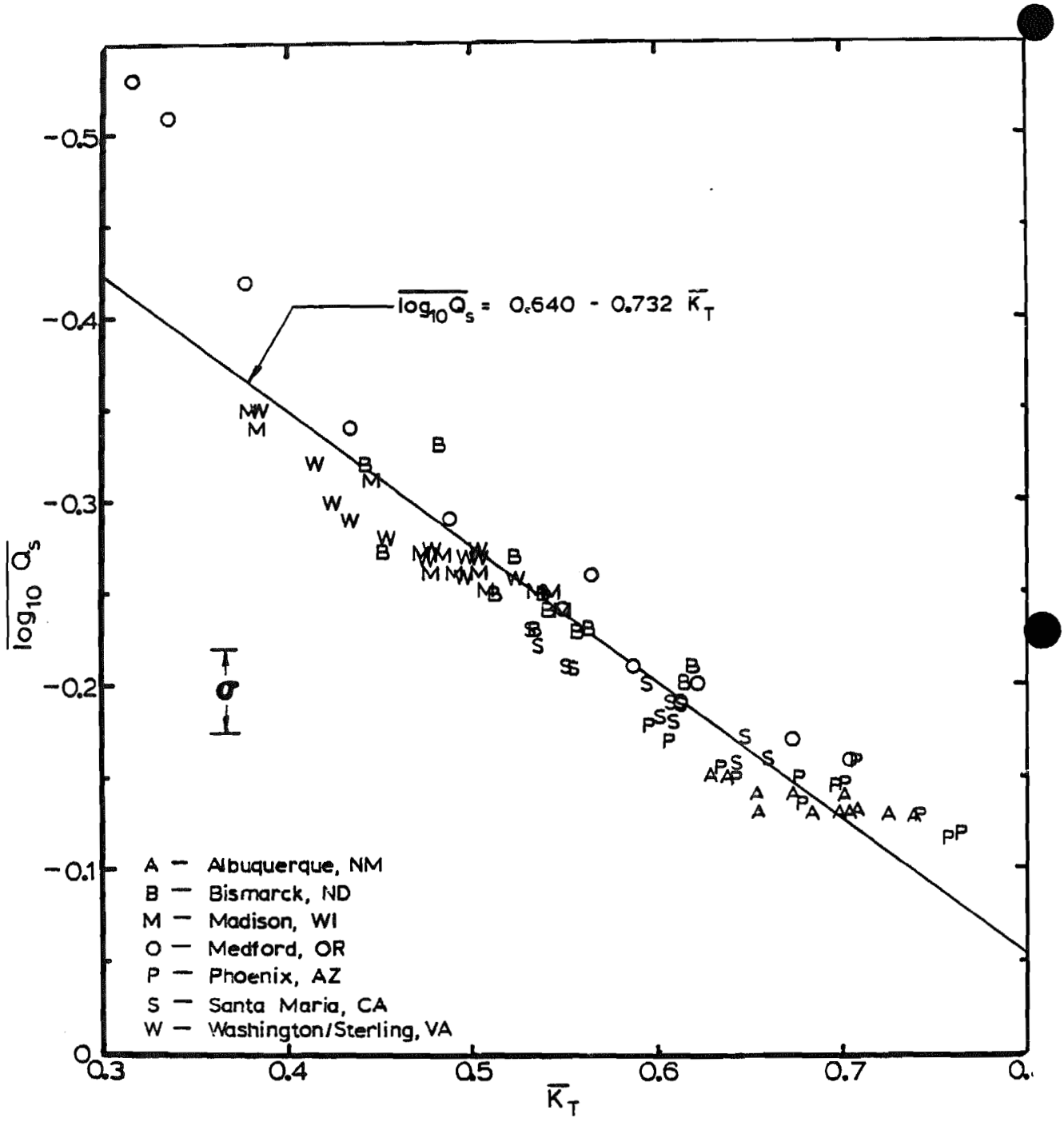

Figure 3.8 Long Term Monthly Results for $\overline{\log_{10} Q_s}$ vs. $\overline{K}_T$ for Seven Cities Using Optimum Tilts Each Month.

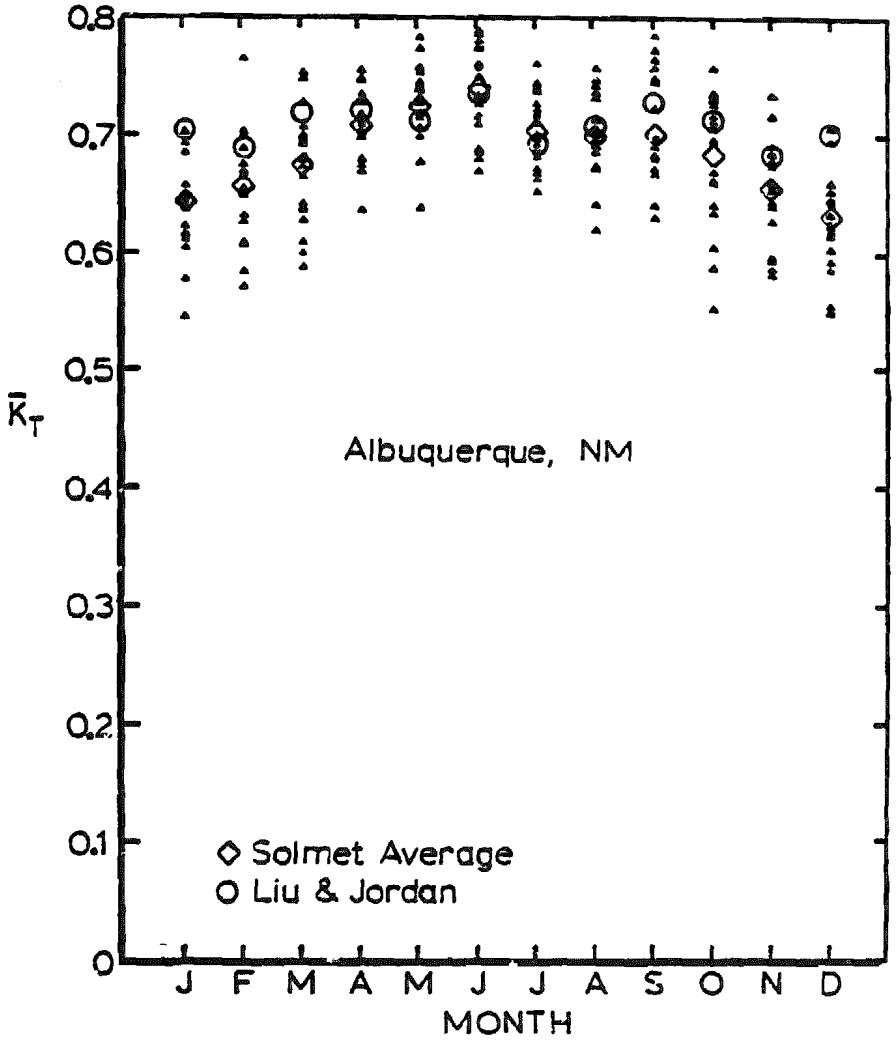

Figure 3.9 SOLMET Derived $\bar{K}_T$'s for Albuquerque, NM. The Solid Triangle Data Points are SOLMET Data.

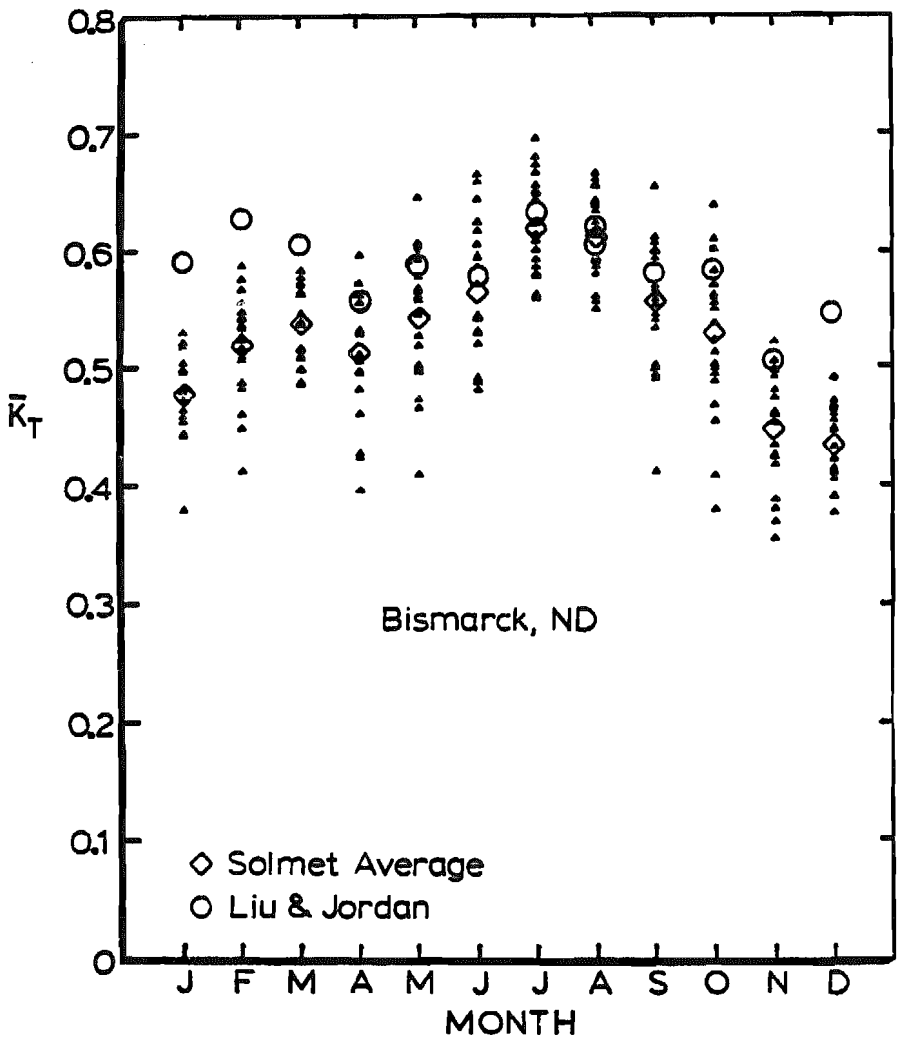

Figure 3.10 SOLMET Derived $\bar{K}_T$'s for Bismarck, ND. Solid Triangle Data Points are SOLMET Data.

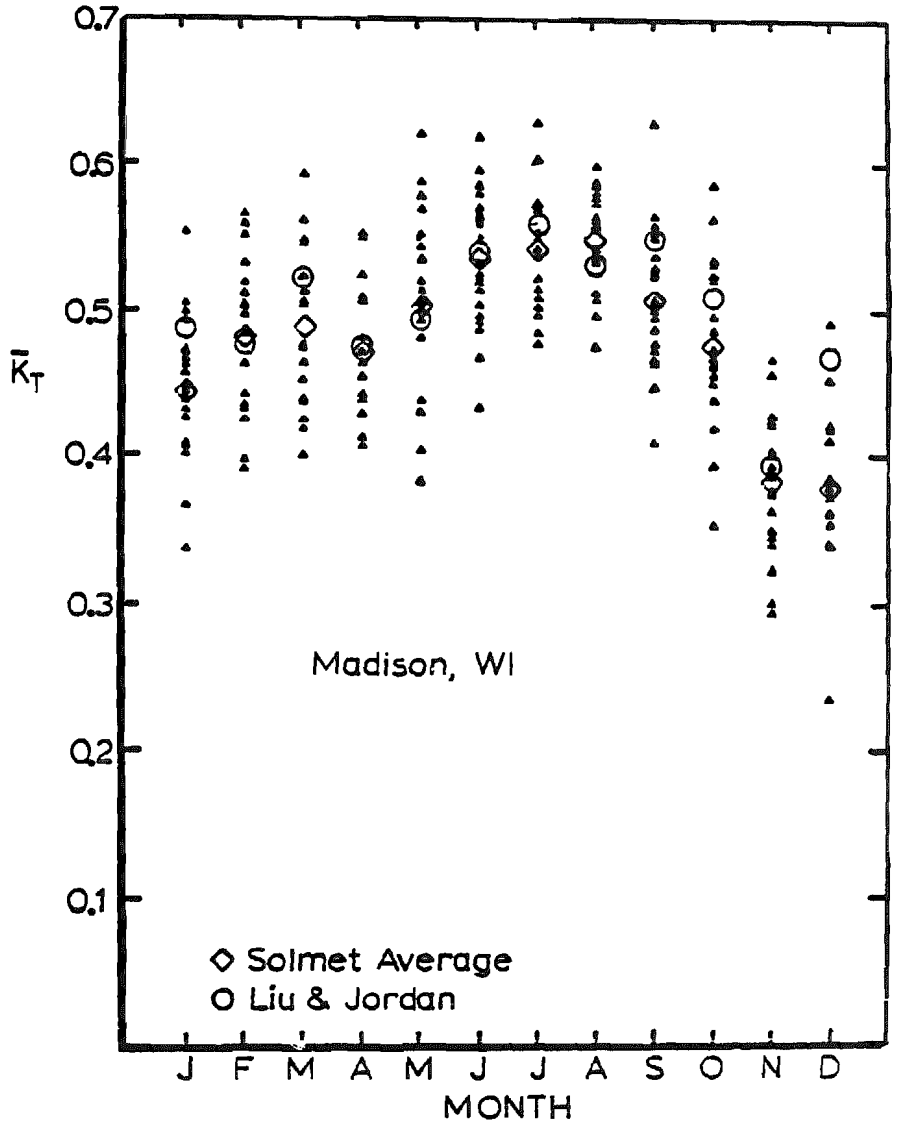

Figure 3.11 SOLMET Derived $\bar{K}_T$'s for Madison, WI. The Solid Triangle Data Points are SOLMET Data.

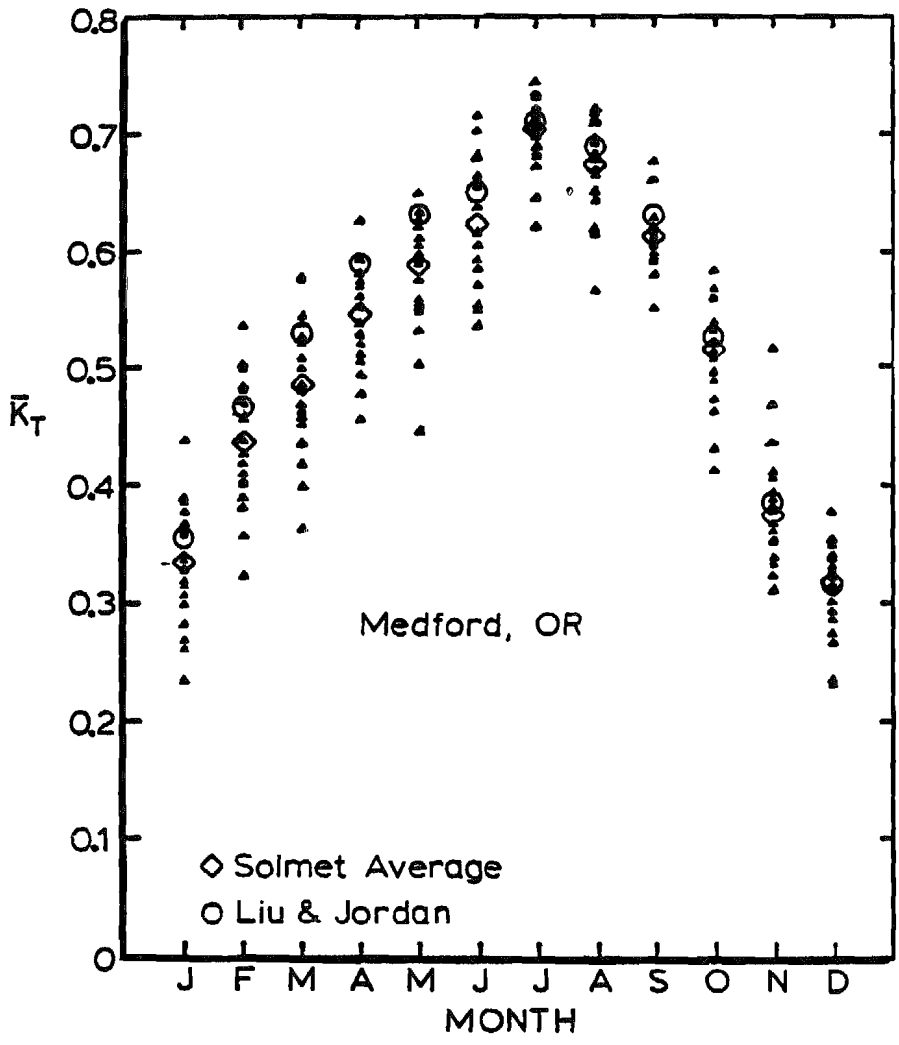

Figure 3.12 SOLMET Derived $\bar{K}_T$'s for Medford, OR. The Solid Triangle Data Points are SOLMET Data.

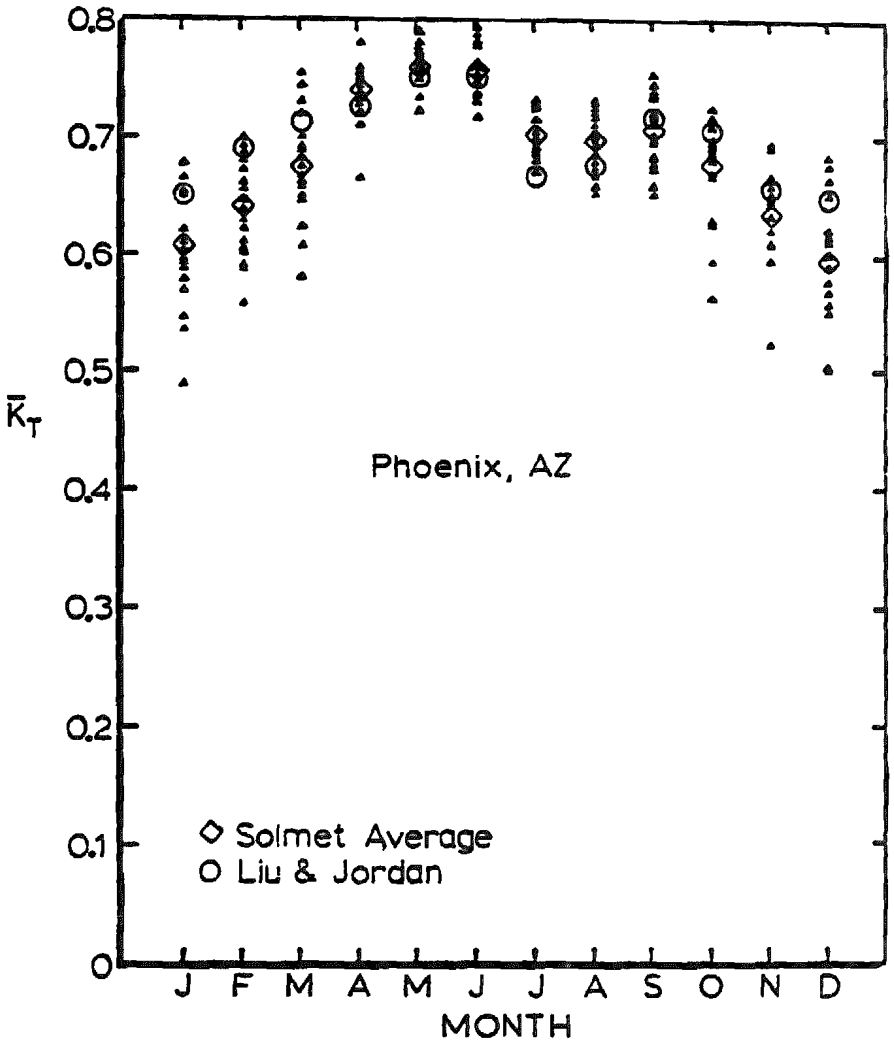

Figure 3.13 SOLMET Derived $\bar{K}_T$'s for Phoenix, AZ. The Solid Triangle Data Points are SOLMET Data.

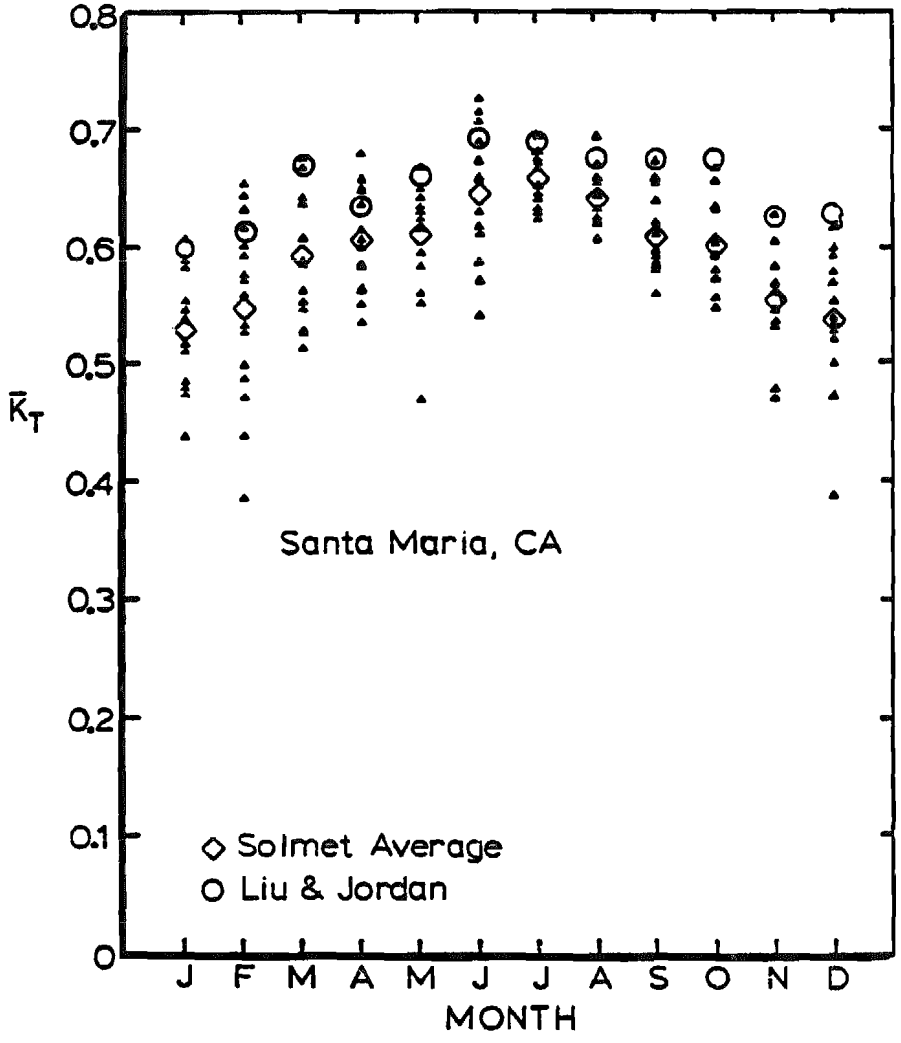

Figure 3.14 SOLMET Derived $\bar{K}_T$'s for Santa Maria, CA. The Solid Triangle Data Points are SOLMET Data.

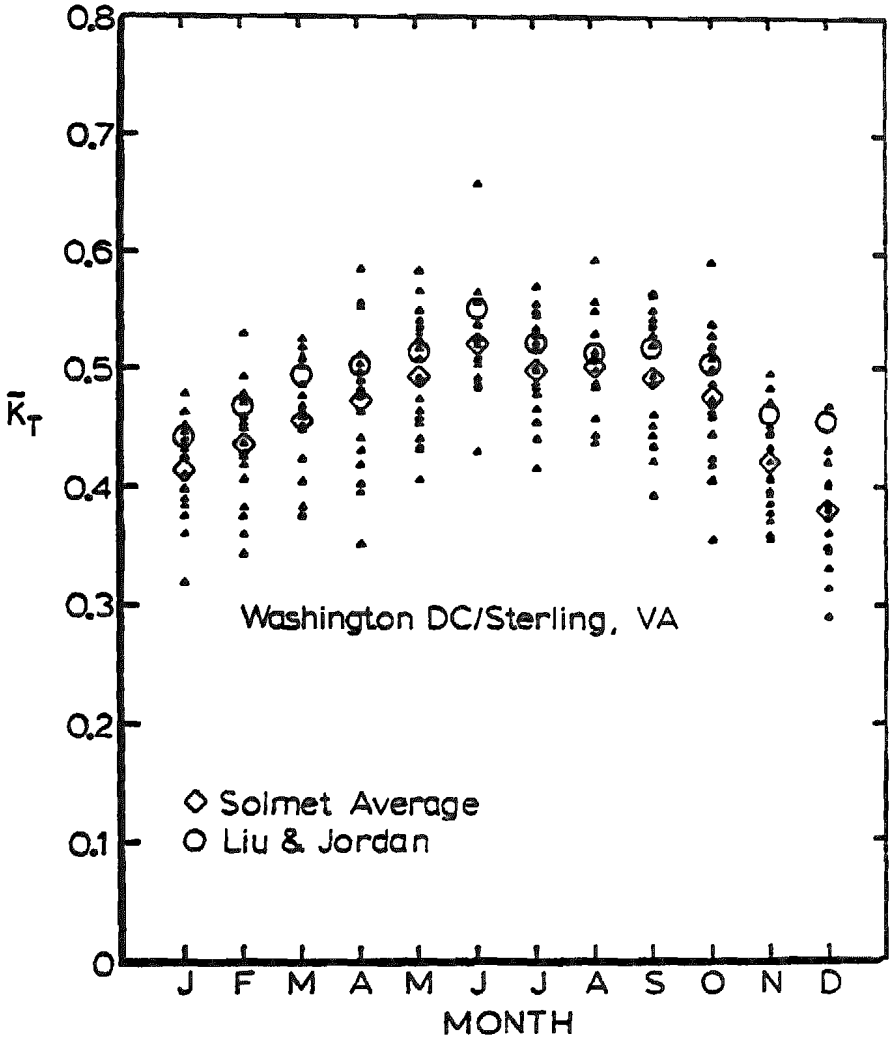

Figure 3.15 SOLMET Derived $\bar{K}_T$'s for Washington D.C./ Sterling, VA. The Solid Triangle Data Points are SOLMET Data.

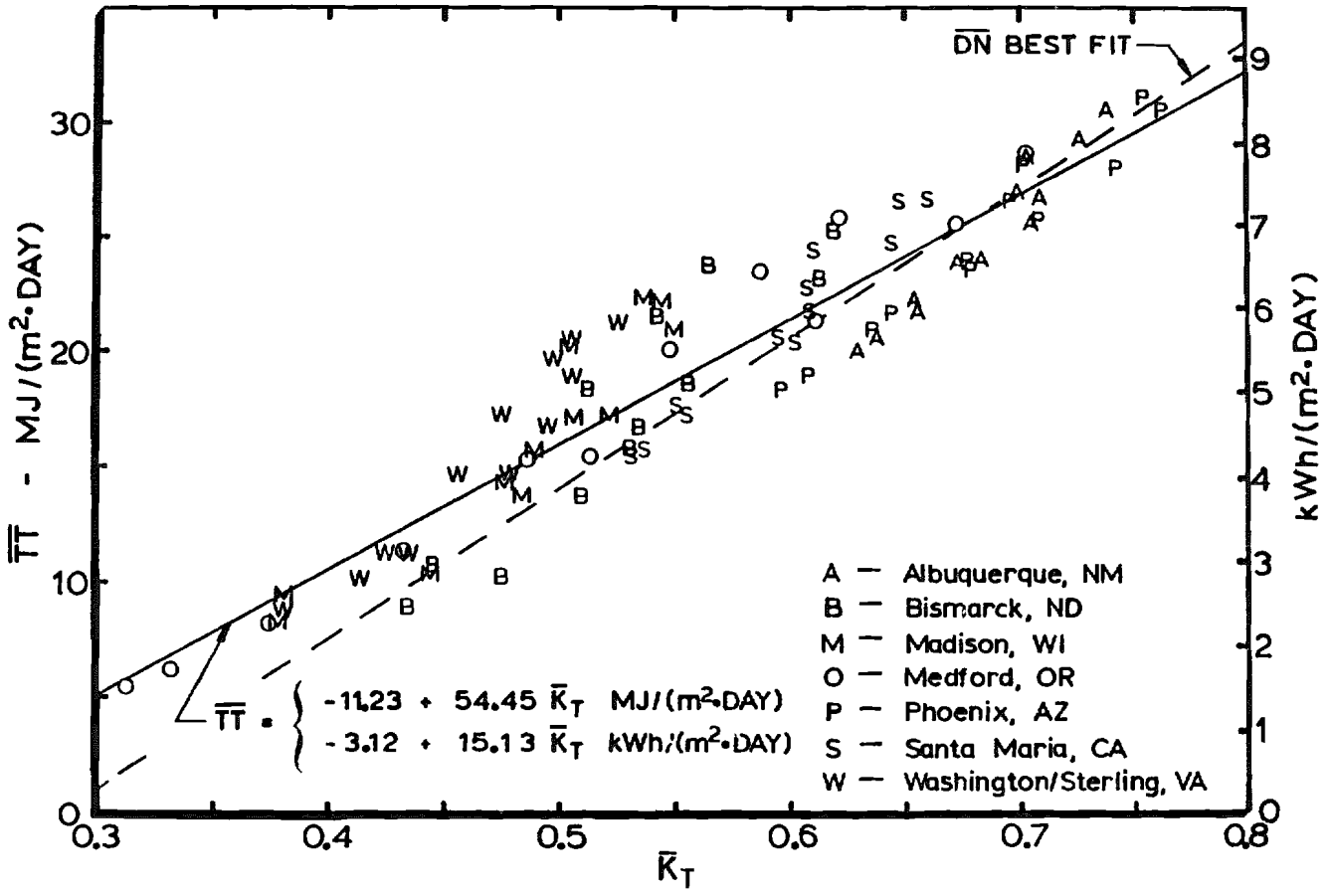

Figure 3.16 Long Term Monthly Average Daily Total Radiation on Monthly Optimally Tilted (TT) Array for Seven Cities. The Direct Normal (DN) Data are Shown in Fig. 3.17.

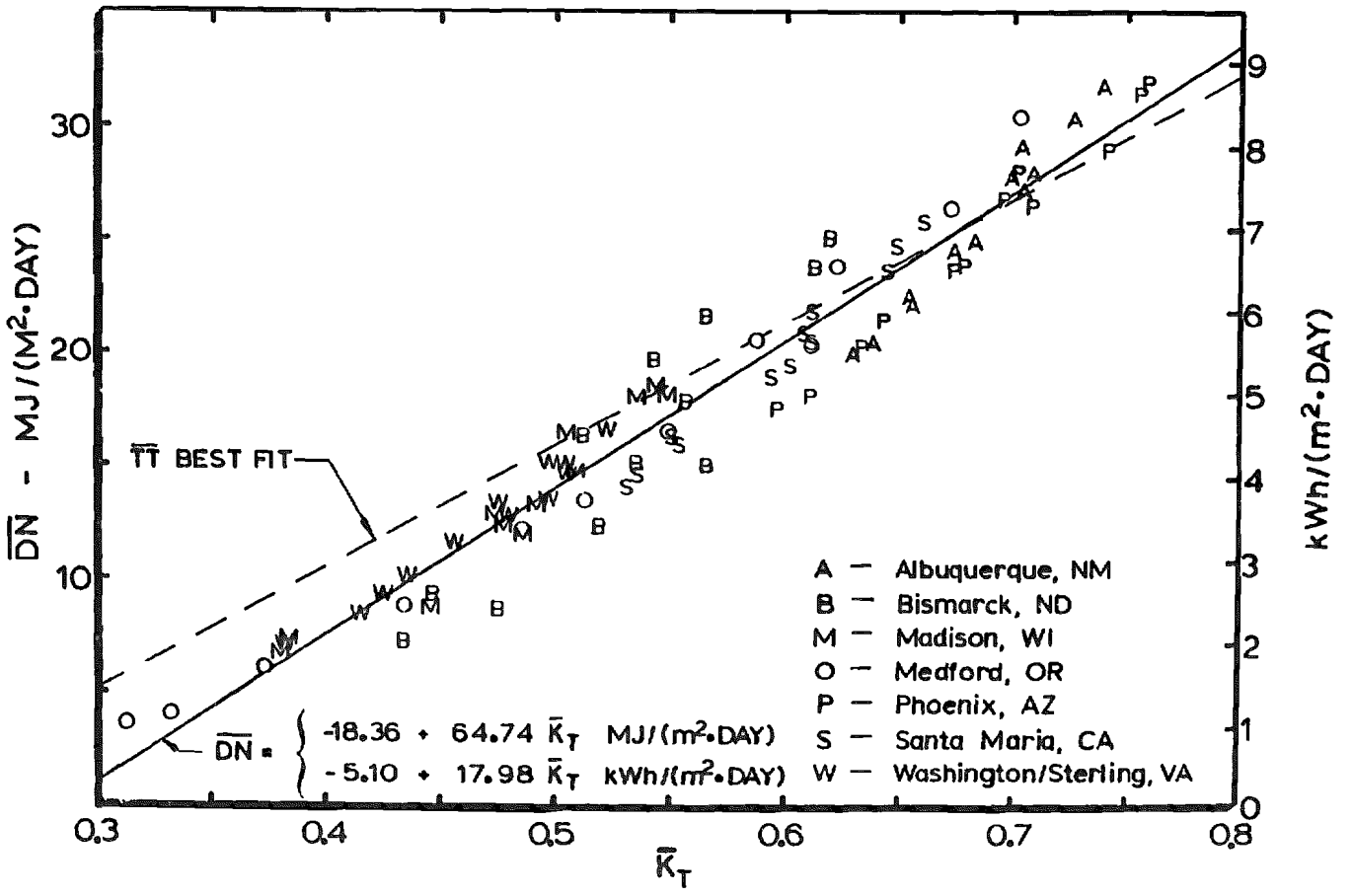

Figure 3.17 Long Term Monthly Average Daily Direct Normal Radiation (DN) for Seven Cities. The Total Radiation on the Tilt (TT) Data are Shown in Fig. 3.16.

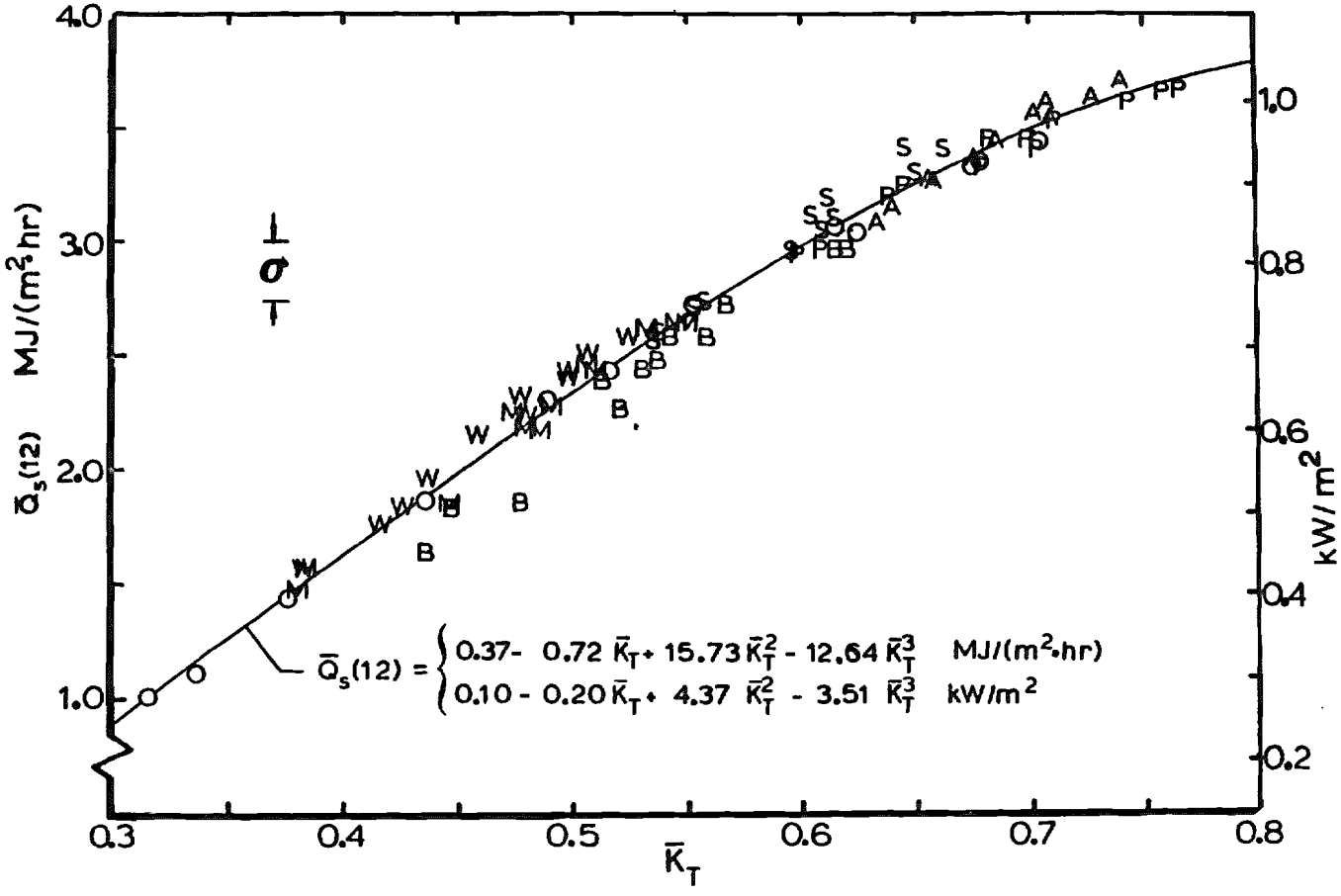

Figure 3.18 Midday Long Term Average Total Insolation on Optimally Tilted Array for Seven Cities. For Legend see Fig. 3.2.

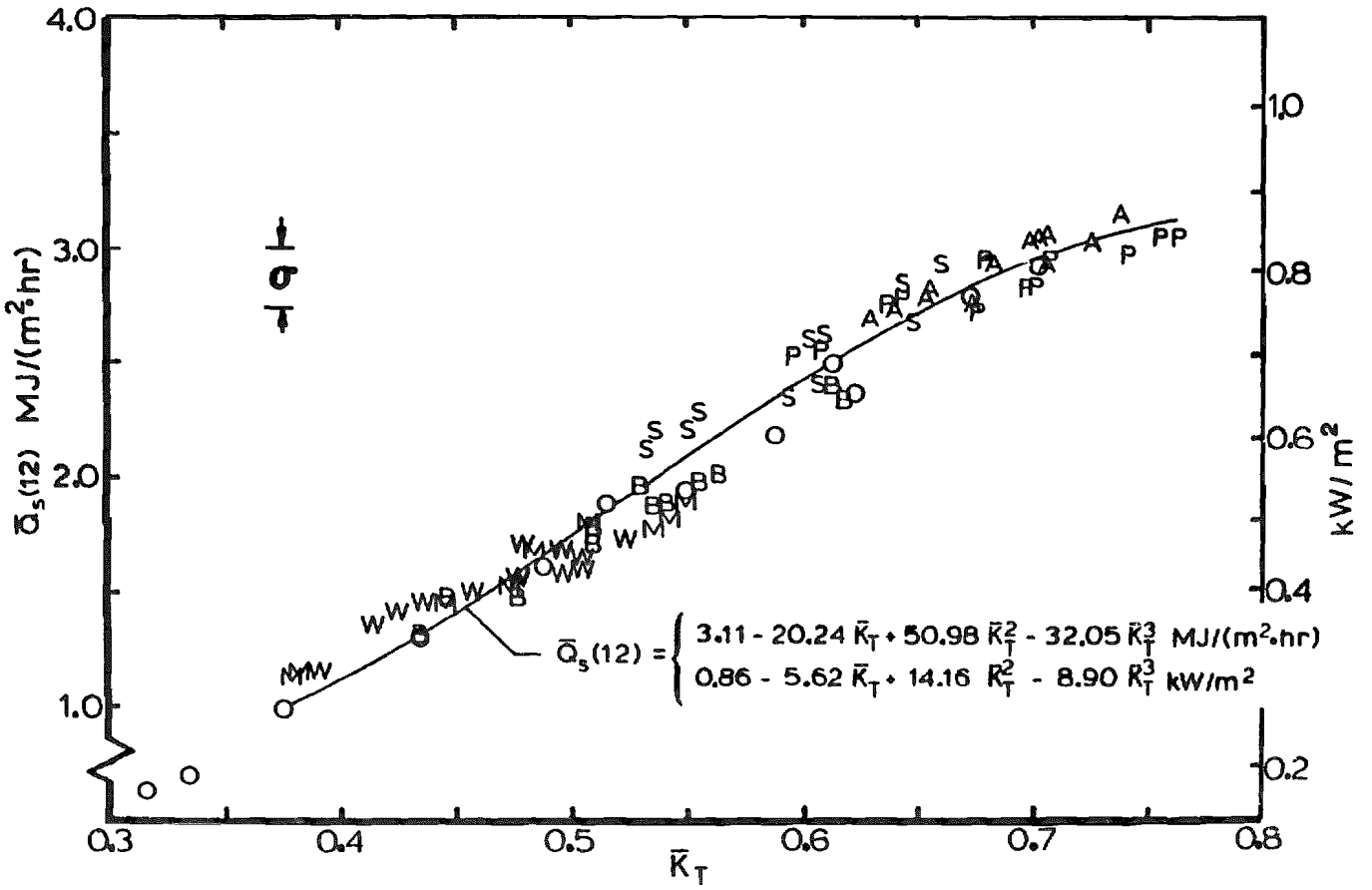

Figure 3.19 Midday Long Term Average Direct Normal Insolation for Seven Cities. For Legend see Fig. 3.2.

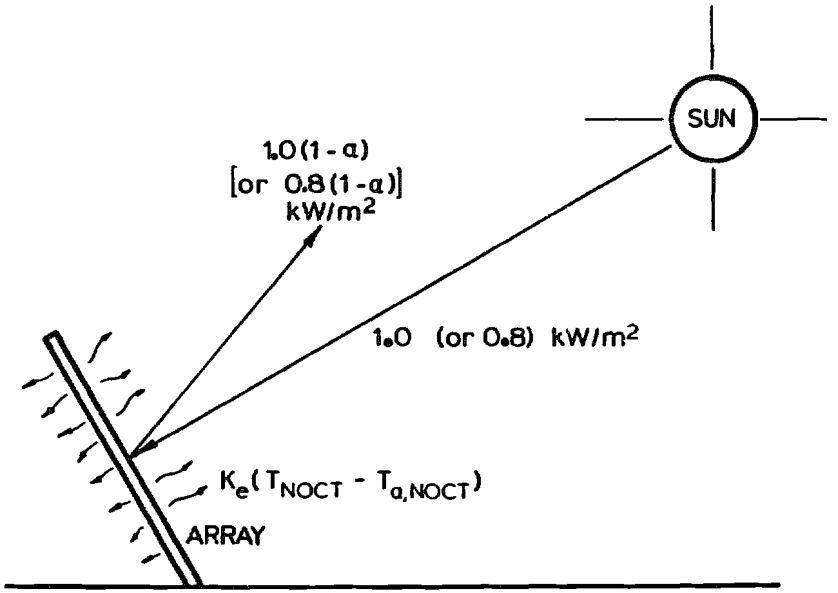

Figure 3.20 Energy Balance Schematic for NOCT Test

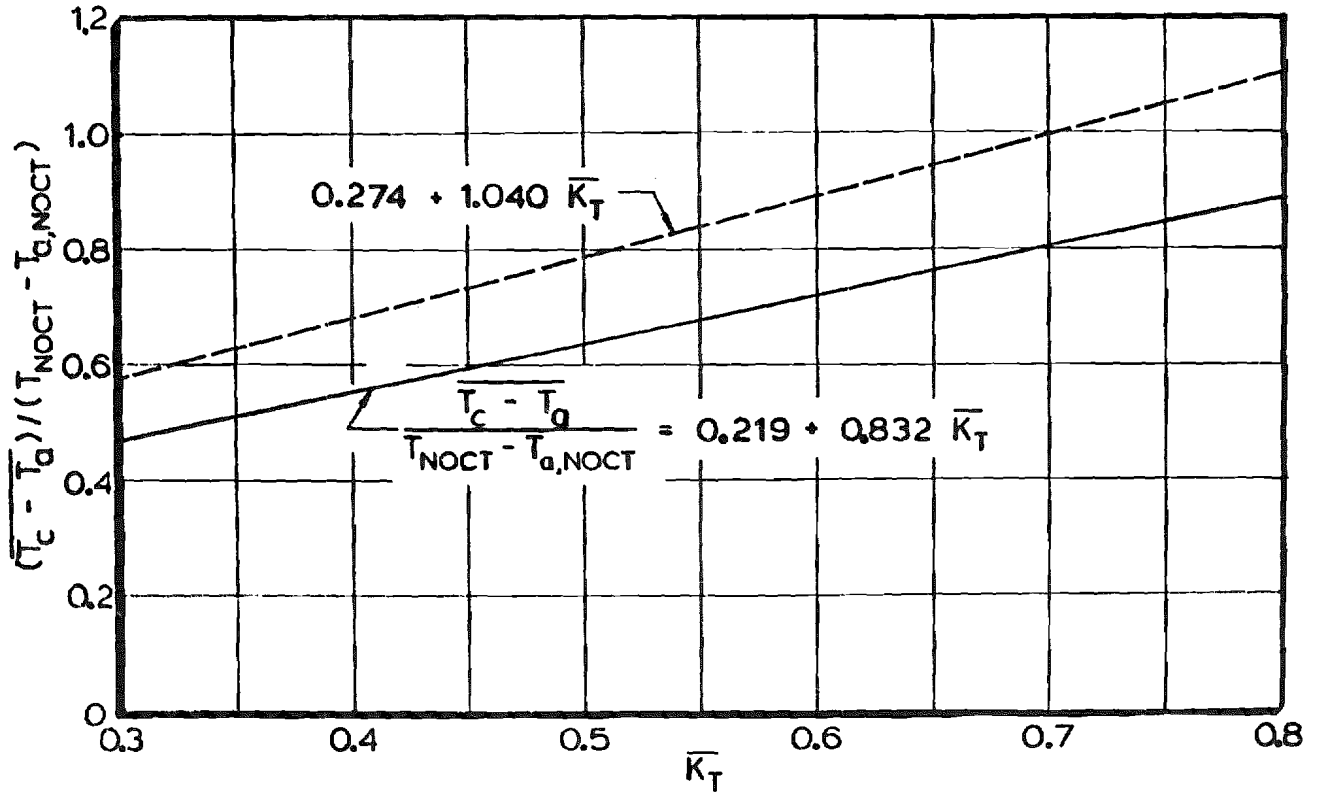

Figure 3.21 Fig. 3.2 Converted for Use with NOCT Data. The Solid Curve is for NOCT Data Taken at 1.0 kW/m^2 Insolation. The Dotted Curve is for NOCT Data Taken at 0.8 kW/m^2.

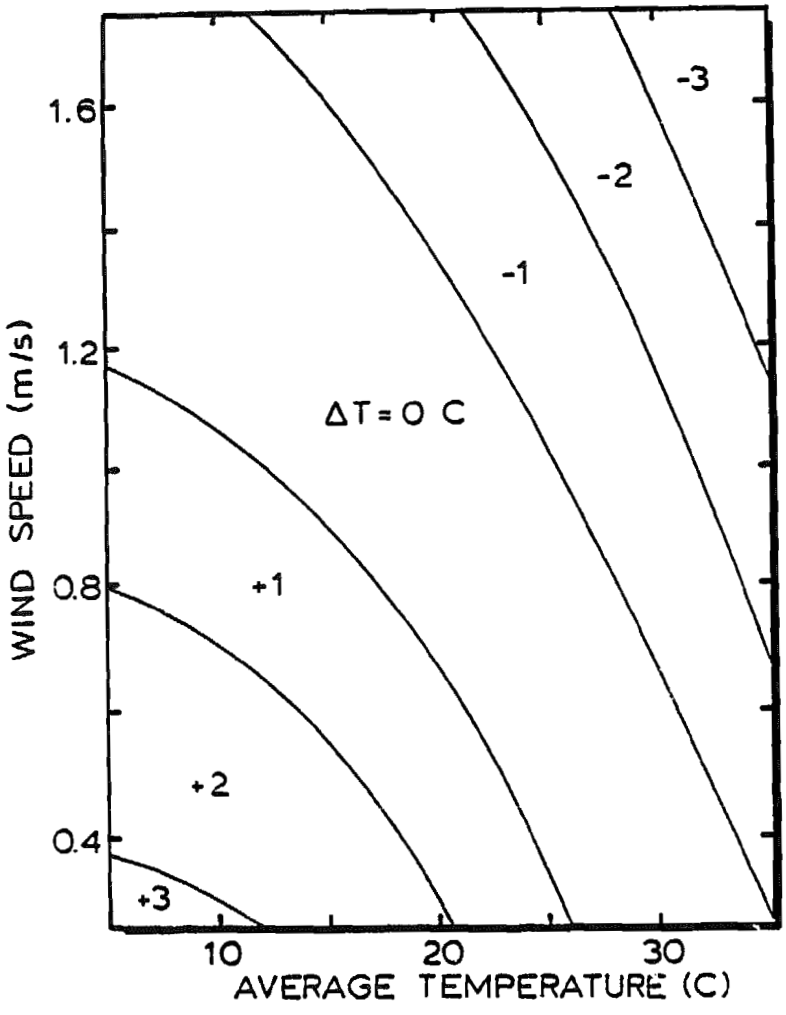

Figure 3.22 ΔT Corrections to be Applied to NOCT Data to Adjust Wind Speed and Average Temperature to Local Conditions. (Modified from Ref. 3.19)

4.0 SIMPLIFIED METHOD FOR MAX-POWER TRACKED SYSTEM PERFORMANCE

4.1 Introduction

In this chapter, a fairly general simplified procedure for estimating the performance of PV systems of the type described in Fig. 2-1 is developed. This procedure is for max-power tracked, passively cooled, flat plate arrays with battery storage and a back-up energy source. The special case of zero storage is also considered. Results from this procedure are compared with those from detailed computer simulations and shown to agree to within a standard deviation of 2.6% (absolute) for the cases considered. Limitations to the procedure are discussed and an example is included.

4.2 System Parameters

The simulation studies described in Chapter 2 are presented in terms of the groups $S/\bar{\eta}A$ and $\bar{Q}_e/\bar{L}$. These arose through an empirically based effort to collapse different families of curves and are largely successful in doing so. However, the results of Chapter 2 also indicate that several additional variables (viz., load characteristics, time of year, and, to a lesser extent, location) need to be considered in order to accurately estimate system performance. Only when the time of year and expected load match those used in the simulations can the Chapter 2 figures be used to predict performance. In order to predict performance for more general situations then, one needs additional or alternative parameters, general in nature, to characterize system behavior. Ideally these parameters involve only monthly mean values since the object here is to obtain monthly performance estimates.

One such set of parameters arises from considering the interaction of the monthly average daily array output and demand curves for an arbitrary month and location, as shown for example in Figs. 4.1a,b. The ordinate in both figures has units of power and the abscissa those of time, so the various areas indicated represent energies. The area under the demand curve is $\bar{L}$, the total daily energy load. The area under the output curve is $\bar{Q}_e$, the mean daily effective energy output from the array for the month in question. The area under the array output curve and above the demand curve will be referred to as excess (XS), the energy which must either be stored or dumped. Finally, the storage capacity (S) is also represented as an area which is shown in Fig. 4.1b superposed on part of the XS energy.

The four energies ($\bar{L}$, $\bar{Q}_e$, XS, S) constitute a set of dimensional parameters which may be normalized in different fashions. One such normalization scheme forms the basis for the design procedure described later in this chapter. The scheme results in three parameters, each of which is a dimensionless energy.

One dimensionless parameter is the same $\bar{Q}_e/\bar{L}$ used in Chapter 2. It represents the ultimate fraction of the daily load which would be supplied by the system if the load were ideally matched to the array output. A second group, $XS/\bar{Q}_e$, is the fraction of electrical output which cannot be used directly because of an insufficient immediate demand. $XS/\bar{Q}_e$ thus represents the fraction of array energy which must be either stored or dumped. A third parameter, S/XS, is the ratio of battery storage to the amount of energy available to be stored.

Mathematically, the three parameters are as follows:

$$\bar{Q}_e/\bar{L} = \int \dot{Q}_e\,(t)dt / \int \dot{L}(t)dt \qquad (4.1)$$

$$XS/\bar{Q}_e = \text{pos} \int [\dot{Q}_e(t)-\dot{L}(t)]dt / \int \dot{Q}_e(t)dt \qquad (4.2)$$

$$S/XS = S\,N_d/\{\text{pos} \int [\dot{Q}_e(t)-\dot{L}(t)]dt\} \qquad (4.3)$$

The integrations in the above equations are carried out over monthly periods.

One additional parameter, not readily apparent in Figs. 4.1a,b, accounts for storage losses. A battery efficiency is defined by

$$\eta_b = S_D/S \qquad (4.4)$$

where S_D is the stored energy which is ultimately delivered to the load. The functional dependencies of η_b were not investigated. However, results from the Chapter 2 simulation studies indicated that, at least for the battery model and range of operation used here, storage efficiency is effectively constant with a value of 0.87.

4.3 Simplified Design - Single Day Approach to Monthly Behavior

4.3.1 Energy Allocation - Single Day

The distribution of electrical energy produced by the PV array on a given day, denoted by the subscript n, is defined by parameters very similar to those of the previous section. However, the integrations in Eqs. (4.1-4.3) are now carried out over day n. The daily distribution is depicted by the flow chart of Fig. 4.2 as a series of binary branches with the division of energy flow at each branch determined by the value of one of the daily system parameters. Thus, of the total effective daily energy produced, $Q_{e,n}$, a fraction $(1- XS/Q_{e,n})$ flows directly to the load. Of the remainder, a fraction S/XS_n is stored, and the rest is dumped. Finally, of the stored energy, a fraction η_b

supplies the load, and the remainder is lost. The net fraction of load satisfied by the system is easily computed as

$$f_{e,n} = \{1 + XS_n [\eta_b S/XS_n - 1] Q_{e,n}\} Q_{e,n}/L_n \qquad (4.5)$$

with $S/XS_n < 1$

and $f_{e,n} < 1$

The constraints on S/XS_n and $f_{e,n}$ simply indicate that the batteries cannot generate energy and the system cannot supply more of the load than exists. In systems with large $Q_{e,n}/\bar{L}$ and sufficient storage, the system output for one day in some cases (notably a clear day followed by a cloudy day) can supply a part of the day's load; in this case of day to day interaction the solar fraction is not subject to the constraint. However, the simplified design procedure will ignore this day to day interaction.

In eq. (4.5), the parameters η_b and S/XS_n occur as a product. For the purpose of estimating system performance, the two may thus be condensed into a single system storage parameter, $\eta_b S/XS_n$.

4.3.2 Monthly Distribution

The single day energy distribution equation, eq. (4.5) using monthly mean values $(XS, \bar{Q}_e)$ for XS_n and $Q_{e,n}$ is not generally valid for estimating monthly system performance. Array output is not uniform from day to day throughout a month because of differences in atmospheric conditions, and $Q_{e,n}/\bar{L}$ varies accordingly. Since XS_n is strongly dependent on $Q_{e,n}$, it too varies and affects both $XS_n/Q_{e,n}$ and S/XS_n. Application of eq. (4.5) is therefore not useful without some consideration being given to the day to day variation within a month.

This section, then, describes a method for representing such variation in array output from knowledge only of $\bar{K}_T$ and the mean daily output, $\bar{Q}_e$. Knowledge of the variation permits eq. (4.5) to be used to compute a distribution of daily performances for the month which in turn may be used to obtain an estimate of monthly performance.

The results of Liu and Jordan (Ref. 4.1) on generalized radiation distribution curves are useful in describing the desired distribution of array output. As a part of the work on data for seven SOLMET sites described in Chapter 3 of this report, the generalized radiation distribution curves were redone. The new curves along aith a comparison with the Liu and Jordan curves are shown in Fig. 4.3. While those results specifically apply to total horizontal radiation data, they may be expected to be at least approximately correct for tilted array output as well. Combined with the mean daily effective array output, $\bar{Q}_e$, determined by the methods of Chapter 3, the insolation distributions of Fig. 4.3 can be used to construct a pattern of daily outputs which yield the appropriate monthly mean value and which reflect the expected variability within the month. The distribution is based on long term results and in this sense is preferable to simulation results based on a single, typical month.

Using Fig. 4.3 it is possible to obtain 30 separate values of $Q_{e,n}$ (a 30-day distribution) corresponding to predicted array output for each day of the month. While this makes the most sense in terms of referring to eq. (4.5) as a single day equation, it is equally possible to approximate monthly performance using N values of $Q_{e,n}$ (an N-day distribution) where N is arbitrary. Since application of eq. (4.5) is somewhat involved (as is seen later), it is advantageous to choose the smallest N which still approximates the variability of output during a month. The results of this work suggest that in most cases N=3 is sufficient. This was established by taking successively smaller numbers for N and noting the resulting solar fraction. The

3-day distribution corresponds t. representing the monthly weather with typical ''good,'' ''mediocre,'' and ''poor'' days.

Figure 4.4 is an abbreviated cross plot of Fig. 4.3. It shows the values of $Q_{e,n}$ appropriate for a 3-day distribution. At a fixed $\bar{K}_T$, the uppermost curve gives a value of $Q_{e,n}$ for the good day, the intermediate curve yields a value for the mediocre day, and the lowest curve yields a poor day value of $Q_{e,n}$. The upper and lower curves in Fig. 4.4 are obtained from the values of $\bar{E}/\bar{H}$ corresponding to the 1/6 and 5/6 points on the cumulative frequency distribution axis in Fig. 4.3. These closely approximate the 5th best and 5th worst days of a 30-day distribution. The middle curve is adjusted so that a point on this third curve when taken with points on the 1/6 (poor day) and 5/6 (good day) curves at the same $\bar{K}_T$, averages to 1.0. That is, the mean array output for the 3-day distribution equals the actual monthly mean value.

4.3.3 The Design Procedure

The ideas of Sections 4.2.1 and 4.2.2 are now merged into a procedure for estimating system performance. The procedure is valid for systems with an arbitrary amount of storage and a known but arbitrary daily load profile. It treats a load which does not vary from day to day but is readily adapted to situations in which the load profile does change (e.g., distinct weekend and weekday profiles). The method provides for consideration of both seasonal and geographic variations.

The technique presumes that the monthly average daily effective energy output from the array is already determined (e.g., through the procedure described in Chapter 3). The designer is required to specify the quantity of available storage, a daily load profile (shape and magnitude), and the average daylength of the month at the location for which he is designing. He must also know $\bar{K}_T$ for the month and site involved.

The method proceeds in four steps. First, a 3-day distribution of array outputs is obtained using Fig. 4.3, and three values of $Q_{e,n}/\bar{L}$ are determined. Next, an $XS_n/Q_{e,n}$ is computed for each of three values of $Q_{e,n}/\bar{L}$. Then, the system storage parameter $\eta_b S/XS_n$ is evaluated directly, again for each of the three representative days. Finally, eq. (4.5) is applied three times, and the resulting values of the solar fraction are averaged to give an estimate for the expected monthly system performance.

The bulk of the procedure lies in computing $XS_n/Q_{e,n}$ from a given value of $Q_{e,n}/\bar{L}$. This is accomplished by curve-fitting a normalized effective array power output, $\dot{Q}_{e,n}(t)/\bar{L}$, using a cosine function centered at noon, with a half-period related to the daylength and with the amplitude adjusted to obtain the specified $Q_{e,n}$. The resulting fit is

$$\dot{Q}_e(t)/\bar{L} = \{Q_{e,n}/\bar{L}\}\ \{\pi/[2(t_D-c)]\}\ \cos\ [\pi(t-12)/(t_D-c)] \qquad (4.6)$$

for

$$[12 - (t_D-c)/2] < t < [12 + (t_D-c)/2]$$

and

$$\dot{Q}_{e,n}/\bar{L} = 0$$

for other values of t.

Experience suggests $c = 1$ hour gives accurate estimates of XS_n. This constant truncates a slight Gaussian-like tail in the periods just following sunrise and preceding sunset and improves the curve-fit during the hours when interaction with the load curve is important. Figures 4.5a,b show examples of the cosine curve-fit for June and December in Albuquerque.

With $\dot{Q}_{e,n}(t)/\bar{L}$ approximated by eq. (4.6), $XS_n/Q_{e,n}$ is computed using the daily equivalent of eq. (4.2). This is accomplished analytically if $\dot{L}(t)$ can be expressed analytically and numerically (or graphically) otherwise.

Using the calculated values of $XS_n/Q_{e,n}$ and $Q_{e,n}/\bar{L}$, the combined parameter $\eta_b S/XS_n$ is readily determined. With each of the system parameters now calculated, eq. (4.5) is applied. A separate solar fraction is computed for each of the three representative days. This introduces the effect of varying array performance within the month so that when the three fractions are averaged this effect is included in the final result.

Table 4.1 summarizes the procedure, and an example in the ensuing section demonstrates it.

4.4 Example

As an example of the procedure described in Section 4.4, consider the estimation of the performance of a PV system to be operated in Albuquerque during March. The following is known from the month and location.

$$\bar{K}_T = 0.64 \tag{4.7}$$

$$t_D = 11.7 \text{ hrs} \tag{4.8}$$

Sources for the first of these were discussed in Section 3.3. The second can be calculated from

$$t_D = 2[\arccos(-\tan\phi \cdot \tan\delta)]/15 \tag{4.9}$$

The solar declination, δ, is calculated from

$$\delta = 23.45 \sin[360(284+n)/365] \tag{4.10}$$

where n is the Julian day of the year.

Suppose that the expected load is constant,

$$\dot{L}(t) = L_o = 1985 \text{ kJ/hr} = 0.55 \text{ kW} \tag{4.11}$$

$$\bar{L} = 24L_o = 4.76 \times 10^4 \text{kJ} = 13.2 \text{ kW-hr} \tag{4.12}$$

Suppose further that the product of storage capacity and efficiency for the system in question is chosen by a designer to be

$$\eta_b S = 5265 \text{ kJ} = 1.46 \text{ kW-hrs} \tag{4.13}$$

Finally, suppose that using the procedure of Chapter 3, the monthly mean daily array output as it comes from the inverter is determined to be

$$\bar{Q}_e/\bar{L} = 0.6 \tag{4.14}$$

Estimation of the sytem performance now proceeds following Table 4.1.

Step 1. Obtain a 3-day distribution of array outputs using Fig. 4.4 and $\bar{K}_T = 0.64$. The figure gives

$$Q_{e,1}/\bar{Q}_e = 1.16; \; Q_{e,2}/\bar{Q}_e = 1.00; \; Q_{e,3}/\bar{Q}_e = 0.84 \tag{4.15}$$

Thus

$$\begin{aligned} Q_{e,1}/\bar{L} &= 1.16(0.6) = 0.696; \\ Q_{e,2}/\bar{L} &= 0.60; \\ Q_{e,3}/\bar{L} &= 0.504 \end{aligned} \tag{4.16}$$

Step 2 a) Approximate the instantaneous array output. Consider the first of the three values from Step 1. From eq. (4.6),

$$\dot{Q}_{e,1}/\bar{L} = 0.696\ \{\pi/[2(11.7-1)]\}\ \cos\ [\pi(t-12)/(11.7-1)]$$

$$= 0.102\ \cos\ [\pi(t-12)/10.7] \qquad (4.17)$$

b) Compute $XS_n/Q_{e,n}$. The load curve is expressed analytically, hence, $XS_n/Q_{e,n}$ can be computed analytically. Again consider the first point in the distribution:

$$XS_1/Q_{e,1} = [\bar{L}/Q_{e,1}] \int_{t_1}^{t_2} [Q_{e,1}/\bar{L} - L_o/\bar{L}]\ dt \qquad (4.18)$$

where

t_1 is the 1st time that the array output equals the load

and

t_2 is the 2nd time that the array output equals the load.

To determine t_1 and t_2, set $\dot{Q}_{e,1} = L_o$. Thus,

$$(0.102)\ (24L_o)\ \cos\ [\pi(t-12)/10.7] = L_o \qquad (4.19)$$

which gives

$$t_1 = 12 - \{10.7/\pi\}\ \text{arc cos}\ [(0.102)(24)]^{-1} = 8.1 \qquad (4.20)$$

and

$$t_2 = 12 + \{10.7/\pi\}\ \text{arc cos}\ [(0.102)(24)]^{-1} = 15.9 \qquad (4.21)$$

Use eq. (4.6) with eq. (4.18) to obtain

$$XS_1/Q_{e,1} = \pi/2(t_D-1) \int_{t_1}^{t_2} \cos [\pi(t-12)/(t_D-1)]dt$$

$$- \int_{t_1}^{t_2} L_o/Q_{e,1}\, dt$$

$$= 1/2 \{\sin [\pi(t_2-12)/(t_D-1)]$$

$$- \sin [\pi(t_1-12)/(t_D-1)]\}$$

$$- L_o/Q_{e,1} (t_2-t_1)$$

$$= 0.44 \qquad (4.22)$$

Repeating the procedure for the remaining two days yields

$$XS_2/Q_{e,2} = 0.37 \qquad (4.23)$$

and

$$XS_3/Q_{e,3} = 0.28 \qquad (4.24)$$

Step 3 Compute the effective storage fraction, $\eta_b S/XS_n$.

Use

$$\eta_b S/XS_n = \eta_b S/[(XS_n/Q_{e,n})(Q_{e,n}/\bar{L})\ \bar{L}] \qquad (4.25)$$

For the 1st day this gives

$$\eta_b S/XS_1 = 5265/[(0.44)(0.696)(24)\ 1985)] = 0.36 \qquad (4.26)$$

Similarly,

$$\eta_b S/XS_2 = 0.50;\ \eta_b S/XS_3 = 0.792 \qquad (4.27)$$

Step 4 Compute the monthly solar fraction

a) apply eq. (4.5) using values for the 1st day.

$$f_{e,1} = [1 + 0.442\ (0.36 - 1)]\ \ (0.696)$$

$$= 0.50 \qquad (4.28)$$

Similarly,

$$f_{e,2} = 0.49 \qquad (4.29)$$

and

$$f_{e,3} = 0.47 \qquad (4.30)$$

b) Average the results

$$f_e = (0.50 + 0.49 + 0.47)/3$$

$$= 0.49 \qquad (4.31)$$

Thus, the procedure predicts that 49% of the load will be satisfied by the system for the month of March. This compares with 46.7% predicted by computer simulation using TMY weather data.

In this example, assuming uniform weather throughout the month does not significantly affect the final estimate of f_e. This is seen by observing that $f_e = f_{e,2}$ in Step 4 above and recognizing that that $f_{e,2}$ is obtained from the monthly average values, $\bar{Q}_e$ and XS. Such a uniform weather assumption is not always valid. For instance, for Madison in June with $\bar{Q}_e/\bar{L} = 0.6$, the baseline load shape, and a storage capacity corresponding to $S/\bar{\eta}A = 5$ Amp-hr/(%·m²), the solar fraction obtained using only monthly average values is $f_e = .59$, while the 3-pt. procedure yields $f_e = .54$. The value from hourly simulation is $f_e = .538$; hence, the 3-pt procedure in this case is crucial.

4.5 Discussion

4.5.1 Comparison of Results

Table 4.2 shows additional comparisons of predictions using the simplified technique with those of computer simulations. The table displays cases for which the baseline load defined in Chapter 2 was specified. The examples without storage best indicate the accuracy in estimating XS. Those corresponding to $\bar{S}/\eta\bar{A}$ = 5 amp-hrs/(%·m²) include storage, obviously, but not enough to eliminate dumping. The $\bar{S}/\eta\bar{A}$ = 10amp-hrs/(%·m²) cases for $\bar{Q}_e/\bar{L}$ = 0.6 experience only minor amounts of dumping.

In virtually all instances, results from the simplified procedure are within 10% relative and 5% absolute of the simulated values. The standard deviation of the predicted values from the simulated values is 2.6% (absolute). Typically, results are very good for summer months when weather patterns tend to be good (more consistent). Poorest results occur in winter months. Also, results for larger storage sizes tend to be very good.

Several factors contribute to differences between simply predicted and computer simulated results. Simulation results are based on a particular month which is likely to differ at least somewhat from the long term average which forms the basis for the simplified procedure. That is, insolation distributions for any one month can differ from the long term (~22 years) results shown in Fig. 4.3. This effect can readily be investigated by simulating the system over several years and comparing the corresponding estimate of the simplified procedure with the long term average of the simulations for any given month. Such a study has not as yet been performed.

Use of an insolation distribution to approximate a distribution in array output also is not completely correct. In particular, temperature variation within a month causes changes in solar cell efficiency and so affects the distribution of array

output. This effect is ignored by using strictly an insolation distribution.

Another obvious source of error in the simplified procedure lies in the cosine fit for the array power output. Individual poor days do not have cosine-like daily distributions although, averaging the poor days over the month, it may appear that they do. This is probably the largest source of error for winter months.

There is also an uncertainty in specifying storage capacity in energy units. Both the charging and discharging voltages enter into the determination of the energy capacity of the batteries. Since these voltages vary during the course of system operation, it is difficult to precisely estimate the energy storage capacity from the rated capacity in amp-hrs. Two schemes have been used to estimate effective energy capacity. The first of these uses the storage efficiency value 0.87, determined from simulation results with a nominal 2.0 volt battery voltage for converting amp-hrs to W-hrs. The second approach employs the well-defined open circuit battery voltage, 2.175 volts, with a nominal storage efficiency of 0.80. The two procedures yield equivalent estimates of the solar fraction and differ only in the apportionment of losses due to dumping and storage inefficiencies.

4.5.2 Interaction on Successive Days

One other phenomenon poses difficulties for the simplified procedure. Consider a system with $Q_e/\bar{L} = 1$ and large storage capacity during a low $\bar{K}_T$ month. Cloudy days within the month result in generation which satisfies less than the full load, while clear days convert more than enough energy to meet the daily load. The load on a clear day then is completely satisfied and, in addition, storage may be filled to where it is not completely depleted by sunrise of the following day. if the following day is also clear, the system will again store energy. However, because

storage is already partly filled, the available storage is less than on the previous day, and more energy must be dumped.

This ''end-of-the-day dumping'' is the situation presumed in the simplified procedure. Constraining the solar fraction to not exceed unity effectively requires that no energy produced on one day be used on the next. However, if the representative good day solar fraction (i.e., the largest $f_{e,n}$ of the 3-day distribution) is near unity, then some of the ''better'' good days contribute $f_{e,n} > 1$ to its value. The procedure imposes the constraint only on the representative $f_{e,n}$ and not on the ''better'' good day $f_{e,n}$'s; hence, the good day fraction is higher than if the constraint were strictly imposed. Including additional days in the distribution allows the constraint on the solar fraction to be more completely enforced.

For the same system as above, if a clear day is followed by a cloudy day, part of the production of the clear day contributes toward satisfying the cloudy day load. When such interaction on successive days occurs, the constraint on f_e is not valid. Since enforcing the constraint tends toward conservative estimates of system performance, however, the recommended procedure is to enforce it as strictly as possible. Thus, predictions for which the good day fraction is greater than about 0.95 should be viewed as optimistic and consideration should be given to using more than a 3-day distribution in order to permit stricter enforcement of the constraint on solar fraction.

4.5.3 High $\bar{K}_T$ Months

In months with high $\bar{K}_T$, the 3-day distribution offers little advantage over a uniform day assumption. Hence, for $\bar{K}_T > 0.65$, eq. (4.5) applied once using $\bar{Q}_e/\bar{L}$ gives results essentially equivalent to those obtained with the 3-day distribution calculation.

4.5.4 Varying Load Profile

The procedure developed here assumes that the load profile is uniform from day to day through a month. To estimate monthly performance in situations where the load profile varies (e.g., a weekend load which differs from that during the week) it is necessary to approximate monthly performance for each load shape and weight the results appropriately (e.g., weight the weekend results by 2/7 and those for the week days by 5/7).

4.5.5 Utility Sellback

The situation in which the utility serves as system storage, purchasing power which is not immediately needed and selling power when the array alone cannot satisfy the load, is merely a special case of the procedure already discussed. Here, the single-day direct fraction, that supplied directly by the array, is

$$f_{e,n} = [1 - XS_n/Q_{e,n}]\ Q_{e,n}/\bar{L} \qquad (4.32)$$

The fraction of the output which is sold to the utility is just $XS_n/\bar{L}$ and that purchased from the utility is $(1 - f_e)$. These are readily computed on a monthly basis using the same 3-day procedure described previously. As shown in the results of Chapter 2, random fluctuations in the load do not significantly affect the monthly two-way energy flow, hence neglecting such fluctuations in the simplified procedure should introduce little additional error.

4.5.6 Alternative Procedures

Two alternative design approaches investigated in the course of this study showed promise, but ultimately proved to be inadequate. Both are empirical in that they rely strictly on simulation results. Both, also, arrive at estimates of system performance by approximating losses. In the first procedure, the total monthly losses (dumping plus storage losses), expressed as a

percentage of the monthly load, are plotted as a function of $\overline{XS}/\overline{L}$, with the storage group $\overline{S}/\eta A$ retained from Chapter 2 as a parameter. Figure 4.6 shows such a plot with linear least squares curves shown in lieu of simulation points. (The lowermost line in Fig. 4.5 represents cases with negligible dumping losses and displays, with simple manipulation, the 0.87 storage efficiency cited earlier.) In the second approach monthly dumping losses, normalized by $\overline{XS}$, are plotted as a function of the storage variable $S/\overline{XS}$. The standard deviation, $\sigma_{H/\overline{H}}$, of daily total radiation on the horizontal from the monthly mean value is included as a parameter. Figure 4.7 shows this second alternative approach.

Both of these empirical approaches work reasonably well in predicting performance for months with large $\overline{K}_T$ (i.e., for months where there is little weather variation). Neither, however, adequately accounts for weather variations in months of low $\overline{K}_T$.

The first scheme does not consider day to day variation at all, but considers parameters based strictly on monthly mean values. This leads to errors in the solar fraction of as much as 25% (absolute) compared with the corresponding simulation results.

The second approach also uses monthly mean values but attempts to consider variations through the use of an additional monthly mean parameter, namely $\sigma_{H/\overline{H}}$. This, however, does not recognize that weather variations of a given magnitude have a greater effect on the smaller of two systems even when the two systems have the same ratio of $S/\overline{XS}$. As a result, the second approach for correlating simulation results can yield poor results for low $\overline{K}_T$ months.

4.6 Summary

The results of Chapter 2 were used to discern parameters which characterize the interaction of PV system components. A practical

simplified design procedure for predicting the fraction of a given load supplied by solar was developed around these parameters and was shown to be adequate for most design purposes.

The technique, although perhaps laborious for hand calculations, has potential for adoption to hand-held programmable calculators. It certainly can be instituted on any small computer in a simple and computationally efficient manner.

The developed technique allows for assessing the impact of many design alternatives, such as array efficiency, array size, battery size, battery efficiency, power conversion efficiency, load shape and location. Since the technique uses cosine fits to the daily insolation profile it is restricted to flat arrays. However, other analytical shapes could be used to represent 2-D tracking systems.

CHAPTER 4 REFERENCES

4.1 B.Y.H. Liu and R.C Jordan, ''The Long-Term Average Performance of Flat-Plate Solar-Energy Collectors,'' Solar Energy 2, 53 (1963).

Table 4.1
Summary of Procedure for
Estimating System Performance

1. Compute $\overline{Q}_{e,n}/\overline{L}$:

   Use $\overline{K}_T$ and Fig. 4.4 to obtain a distribution of effective array outputs:

   $$Q_{e,n}/\overline{Q}_e \,, \qquad n = 1, 2, 3$$

   Use these with known $\overline{Q}_e$ and $\overline{L}$ to obtain:

   $$Q_{e,n}/\overline{L} \qquad n = 1, 2, 3$$

2. Compute $XS_n/Q_{e,n}$:

   a) Approximate the instantaneous array output using a cosine fit:

   $$\dot{Q}_{e,n}/\overline{L} = \frac{Q_{e,n}}{\overline{L}} \cdot \frac{\pi}{2(t_D - 1)} \cos\left[\frac{\pi(t - 12)}{(t_D - 1)}\right]$$

   b) Use the above output profile to compute $XS_n/Q_{e,n}$ analytically, numerically or graphically:

   $$XS_n/Q_{e,n} = \frac{1}{Q_{e,n}/\overline{L}} \left\{ \text{pos} \int_{24} \left[\frac{\dot{Q}_{e,n}}{\overline{L}} - \frac{\dot{L}}{\overline{L}} \right] dt \right\}, \qquad n = 1, 2, 3$$

3. Compute $\eta_b S/XS_n$:

   Use:

   $$\eta_b S/XS_n = \frac{\eta_b S}{(XS_n/Q_{e,n}) \cdot (Q_{e,n}/\overline{L})\ \overline{L}} \,, \qquad n = 1, 2, 3$$

4. Compute the monthly solar fraction:

   a) Use:

   $$f_{e,n} = \left\{ 1 + (XS_n/Q_{e,n}) \left[\eta_b S/XS_n - 1 \right] \right\} \cdot Q_{e,n}/\overline{L}, \qquad n = 1, 2, 3$$

   b) Average the results:

   $$f_e = \frac{1}{3} \sum_{n=1}^{3} f_{e,n}$$

Table 4.2
Comparison of Results from Simplified Procedure with Simulation Results

Location	Q_e/L	TMY Month	$S/\bar{\eta}A=0$				$S/\bar{\eta}A \equiv 10$ W-hrs/(%·m²)				$S/\bar{\eta}A \equiv 20$ W-hrs/(%·m²)			
			Solar Fraction		Difference		Solar Fraction		Difference		Solar Fraction		Difference	
			predicted	simulation	Δ	%	predicted	simulation	Δ	%	predicted	simulation	Δ	%
Albuquerque	0.6	March	0.391	0.398	-0.008	-1.9	0.503	0.488	+0.016	+3.2	0.558	0.562	-0.009	-0.7
		June	0.459	0.476	-0.018	-3.7	0.552	0.561	-0.009	-1.6	0.572	0.577	-0.006	-1.0
		September	0.404	0.411	-0.007	-1.7	0.518	0.509	+0.009	+1.8	0.561	0.566	-0.005	-0.9
		December	0.330	0.355	-0.026	-7.4	0.472	0.469	+0.003	+0.7	0.546	0.555	-0.010	-1.7
	1.0	March	0.422	0.444	-0.021	-4.8	0.619	0.623	-0.004	-0.7	0.798	0.801	-0.003	-0.4
		June	0.508	0.540	-0.032	-5.8	0.684	0.712	-0.028	-4.0	0.844	0.884	-0.040	-4.6
		September	0.439	0.456	-0.018	-3.9	0.636	0.642	-0.006	-0.9	0.819	0.842	-0.023	-2.7
		December	0.349	0.393	-0.044	-11.2	0.588	0.610	-0.022	-3.6	0.803	0.827	-0.024	-2.9
Madison	0.6	March	0.381	0.347	+0.035	+10.0	0.495	0.440	+0.056	+12.6	0.556	0.529	+0.027	+5.0
		June	0.459	0.447	+0.010	+2.2	0.542	0.538	+0.004	+0.7	0.571	0.574	-0.002	-0.4
		September	0.398	0.379	+0.018	+4.8	0.516	0.495	+0.021	+4.2	0.556	0.562	-0.006	-1.0
		December	0.290	0.242	+0.048	+19.6	0.490	0.443	+0.047	+10.7	0.538	0.535	+0.003	+0.6
	1.0	March	0.416	0.399	+0.017	+4.2	0.653	0.593	+0.061	+10.2	0.816	0.761	+0.055	+7.2
		June	0.526	0.518	+0.008	+1.4	0.723	0.732	-0.009	-1.3	0.841	0.856	-0.014	-1.6
		September	0.437	0.432	+0.005	+1.2	0.687	0.665	+0.022	+3.3	0.843	0.859	-0.016	-1.9
		December	0.312	0.278	+0.034	+12.3	0.729	0.651	+0.078	+11.9	0.755	0.782	-0.026	-3.4
Medford	0.6	March	0.380	0.357	+0.023	+6.3	0.496	0.464	+0.032	+6.9	0.554	0.553	+0.002	+0.3
		June	0.474	0.469	+0.006	+1.2	0.561	0.552	+0.009	+1.7	0.575	0.576	-0.001	-0.2
		September	0.405	0.403	+0.002	+0.6	0.525	0.515	+0.010	+2.0	0.561	0.565	-0.004	-0.7
		December	0.292	0.272	+0.020	+7.3	0.538	0.480	+0.058	+12.1	0.538	0.532	+0.006	+1.1
	1.0	March	0.413	0.413	-	-	0.652	0.643	+0.010	+1.5	0.808	0.792	+0.016	+2.0
		June	0.531	0.540	-0.009	-1.6	0.723	0.716	+0.006	+0.9	0.872	0.893	-0.021	-2.4
		September	0.440	0.450	-0.009	-2.1	0.671	0.667	+0.004	+0.6	0.847	0.872	-0.026	-2.9
		December	0.315	0.319	-0.004	-1.2	0.756	0.697	+0.059	+8.5	0.756	0.794	-0.038	-4.8

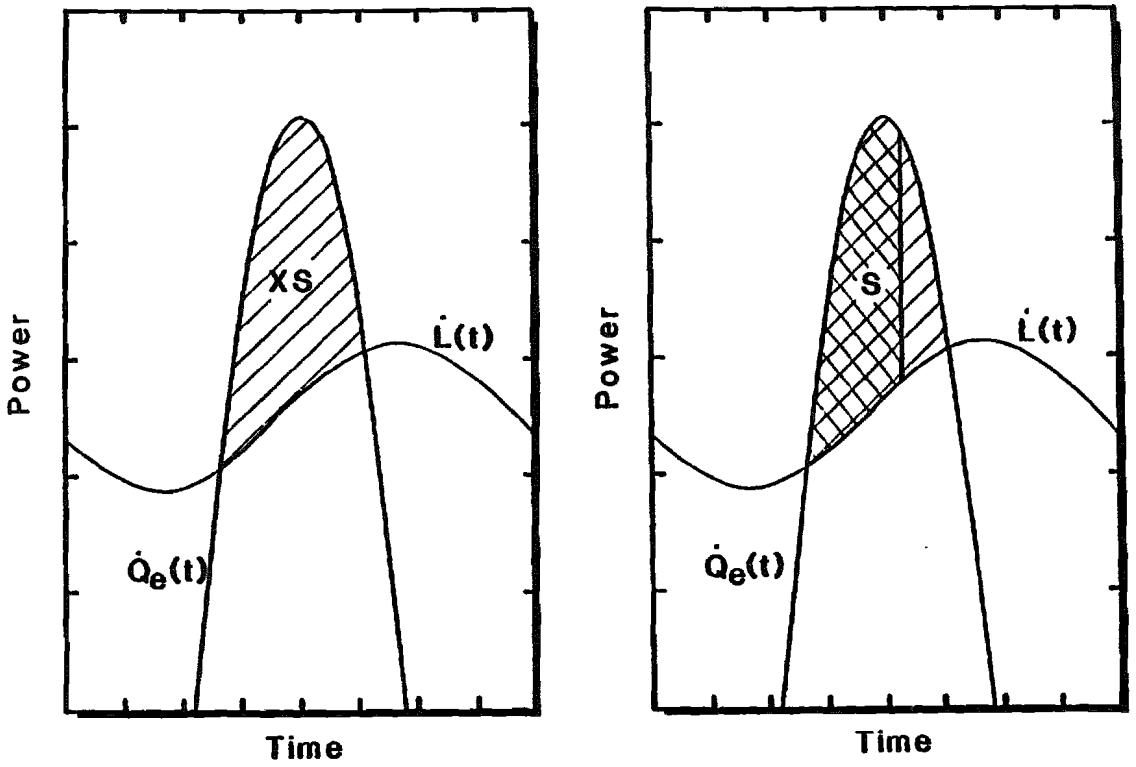

Figure 4.1 Pictoral Representation of the System Parameters $\dot{Q}_e$, $\dot{L}$, XS, and S.

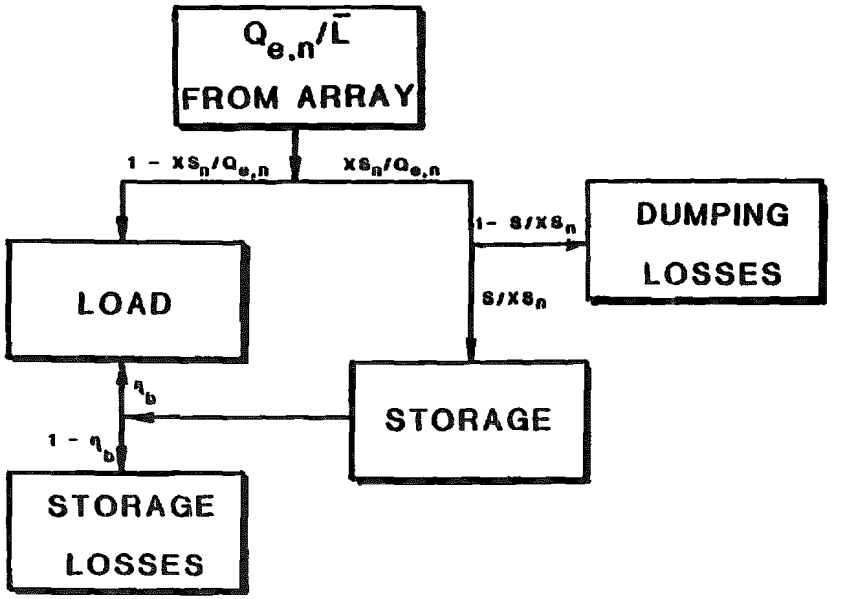

Figure 4.2 Apportionment of Effective Array Output on an Arbitrary Day.

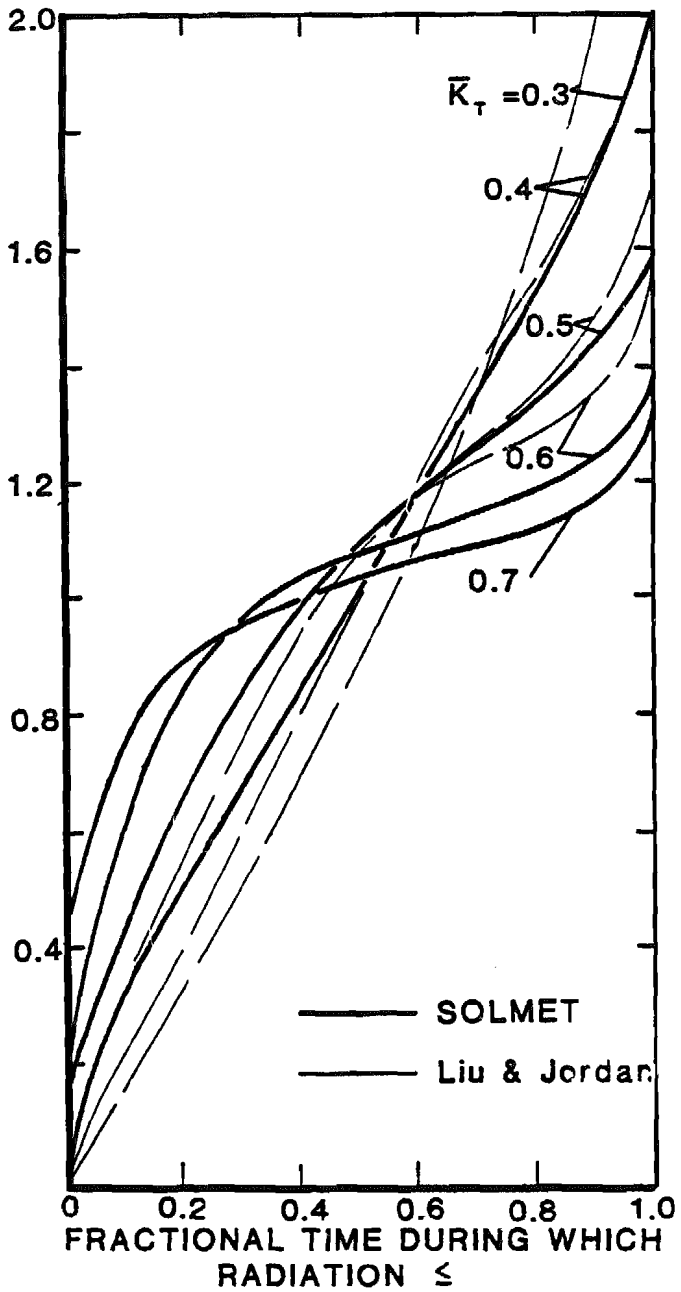

Figure 4.3 Generalized Distribution of Daily Total Radiation on a Horizontal Surface for Various $\bar{K}_T$.

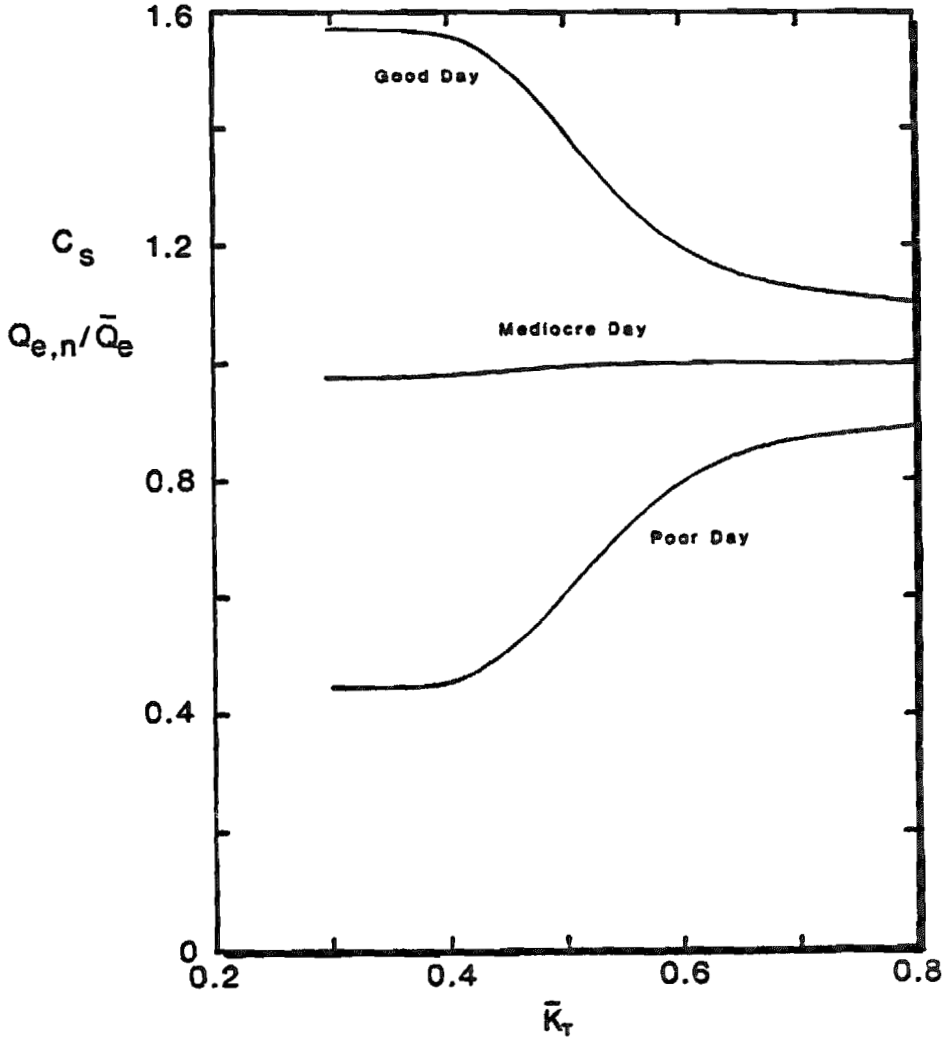

Figure 4.4 Daily Effective Array Output as a Function of $\bar{K}_T$ (3-Day Distribution).

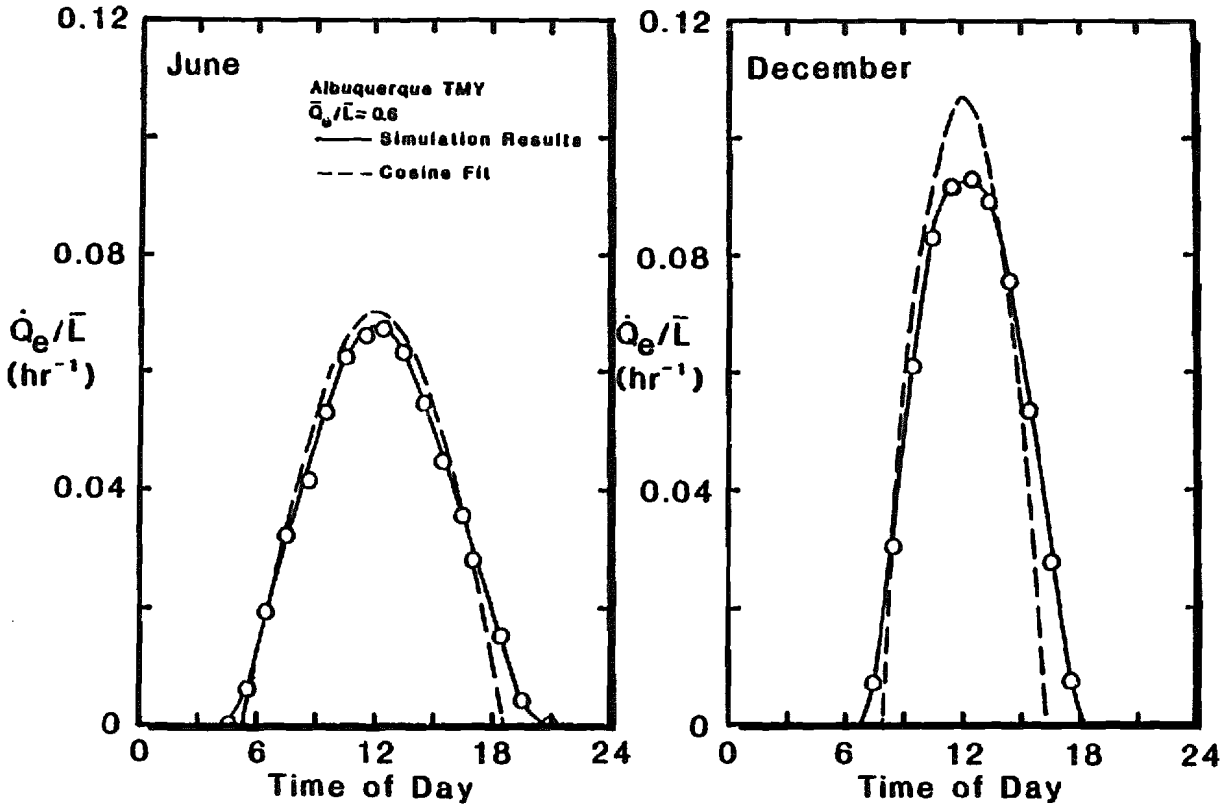

Figure 4.5 Comparison of Simulated Monthly Average Effective Array Output with Cosine Approximation for Albuquerque in June and December.

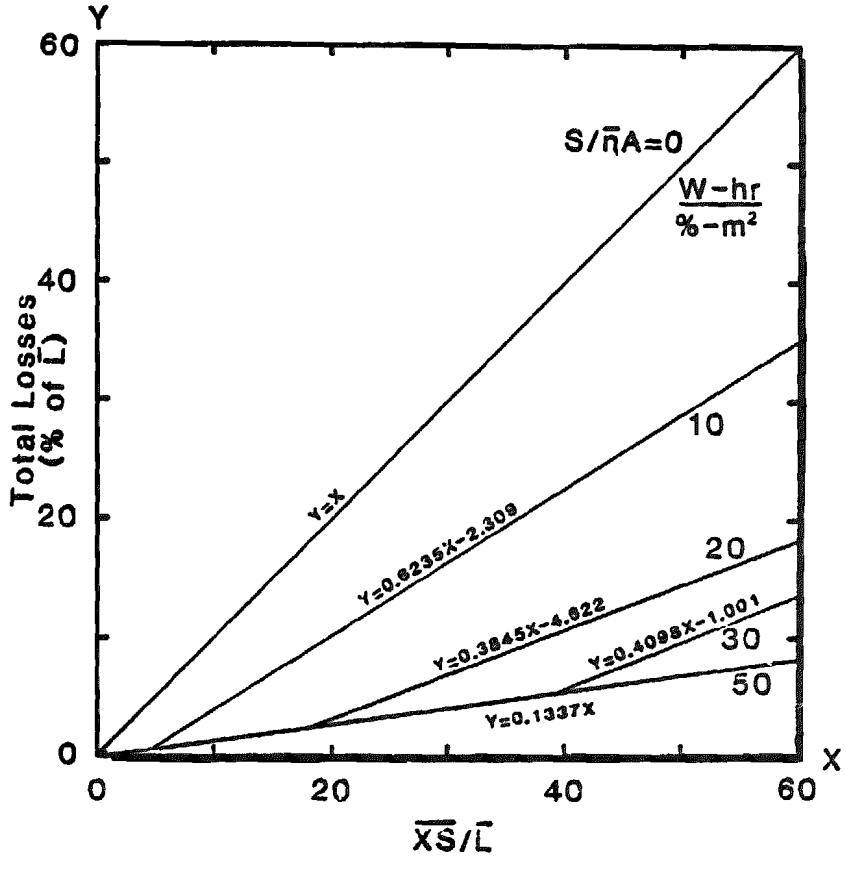

Figure 4.6 Alternative Design Procedure. Linear Least Squares Plots of Simulation Results Showing Total Losses as a Function of Monthly Mean $\overline{XS}$ and the Storage Parameter, $S/\bar{\eta}A$.

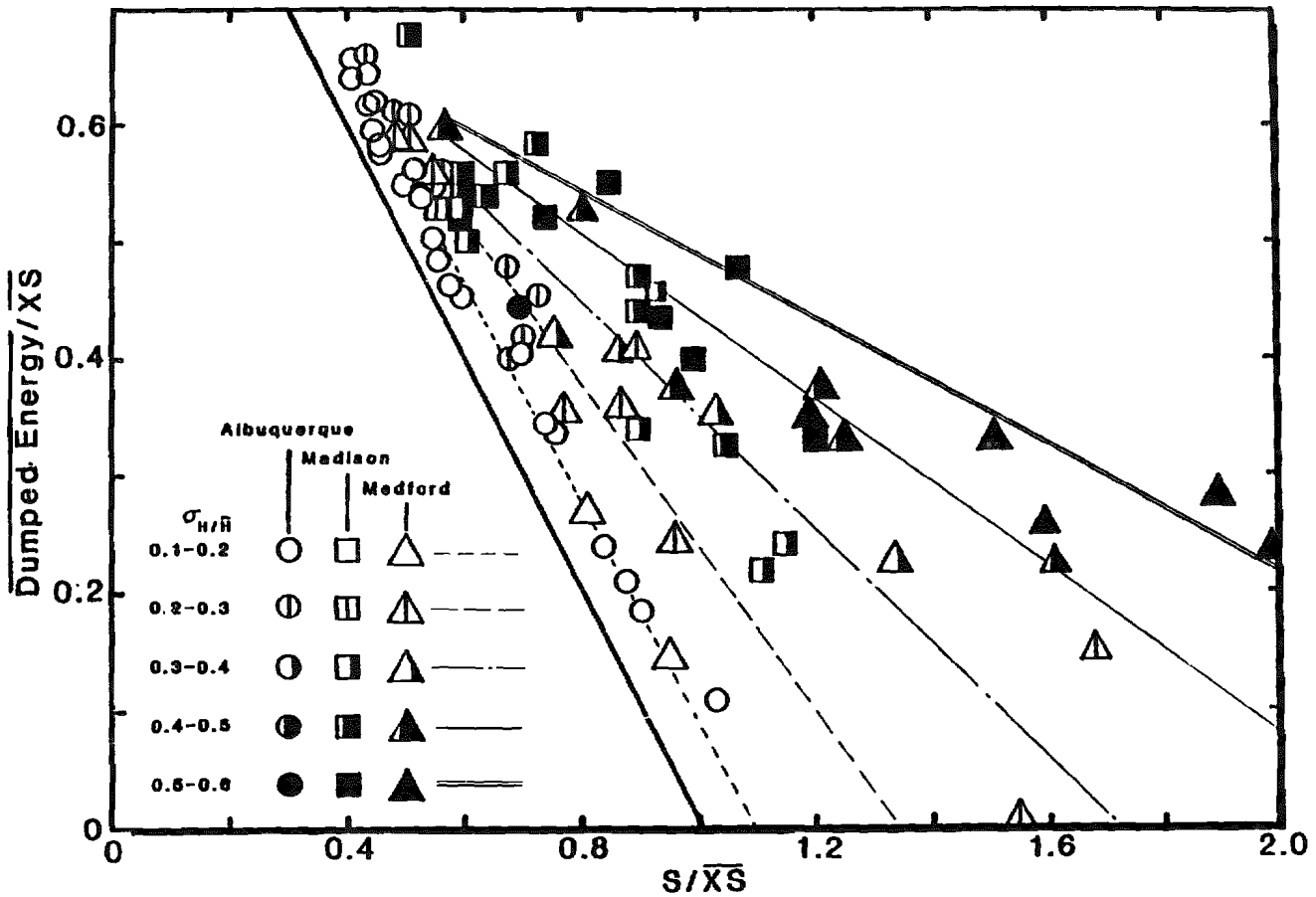

Figure 4.7 Alternative Design Procedure. Simulated Monthly Dumping Losses as a Function of Monthly Mean Values of S/$\overline{XS}$ and $\bar{K}_T$.

5.0 SIMPLIFIED METHOD FOR CLAMPED-VOLTAGE SYSTEM PERFORMANCE

All the simulations mentioned in the previous chapters are of systems operating in the max-power mode in which the voltage imposed on the photovoltaic array is dynamically adjusted to give the maximum power output at any given insolation and temperature. The other mode of operation, to be discussed in this chapter, is called the ''clamped-voltage'' mode. For systems operating in this mode, the array is in parallel with the battery; their voltages are ''clamped'' to one another. The array voltage can no longer be varied independently of that of the battery in order to obtain the maximum power possible; therefore, the power output in this mode is less than in the max-power mode. Estimation of this reduced power output is the subject of this chapter.

5.1 Photovoltaic Cell and Battery Model

5.1.1 Photovoltaic Cell Model

The difficulty encountered in simulation of the clamped-voltage mode is that electrical power produced by the array is no longer related to the insolation by the simple max-power efficiency relationship of eq. (2.4). The complete current-voltage (I-V) curve and its dependence on insolation and temperature must be expressed in some functional form.

Perhaps the most common method is to represent the cells as single or multiple diodes in parallel with direct current sources (Ref. 5.1). Although this method is suitable for computer simulation (Ref. 5.2), the equations which must be solved are too cumbersome for any simplified design.

More reasonable and straightforward is the set of equations given by:

$$V_{mp} = C_1 - C_2 (T_c - T_{r1}) + C_3 \cdot \log_{10} \dot{Q}_{sc}$$

$$I_{mp} = C_4 \cdot \dot{Q}_{sc} + C_5 (T_c - T_{r1})$$

$$V_o = C_6 (T_c + T_{r2}) \qquad (5.1)$$

$$I_{sc} = I_{mp} (1 + V_o/V_{mp})$$

$$V_{oc} = V_{mp} + V_o \ln (1 + V_{mp}/V_o)$$

$$I_c = I_{sc} \{[1-\exp[(V_c-V_{oc})/V_o]\}$$

These allow the determination of cell current (I_c), for a given cell voltage (V_c), cell temperature (T_c, C), and insolation ($\dot{Q}_{sc}$, kW/m^2). Here the constant values of the C_i's and T_{ri}'s are chosen to fit the data for a particular cell. The first two equations in (5.1) represent reasonable dependencies for the max-power voltage and current (Ref. 5.3), respectively, while the last three equations follow from the work of Lindmayer (Ref. 5.4). The third equation is merely an expression for what is commonly called the thermal voltage.

The work which follows presents some results for two different types of cell I-V curves distinguished as ''CV1'' and ''CV2''. These two cells differ primarily in their fill factor defined as

$$ff = V_{mp} \cdot I_{mp} / (V_{oc} \cdot I_{sc}) \qquad (5.2)$$

The CV1 cell has a poorer fill factor than CV2 which means that it has a less ''boxy'' I-V curve. The power versus voltage curve is thus a less peaked curve for CV1 than for CV2. This will be apparent in the results that follow.

The values of the C_i's and T_{ri}'s for CV1 and CV2 cells are given in Table 5.1. The CV1 cells are intended to represent a particular flat plate cell that may be commercially available.

The eight parameters for CV2 were chosen by least-squares fitting to duplicate Spectrolab concentrator cells as they had been modeled by the subroutine SOLCEL in TRNSYS-compatible photovoltaic subroutines (Ref. 5.2). The value of T_{r_2} so chosen, 291 C, is close to the expected theoretical value of 273 C, but the former gives a better fit to the empirical data for the Spectrolab/SOLCEL cells.

It should be pointed out that often a designer is not concerned with individual cell I-V curves but rather array I-V curves. This does not change the approach being described here. V_c, I_c, V_{oc}, I_{sc}, V_{mp}, and I_{mp} are then interpreted as array voltages and currents, Q_{sc} becomes insolation on the array and the C_i's take on new values in eqs. (5.1).

5.1.2 Battery Model

The Hyman or modified-Shepherd battery model has been used here. It is described briefly in Section 2.3 and in more detail in Refs. 5.2 and 5.5.

5.2 Dependence of Array Output upon Ratio of Solar Cells to Battery Cells

If the voltage difference across the terminals of a battery cell were constant, say V_b, and if the max-power voltage for each photovoltaic cell were fixed at V_{mp}, then the optimum number of solar cells in series per battery cell in series would simply be

$$SR^* = V_b/V_{mp}, \tag{5.3}$$

where SR is referred to as the series ratio and the asterisk denotes the optimum value.

In reality, variations with time of the insolation and solar cell temperature, upon which V_{mp} depends, and battery state of charge and current, upon which the battery voltage depends, greatly complicate prediction of the optimum series ratio, SR^*. An optimum SR does exist under these conditions, but its determination can be difficult.

Selection of a solar cell to battery cell ratio, SR, different from SR^* can lead to significant losses in array output. These ''mismatch'' losses are clearly depicted in Figs. 5.1 and 5.2 which give results of simulations for arrays CV1 and CV2 for various values of SR. For these simulations the subroutine SOLCEL has been altered to use eqs. (5.1).

The data shown in Figs. 5.1 and 5.2 represent monthly results for four months throughout the Albuquerque TMY using the baseline load (See Section 2.1.7 or Fig. 2.2). In these simulations, the array area is fixed, but L_o is adjusted from month to month so that $\bar{Q}_e/L$ is always equal to 0.6, where $\bar{Q}_e$ is η_{pc} times array output for the same system run in the max-power mode. $S/\eta A$ in these cases is 20 W-hr/(%·m²).

The four short horizontal lines in each of Figs. 5.1 and 5.2 represent the normalized[1] $\bar{Q}_{ae}$ (max-power) values for the four months graphed. The $\bar{Q}_{ae}$ results are independent of the battery and load and consequently are independent of SR.

The array, battery and load all interact in the battery-clamped mode. Thus, the results are system and load dependent, and the figures indicate the strong variation of $\bar{Q}_{ae,cv}$ with SR. However, $\bar{Q}_{ae,cv}^*$, the maximum value of $\bar{Q}_{ae,cv}$, is within 2% of $\bar{Q}_{ae}$.

---

[1]The curves in Figs. 5.1 and 5.2 have been normalized with respect to the June $\bar{Q}_{ae}$

Figs. 5.1 and 5.2 also show that SR^* (i.e., the SR corresponding to maximum electrical energy output) varies from month to month due to the different cell operating temperatures and different insolation levels from one month to another. Of these two effects, cell operating temperature is the more significant.

If the system were wired for best operation in December (i.e., $SR^* = 5.3$ for CV1 or 4.6 for CV2), then mismatch losses would be non-negligible in June (i.e., 6% loss for CV1 or 9% loss for CV2). On the other hand, if the system were arranged to give best performance in June, then mismatch losses would be small for the other months, including December. This is because: (1) June has the highest value of SR^* (the cells are typically warmest in June and have the lowest V_{mp}) and (2) the $\bar{Q}_{ae,cv}$ vs SR curves are asymmetric, with the $SR > SR^*$ portions much less steep than the segments for $SR < SR^*$.

The computer simulation required for the results in this section can involve considerable expense. For each system configuration (i.e., array size, battery size, and load) simulations need to be run at a number of SR's in order to define performance curves like those in Figs. 5.1 and 5.2. in addition to the expense involved in design based upon computer simulation, the difficulty in assembling a TRNSYS data deck, particularly for the inexperienced programmer, should not be underestimated.

Sections 5.3 and 5.4 discuss two approaches for estimating system performance which are easier to use than TRNSYS simulations. The non-computer-based approach of Section 5.3 was ultimately unsuccessful, but the method of Section 5.4, although computer-based, yielded high accuracy in a preliminary validation study.

5.3 Non-Computer-Based Prediction Method

5.3.1 Prediction of Performance as a Function of SR for a Given SR*

The shapes of the performance curves in Figs. 5.1 and 5.2 are a result of the solar cell I-V curves and their variation with cell temperature and insolation throughout the month. It is not unreasonable to expect, however, that the most important I-V curve is the one corresponding to average midday cell temperature and average midday insolation. Certainly electrical energy production is greatest near midday since that is typically the time of highest insolation. This period of the day would then contribute most significantly to the total electrical energy production for the month. This reasoning then forms the crux of the hypothesis on which the work described in this section is based. Simply stated, the hypothesis is that once SR^* and $\bar{Q}_{ae,cv}{}^*$ are known, monthly average midday temperatures and insolation can be used to determine the performance curve of $Q_{ae,cv}$ vs SR.

This hypothesis has been validated for 8 different systems (various $\bar{Q}_e/\bar{L}$, $\bar{S}/\eta\bar{A}$ combinations) using CV1 cells and 4 different systems using CV2 cells. The monthly average midday temperature and insolation values are obtained from the results presented in Chapter 3. These are then used in eqs. (5.1) to obtain the midday I-V curve. The following example is included to show both the validity of the hypothesis and all the steps required:

Example: Albuquerque, March TMY

SR^* = 5.6 assumed known (taken from TRNSYS simulations)

$\bar{K}_T$ = 0.664 (from March TMY data)

$\emptyset$ = 35°

CV1 cells

Array: Flat-Plate (south facing)

$s = \emptyset = 35^\circ$ (array tilt equal to latitude)

$\tau = 0.88$

$\rho = 1$

$\alpha = 0.77$

$K_e = 72\ kJ/(hr \cdot m^2 \cdot C) = 0.02\ kW/(m^2 \cdot C)$

$A_{cell} = 0.007854\ m^2$

Midday Insolation (Monthly Average)

From Fig. 3.18: $\dot{Q}_s(12) = 0.929\ kW/m^2$

From Table 3.2: $(s_M - s) = (s_M - \emptyset) = 3^\circ$

Since Fig. 3.18 assumes an optimum tilt, a cosine correction is made to yield the insolation on this non-optimum tilt. The parameters shown in Table 5.1 for the CV1 cells produce a cell I-V curve as opposed to an array I-V curve. Therefore, the insolation must be multiplied by the encapsulant transmittance before it is used in eqs. (5.1). If an array I-V were being studied, τ would be set to 1.0.

$$\dot{Q}_{sc}(12) = \dot{Q}_s(12) \cdot \tau \cdot \cos(s_M - \emptyset) = 0.816\ kW/m^2$$

Midday Cell Temperature, Voltage and Power (First Iteration)[2]

From Fig. 3.6a

$$K_e \overline{(T_c - T_a)}/(\alpha\rho) = 3.517\ MJ/(m^2 \cdot hr)$$

Then

$$\overline{T_c - T_a} = 3.517\alpha\rho/K_e = 37.8\ C$$

Also

$$C_f = \cos(s_M - \emptyset) = 1.0$$

[2]The need for and purpose of iteration is described in Chapter 3

For Albuquerque March TMY

$$T_M = 6.8 \text{ C.}$$

Then the monthly average midday cell temperature, $\bar{T}_c$, is given by[3]:

$$\bar{T}_c = C_f \overline{(T_c - T_a)} + T_M + 3 = 47.6 \text{ C,}$$

For CV1 cells, eqs. (5.1) yield:

$$V_{mp} = 0.396 \text{ V}$$

$$P_{mp} = 0.741 \text{ W}$$

and

$$\eta = P_{mp}/[\dot{Q}_{sc}(12) \cdot A_{cell}] = 0.116$$

Midday Cell Temperature, Voltage, and Power (Second Iteration)[4]

$$\overline{T_c - T_a} = 3.517 \cdot \rho(\alpha - \eta)/K_e = 32.2°C$$

$$\bar{T}_c = C_f \overline{(T_c - T_a)} + T_M + 3 = \underline{42.0 \text{ C}}$$

$$V_{mp} = .410V$$

$$P_{mp} = .758W.$$

These values of midday cell temperature and insolation are then used in eqs. (5.1) to obtain the P-V curve shown in Fig. 5.3.

---

[3]It is assumed here that T_M+3 is representative of monthly average midday ambient temperature.

[4]Op. cit. 2.

The next step in deriving a $\bar{Q}_{ae,cv}$ vs. SR curve is to rescale the vertical axis in Fig. 5.3 as is done in Fig. 5.4. Here it is assumed that $\bar{Q}_{ae,cv}$ is directly proportional to the power output by a single cell at midday on an average day, or

$$\bar{Q}a_{e,cv}/\bar{Q}_{ae,cv}^{*} = P/P_{mp} \tag{5.4}$$

Thus the ordinate in Fig. 5.4 is both the dimensionless midday power output and the predicted dimensionless $\bar{Q}_{ae,cv}$.

With V_{mp} calculated under average midday conditions, it is assumed that the typical cell voltage at noon is inversely proportional to the series ratio, i.e.

$$V/V_{mp} = SR^{*}/SR, \tag{5.5}$$

or

$$SR = SR^{*} \cdot V_{mp}/V \tag{5.6}$$

Eq. (5.6) is used in going from voltage as the abscissa in Fig. 5.3 to SR on the horizontal axis in Fig. 5.4. SR^{*} is taken to be 5.6, which simulations found to be the optimum series ratio in March in Albuquerque, for a system with $\bar{Q}_e/\bar{L} = 0.8$ and $S/\bar{\eta}A = 20.3$ W-hrs/(%·m²).

Replotting to restore a uniform scale on the horizontal axis for the data of Fig. 5.4 gives the dashed performance curve shown in Fig. 5.5. The results of TRNSYS simulations are given by the solid curve in the same figure. The two curves are almost identical for $SR > 5$.

The change of scale and replotting procedure used in going from Fig. 5.3 to 5.5 clearly shows that: (1) the steep side of the $\bar{Q}_{ae,cv}$ vs SR curve corresponds to the steep side of the P–V solar cell curve, and (2) the inflection on the right side of the

curve is due to the change of scale on the abscissa from V units to SR units.

Finally, prediction of array output from the dimensionless ordinate in Fig. 5.5 requires knowledge of $\bar{Q}_{ae,cv}^{*}$. Figs. 5.6 and 5.7 indicate that

$$\bar{Q}_{ae,cv}^{*} = 0.98\ \bar{Q}_{ae}. \tag{5.7}$$

If an estimate of $\bar{Q}_{ae}$ is available (e.g, from the procedure of Chapter 3), then $Q_{ae,cv}^{*}$ can be predicted.

The technique described in this section lumps clamped-voltage system considerations, particularly the photovoltaic array-battery interactions, into the parameter SR^{*}, the choice of which will be discussed in the next section.

5.3.2 Prediction of SR^{*}

In this sub-section a method for predicting the monthly optimum SR is described. It does not rely on the use of computer calculations, but has been found to be erratic and thus, unreliable. A description of the approach is included here in order to show that a complete, non-computer-based method has been attempted and to justify use of the computer-based method of Section 5.4.

A simple approach for determining SR^{*} would involve the use of eq. (5.3) if an appropriate battery voltage and solar cell max-power voltage could be determined. Since the procedure of Section 5.3.1 worked well using midday I-V curves, a similar approach was attempted here. V_{mp} was chosen in the manner demonstrated in the example of that section. Attempts were then made to determine V_b, battery voltage, for the monthly average midday conditions.

Battery voltage at any time of the day depends on the battery charging (or discharging) current and state of charge. (The systems and loads used here typically resulted in battery charging rather than discharging at midday.) V_b can thus be determined from estimates of midday values of these quantities. Unfortunately, these are difficult to predict.

A fairly complicated procedure was developed to estimate battery current and state of charge. It first uses the prediction of P_{mp} at noon to give a value of $\dot{Q}_e$ at noon and also to generate a cosine curve for $\dot{Q}_e(t)$, in a method resembling that of Chapter 4. From these values and $\dot{L}(t)$, an $\dot{X}S$ at noon and an integrated XS from sunrise to noon were determined. Division by the storage capacity and other factors yielded the midday current and state of charge, respectively.

For some systems this approach gave estimates of V_b and thus, SR^* [see eq. (5.3)] which are close to the values from simulation results. However, this is not generally the case; the method is highly erratic.

The difficulty is due to the basic problem of predicting photovoltaic array-battery interactions. Estimating battery behavior is difficult even in the max-power case, when array output is independent of battery fluctuations. In the clamped-voltage mode, prediction is further complicated by the ''feedback'' from battery to array. A simplified design procedure akin to those described in Chapters 3 and 4 does not appear to be feasible for estimating performance of a clamped-voltage system.

5.4 Computer-Based Prediction Method

The results of the previous section indicate that: (1) a technique capable of handling array-battery interactions is necessary in order to predict clamped-voltage system performance,

and 2) use of estimates of cell temperature and insolation at noon is justified to a certain extent. These conclusions suggested the development of the computer program to be described in this section. The program accurately reproduces curves such as those in Figs. 5.1 and 5.2, but with a reduction in computer time by a factor of about 25 in comparison with TRNSYS simulations. It should also be much easier to use in design applications than a detailed program like TRNSYS.

A flowchart for the new algorithm is given in Fig. 5.8. The program essentially simulates a given clamped-voltage system (fixed array size, battery size, and load) with a given SR during three representative days of a month. As indicated in the figure, the primary inputs are the quantities T_M, $\bar{K}_T$, and $\bar{Q}_s$, along with the load profile $\dot{L}(t)$. A listing of the program is not included here since the program is presently not in a state that would allow easy use by others.

The flowchart is explained from the bottom up (from the simple to complex) in the remainder of this section, emphasizing the four concepts embodied in the procedure: (1) simulation of clamped-voltage system performance during a single day, (2) approximation of daily insolation and PV cell temperature profiles by cosine curves, (3) prediction of the peaks of each of these curves, and (4) representation of day-to-day variations in insolation during a month by the insolation patterns on three statistically determined days.

Step 4 of the Fig. 5.8 flowchart simulates a day's operation of a clamped-voltage system by the same iterative procedure used in TRNSYS. At each time step, the inputs $T_c(t)$ and $\dot{Q}_{sc}()$ enter the CV1 or CV2 cell eqs. (1), thereby fixing a solar cell I-V curve. The program combines this information with a value of $\dot{L}(t)$ and with the Hyman model for $V_b = V_b(I,F)$ to match the array and battery voltages. This process is repeated hourly.

Because the program need only determine the array output, $Q_{ae,cv}$, it only simulates the daylight, power-producing hours. Other simplifications make the program much more tractable and less expensive to run than a general TRNSYS simulation. For example, it is assumed that the battery rarely discharges during the daylight hours, so only the charging portion of the Hyman battery model is included in the program.

$T_c(t)$ and $\dot{Q}_{sc}(t)$, the functions input to step 4 of the program, are determined in step 3. Estimates of the peak of the insolation, $\dot{Q}_{sc}(12)$, and of the total daily insolation, Q_{sc}, specify an insolation cosine curve. An ''effective daylength,'' $t_{D,e}$, is then found. This value plus a prediction of the noontime cell temperature, $T_c(12)$, yield a cosine approximation for $T_c(t)$.

The only location considered thus far with regard to clamped-voltage system performance is Albuquerque. Based upon TMY data for this city, TRNSYS-generated average daily insolation and temperature profiles for any month are shifted to the right, with their peaks occurring after 12:00 noon. In the case of the insolation, the shift is apparently due to cloud patterns in Albuquerque. The peak of cell temperature curves occurs at an even later time because of the rise in ambient temperature during the early afternoon.

The phase shift in cell temperature is presently accounted for in the program only by introduction of a time lag of one-half hour after solar noon in the $T_c(t)$ profile. This 30 minute interval approximates the delay found in the monthly outputs of several TRNSYS simulations. The insolation curves have not been shifted.

The peaks of the $T_c(t)$ and $Q_{sc}(t)$ profiles are determined in step 2 of the program by the method analogous to that of Chapter 3 and described via the example in Section 5.3.1.

Step 1 also uses previous results to select three values of the insolation multiplier, C_s. For a given K_T, the values are read directly off the vertical axis of the three-day insolation distribution, Fig. 4.4. C_s then multiplies $\dot{Q}_{sc}(12)$ and $\bar{Q}_s$ to give estimated peak and total insolation values on each of three representative days from a given month.

The computer program which implements the flowchart of Fig. 6 is structured to run three times in succession, once for each of the three values of C_s. The three resulting values of $Q_{ae,cv}$ are then averaged to give $\bar{Q}_{ae,cv}$.

The entire scheme is repeated for incremental SR to yield predictions of $\bar{Q}_{ae,cv}$ vs. SR such as those shown in Fig. 5.9. Comparison with TRNSYS results demonstrates the high accuracy of the simplified program. Depicted are the results for the months of June and December, but comparably close agreement holds for March and September data as well.

Because these studies are only for a certain size system, load profile, and location, the results are only preliminary validations of the simple program. However, the high accuracy achieved thus far and the apparent adaptability of the program (e.g., for various load distributions) point toward continued utilization of the method and perhaps to its eventual use in actual clamped-voltage system design.

CHAPTER 5 REFERENCES

5.1 H.J. Hovel, Semiconductors and Semimetals, Volume 11, Solar Cells, Academic Press, New York, NY (1975).

5.2 D.L. Evans, W.A. Facinelli and R.T. Otterbein, ''Combined Photovoltaic/Thermal System Studies,'' Report SAND78-7031, Arizona State University, Tempe, AZ (1978).

5.3 ''Solar Cell Array Design Handbook, Volume 2,'' Jet Propulsion Laboratory, Pasadena, CA (1976).

5.4 J. Lindmayer, ''Theoretical and Practical Fill Factors in Solar Cells,'' Comsat Technical Review, Vol. 1, No. 2 (1972).

5.5 G.W. Vinal, Storage Batteries, John Wiley and Sons, New York, NY (1955).

Table 5.1

Constants Used in Eqs. 5.1
for Determining I-V Curves

CONSTANT	Cells		UNITS
	CV1	CV2	
C_1	0.452	0.459	volts
C_2	0.00251	0.00236	volts/°C
C_3	0.031	0.0246	volts
C_4	2.200	0.104	amps.m^2/kW
C_5	0.0038	-0.00004	amps/°C
C_6	0.0002	8.47×10^{-5}	volts/°C
T_{r1}	28.	51.3	°C
T_{r2}	273.	291.	°C

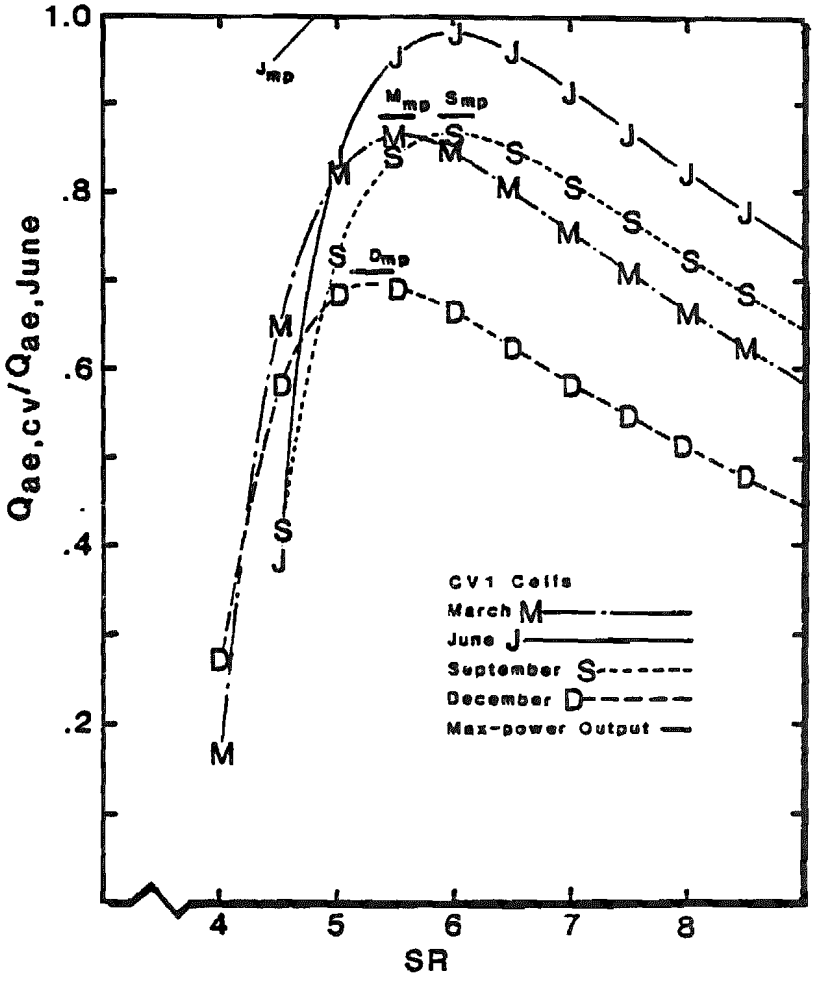

Figure 5.1 Normalized Monthly Performance vs. Series Ratio, CV1 Cells, $\bar{Q}_e/\bar{L}$ = 0.6, $S/\bar{\eta}A$ = 20 W-hrs/(%m^2).

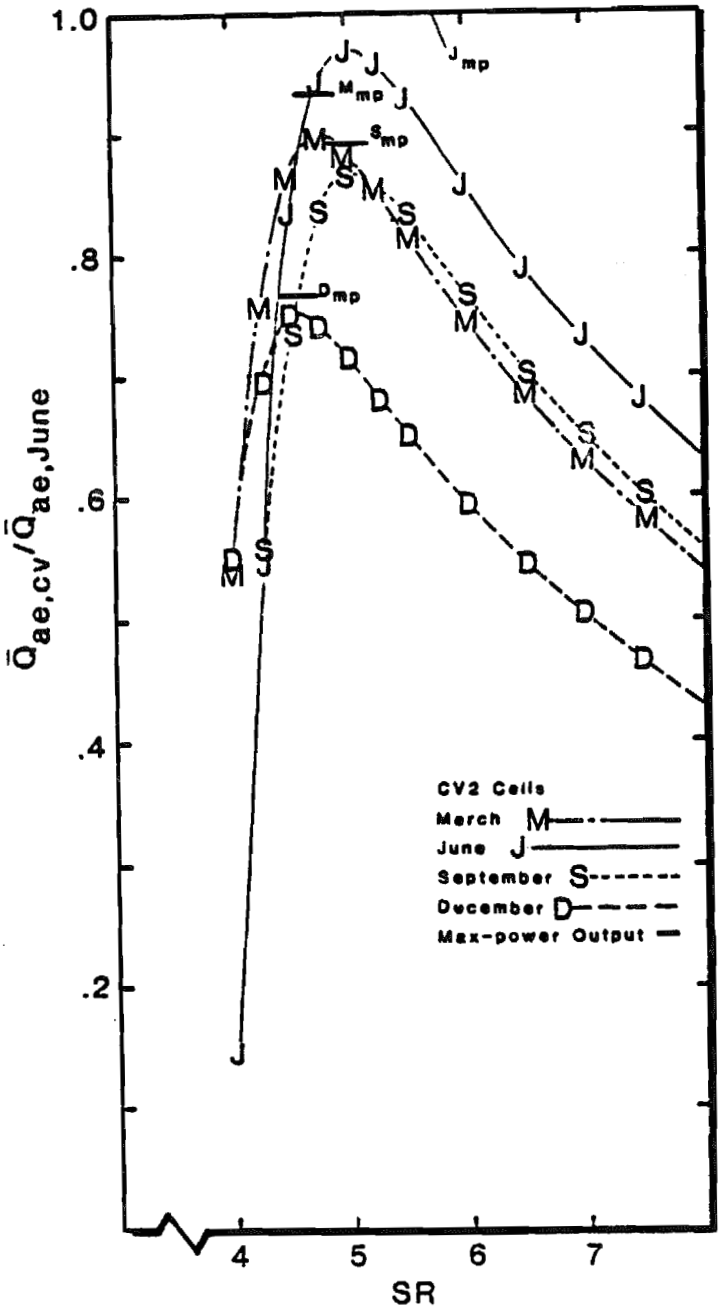

Figure 5.2 Normalized Monthly Performance vs. Series Ratio, CV2 Cells, $\bar{Q}_e/\bar{L}$ = 0.6, $S/\bar{\eta}A$ = 20 W-hrs/(%m^2).

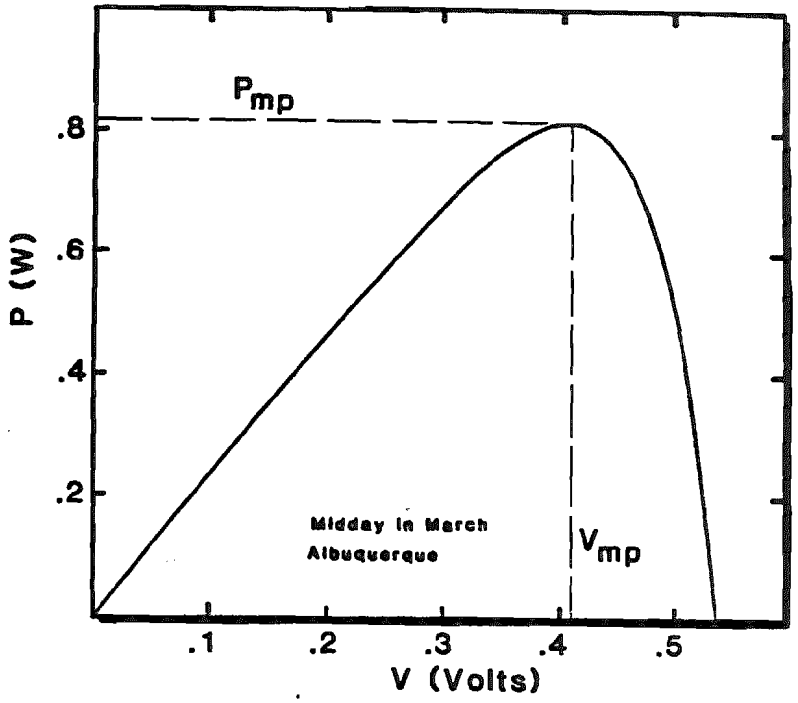

Figure 5.3 Power Output vs. Cell Voltage for a CV1 Cell at Midday on an Average March Day in Albuquerque.

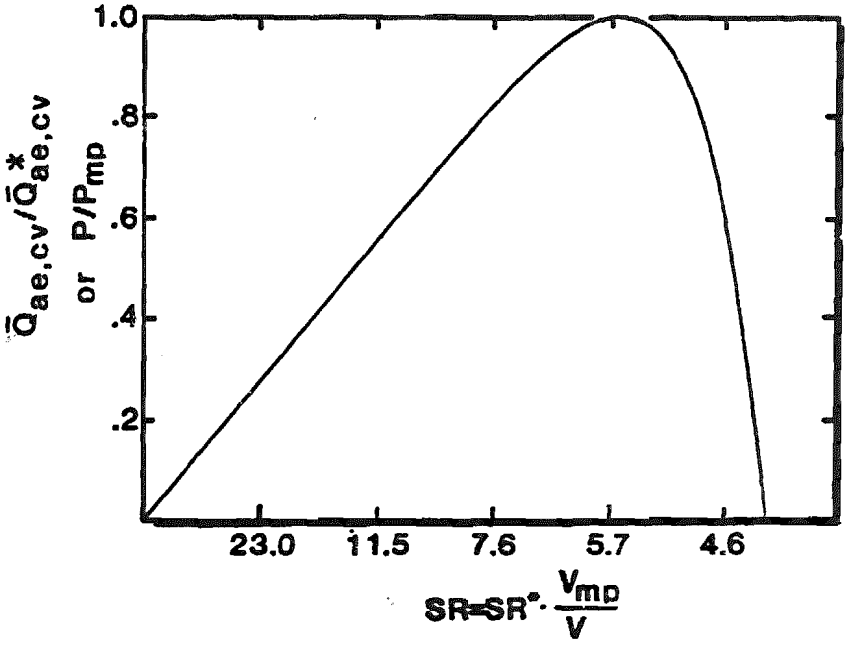

Figure 5.4 Normalized Array Output or Cell Power vs. Series Ratio, Obtained by Rescaling Fig. 5.3 (SR* = 5.6).

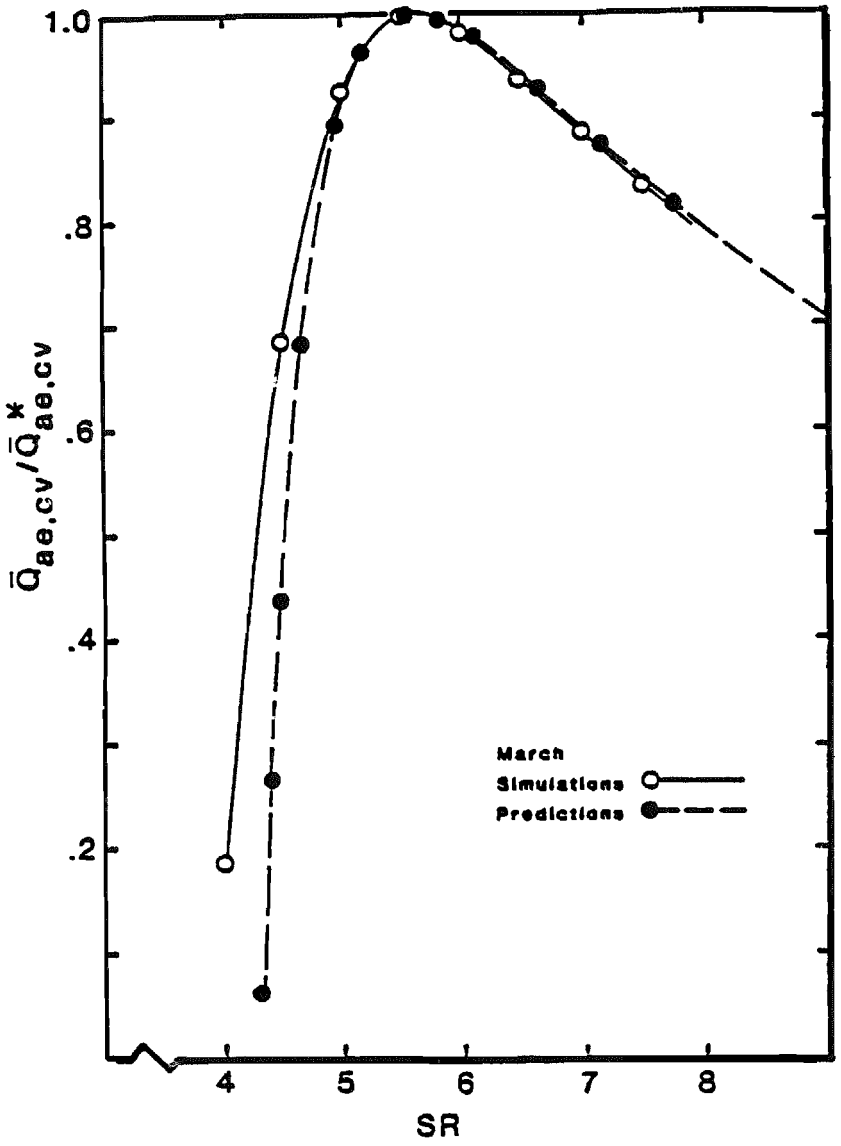

Figure 5.5 Normalized Array Output vs. Series Ratio, from TRNSYS Simulations and from Linearizing the Scale of Fig. 5.4. $\bar{Q}_e/\bar{L}$ = 0.8, $S/\overline{\eta A}$ = 20.3 W-hrs/(%m²)

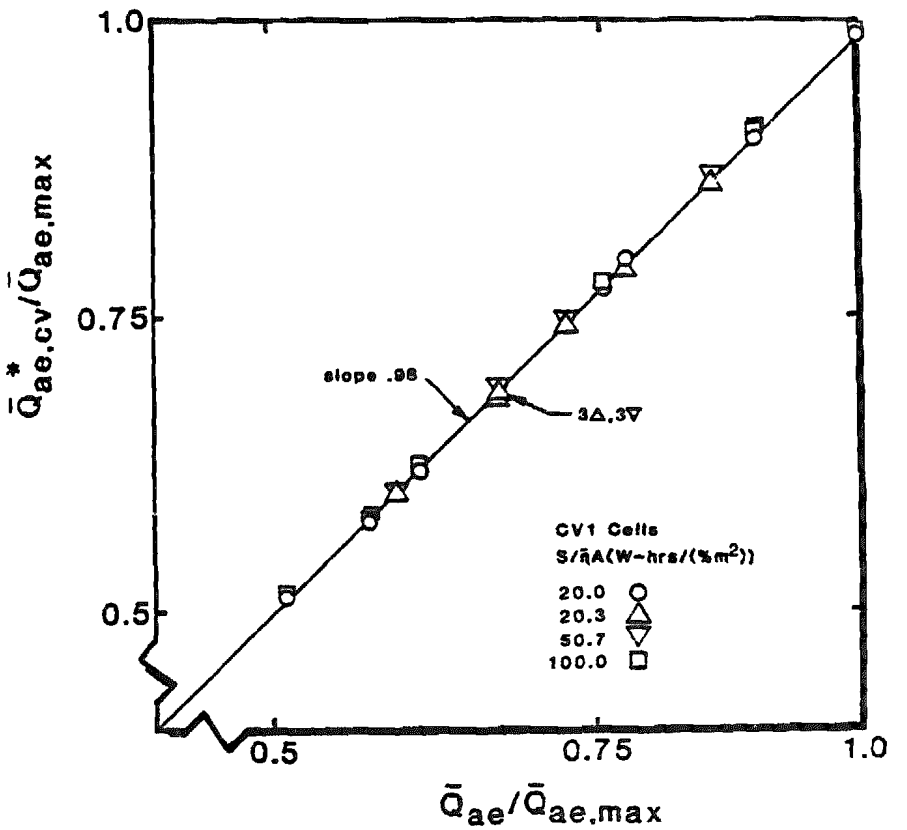

Figure 5.6 Optimum Clamped Voltage Array Output vs. Max-Power Array Output, CV1 Cells, Normalized by Maximum $\bar{Q}_{ae}$.

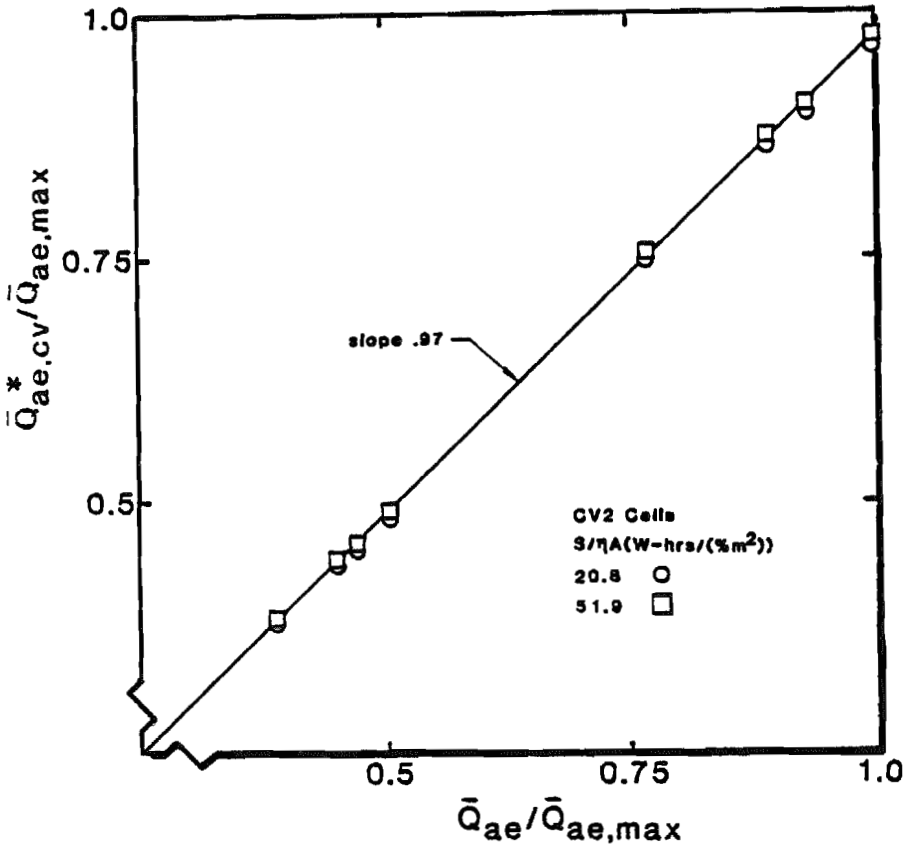

Figure 5.7 Optimum Clamped Voltage Array Output vs. Max-Power Array Output, CV2 Cells, Normalized by Maximum $\bar{Q}_{ae}$.

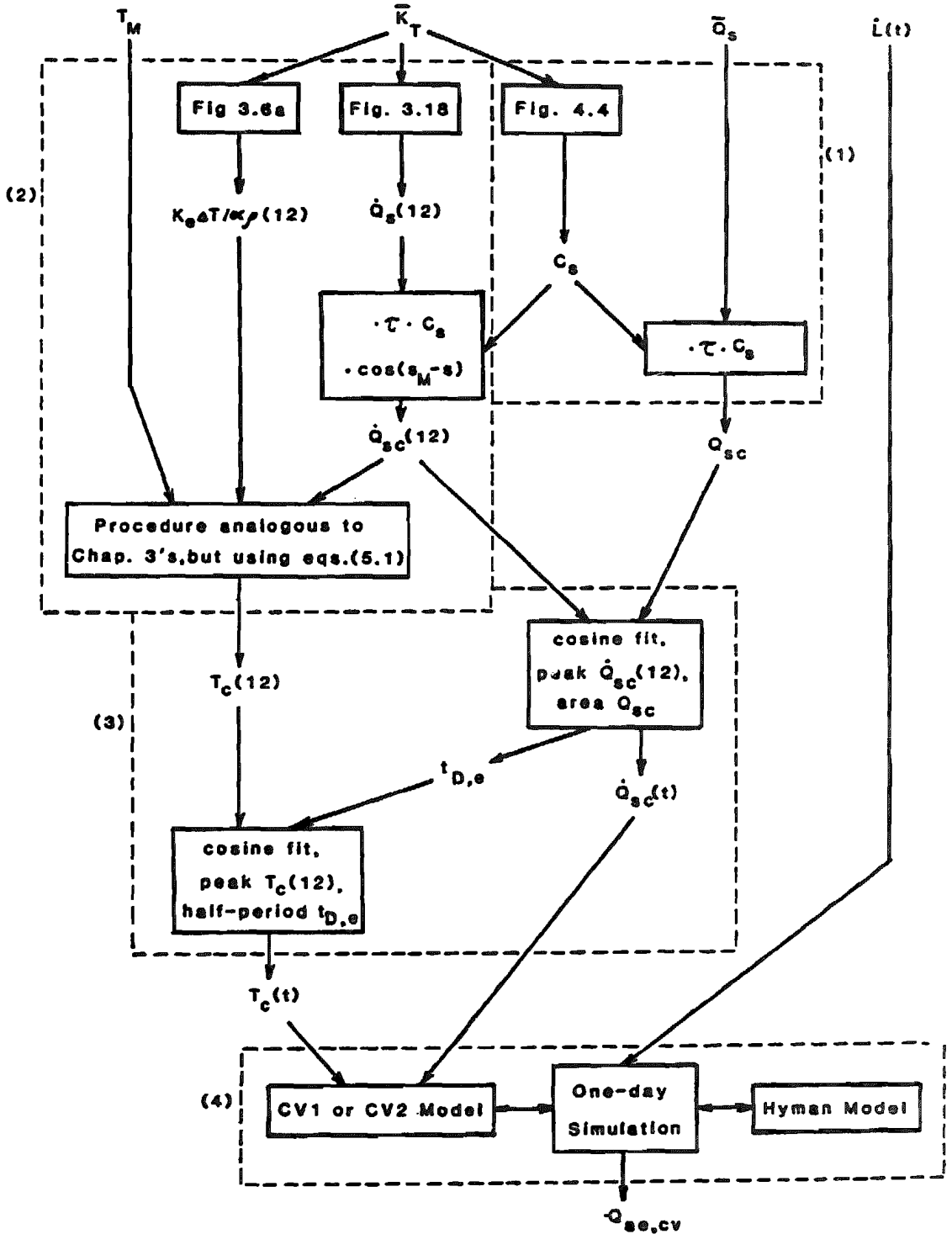

Figure 5.8 Information Flow Diagram of Average-Day Simulation Program for Clamped-Voltage Systems.

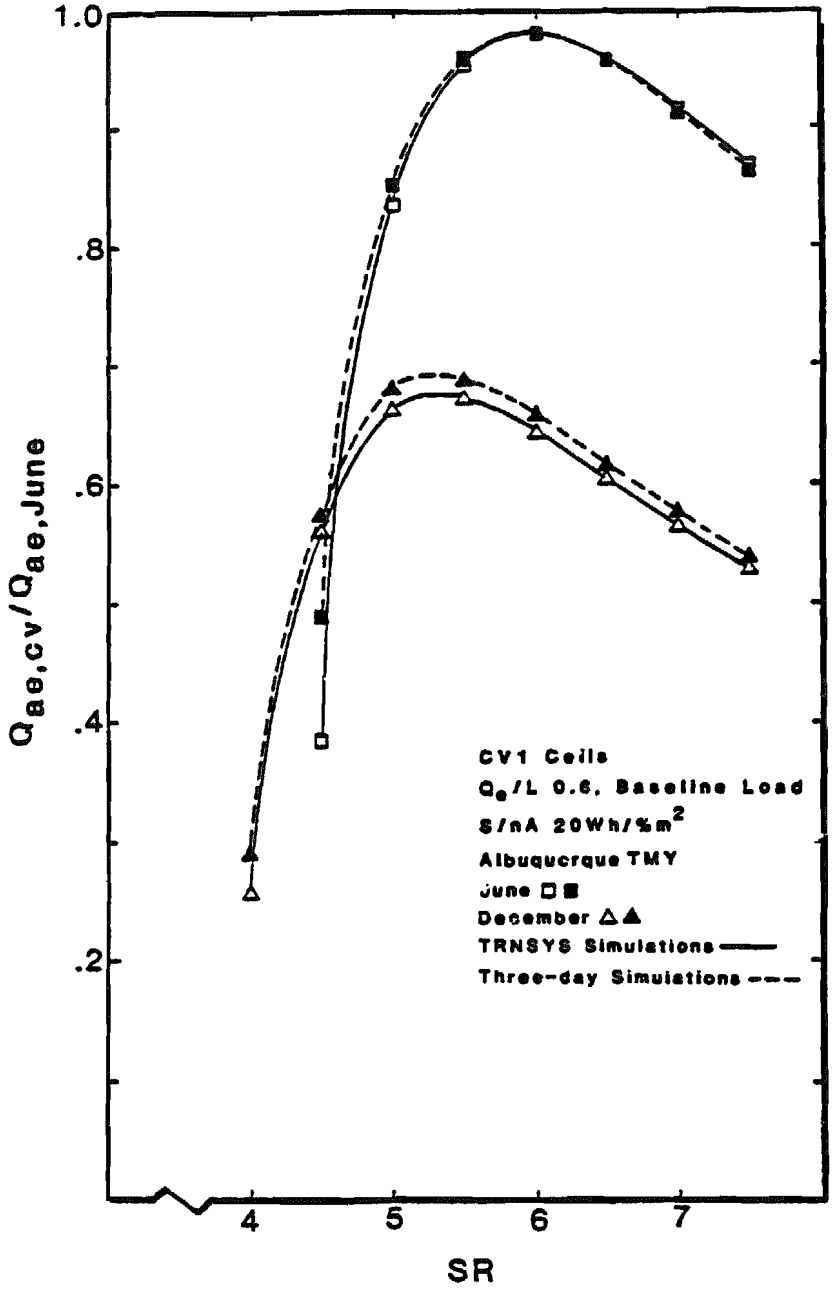

Figure 5.9 Comparison of TRNSYS and Average-Day Program Simulation Results.

6.0 DISCUSSION, CONCLUSIONS AND SUMMARY

The findings of this study are reviewed and discussed in the first four sections of this chapter. The last section includes an example of array and battery sizing for a PV system in two locations.

6.1 Simulation Results

The simulation results discussed in Chapter 2 have been found to correlate well using the parameter $\bar{Q}_e/\bar{L}$ along with either $S/\bar{\eta}\bar{A}$ or $S/\bar{\eta}\bar{A}\bar{Q}_s$. $\bar{Q}_e/\bar{L}$ is the ratio of monthly average daily array output (multiplied by the power conversion efficiency) to the monthly average daily electrical load. $S/\bar{\eta}\bar{A}$ is the ratio of storage capacity to effective array area while $S/\bar{\eta}\bar{A}\bar{Q}_s$ is the ratio of storage capacity to array output. For a given location, $S/\bar{\eta}\bar{A}\bar{Q}_s$ is a better parameter than $S/\bar{\eta}\bar{A}$ when array tilt is used to vary the insolation on the array. The parameter $S/\bar{\eta}\bar{A}$ is very useful when considering optimally tilted arrays or when comparing results for two different locations that have similarly tilted arrays (i.e., tilts that vary from optimum for each location by a fixed increment).

For optimally tilted or similarly tilted arrays, the parameter $S/\bar{\eta}\bar{A}$ collapses the data for many locations onto nearly single curves for equivalent $\bar{Q}_e/\bar{L}$, a given load shape and equal daylengths. The result is analogous to an f-Chart (Ref. 6.1) and yields the fraction of the electrical load supplied by the PV system as a function of array size and battery size, for a given diurnal load shape and time of year (daylength).

Such an f_e-Chart shows that storage sizes greater than that determined from $S/\bar{\eta}\bar{A} \sim 50$ W-hrs/(%·m²) do not improve system performance. For example, for 100 m² of 10% efficienct array, battery sizes in excess of 50 kW-hrs would never be warranted, regardless of daylength, geographical location, or, within reason, diurnal load shape. Below $S/\bar{\eta}\bar{A} = 50$ W-hrs/(%.m²), both daylength and load shape become increasingly important in determining f_e. The knees

of the f_e versus storage curves depend on both $\bar{Q}_e/\bar{L}$ and load shape. But, they typically occur in the range of 20 to 30 W-hrs/(%·m²). These two criteria are useful design ''rules of thumb'' with regard to storage capacity.

The load shape referred to above is the monthly average diurnal shape. Obviously, the better the match between the load and the array output, the higher the solar fraction. However, this study has found that random fluctuations on this load shape have little effect on system performance even for the case of no storage. This information should make simplified design techniques more useful.

Three different battery models were considered in the simulations, but were found to have little effect on overall system performance. Temperature effects were not included in this study, because little data exist on the temperature dependence of battery performance. Available data suggest that batteries which operate in cold environments would have significant decreases in performance.

Although the simulations conducted here (or any finite number of simulations) provide useful insight into system operation and sensitivity and a few useful ''rules of thumb,'' they do not provide a useful tool to the designer for specific applications. For that purpose one needs a fairly general simplified design technique that can accommodate arbitrary load shapes and daylengths. Such techniques were discussed in Chapters 3, 4 and 5 of this report, and are reviewed in the following sections.

6.2 Simplified Procedure for Predicting Array Output

A simplified procedure for predicting array monthly electrical output was developed in Chapter 3. It works for flat arrays and 2-D tracked systems which are passively cooled and max-power tracked. The procedure, estimates a monthly average array efficiency which can be multiplied by the monthly array insolation to yield monthly electrical production.

Input information needed by a designer consists of mean monthly temperature, monthly $\bar{K}_T$ values and wind speed data for the intended location of the array, monthly collector tilts (for a flat array) and some reference information on the arrays. This reference information includes a reference efficiency at a reference temperature and either the thermal conductance between the cells and the ambient or the array NOCT.

The procedure is extremely accurate and easy to use. Although it can be carried out by hand, it can also be programmed on a hand-held calculator for improved ease of use.

Procedures for calculating insolation on the array were not studied here since both calculation schemes and tabular data are available in the solar field.

6.3 Max-Power Tracked System Results

In Chapter 4, a simplified design procedure was developed which estimates monthly overall performance of a PV system having a passively cooled flat PV array. The procedure considers the effects of limitations in storage capacity (including no storage) and equivalent ''round trip'' battery storage efficiencies as they reduce the portion of the array output which eventually reaches the load.

The procedure uses long term distributions of daily insolation of the type first introduced by Liu and Jordan (Ref. 6.2) to obtain an expected distribution of daily array energy production. This distribution, which accounts for the effect of day to day variations on system performance, is used to characterize array performance on three separate days: a good day, a mediocre day and a poor day. The instantaneous power output of the array is reconstructed through the use of a cosine fit based on daylength and the total array output on each of the three days.

The daily interaction between the array output and the load can be calculated from knowledge of only a few monthly mean values. The method requires specification of a daily electrical load profile, battery storage capacity and efficiency along with mean monthly daylength, mean monthly array output (from Chapter 3), and the $\bar{K}_T$ value for the month and location under consideration. It is not restricted to specific load shapes, avoids the need for extensive weather data, and does not require use of a digital computer. It has potential for adoption to hand-held calculators.

Based on comparisons with detailed computer simulation results, the simplified method yields estimates to within a standard deviation of 2.6% (absolute).

6.4 Battery or Voltage-Clamped System Results

Photovoltaic array output from a clamped-voltage system can be considerably less than that from a max-power tracked system with an array of equal area. Reduced output for the battery-clamped case results mainly from improper choce of SR, the number of solar cells in a series per battery cell in series. However, a clamped-voltage system with optimum series ratio, SR*, can produce approximately 98% of the power output by the same size system operated in the max-power mode. Since the value of SR* varies from month to month, the main thrust of this work was to predict SR*.

Estimation of SR* by means of a simplified design procedure akin to those developed for max-power tracked array and system outputs does not appear to be feasible, because a very simple method cannot reliably predict array-battery interactions. Instead, a computer program has been developed which essentially simulates the operation of the system during three representative days in the given month. A value of monthly energy production is obtained for each SR used in the program.

The resulting plots of monthly energy production versus SR compare favorably with TRNSYS simulation results in terms of estimates of $\bar{Q}_{ae,cv}$ and SR, on the basis of a preliminary validation study. Further testing and development of the program should lead to a simple, inexpensive, and accurate method of clamped-voltage system design.

6.5 A Sizing Example in Phoenix and Madison

A commercially available silicon flat array is considered here as an example of using available data and selecting system sizes. A summary of the specifications available in the manufacturer's data is given in Table 6.1.

From items 1 and 2 in Table 6.1 and eq. (3.5), it can be determined that

$$\beta = 0.0039 \ C^{-1}$$

Items 1 and 3 in Table 6.1 and eq. (3.5), along with β from above, can be used to show

$$\gamma = 0.117.$$

Items 1 and 4 in Table 6.1 and eq. (3.5), along with β from above, yield

$$\gamma = 0.092.$$

This discrepancy in γ results in an extremely small uncertainty in any $\bar{\eta}$ that might be desired. Although γ could be neglected in eq. (3.5) without significant loss of accuracy, the value of 0.117 will be used here.

Consider placing these arrays in Phoenix, AZ, and Madison, WI, in order to satisfy 50% of a September average daily load of 35 kW-hrs/day distributed diurnally much like the baseline load discussed in Section 2.1.7. The arrays are south-facing and tilted at the local latitude (33.4° in Phoenix and 41.9° in Madison).

There are several combinations of array size and battery capacity which will yield an f_e of 0.5 but $\bar{Q}_e/\bar{L} = 0.6$ and $S/\eta A = 20$ W-hrs/(%·m²) will be used here for demonstration (see Fig. 2.7). A straight-through power conversion efficiency (η_{pc}) of 90% will be considered. The array areas and battery sizes that are necessary in the two chosen locations will be determined.

Phoenix: For September, SOLMET data give a long term $\bar{K}_T = 0.709$. Then from Fig. 3.21

$$\overline{(T_c - T_a)} = [0.274 + 1.04\,\bar{K}_T]\,(T_{NOCT} - T_{a,NOCT})$$

$$= [0.274 + 1.04(0.709)]\,(45 - 20)$$

$$= 25\ C.$$

This value needs no tilt correction since the tilt is nearly optimum for the month and $C_f \approx 1.0$.

Also, Fig. 3.8 gives

$$\overline{\log_{10} Q_s} = 0.12.$$

For September and Phoenix

$$T_M = 31\ C.$$

Equation (3.23a) now yields

$$\bar{\eta} = \eta_r \{ 1 - \beta[\overline{(T_c - T_a)} - \overline{(T_a - T_M)} - (T_m - T_r)] + \gamma \overline{\log_{10} Q_s} \}$$

$$= 0.0992 \{ 1 - 0.0039 [(25) - (3) - (31-28)] + 0.117 (0.12)] \}$$

$$= 0.086 = 8.6\%$$

SOLMET data also show for a latitude tilt in September

$$\bar{Q}_s = 25.7 \text{ MJ/(day·m}^2\text{)}$$

$$= 7.14 \text{ kW-hrs/(day·m}^2\text{).}$$

Thus, to produce a $\bar{Q}_e/\bar{L} = 0.6$, an array area of

$$A = 0.6 \bar{L}/[\eta_{pc} \overline{\eta Q_s}]$$

$$= 0.6(35)/[0.9(0.086)7.14] \text{ m}^2$$

$$= 38 \text{ m}^2$$

would be required. To obtain an $S/\bar{\eta}A = 20$ W-hrs/(%·m²), a storage capacity of

$$S = 20 \bar{\eta}A$$

$$= [20 \text{ W-hrs/(\%·m}^2\text{)}](8.58\%) (38 \text{ m}^2)$$

$$= 6500 \text{ W-hrs}$$

would be required.

Madison: In Madison, for September, $\bar{K}_T = 0.509$ and $T_M = 15$ C.

Then

$$\overline{(T_c - T_a)} = 20 \text{ C}$$

$$\overline{\log_{10} Q_s} = 0.27$$

$$\bar{\eta} = 0.092 = 9.2\%$$

Also for a latitude tilt

$$\bar{Q}_s = 17.1 \text{ MJ/(day·m}^2\text{)}$$

$$= 4.75 \text{ kW-hrs/(day·m}^2\text{)}$$

Therefore

$$A = (0.6)(35)/[0.9(0.092)4.75]/(0.9)(0.092)(4.75) = 53 \text{ m}^2$$

and

$$S = 20\ (9.2)\ (53) \text{ W-hrs}$$

$$= 9750 \text{ W-hrs}$$

Notice that, for the same $\bar{Q}_e/\bar{L}$, the array area scales inversely with the product of monthly average efficiency and array insolation, since

$$\bar{\eta}_{Phx}\ A_{Phx}\ \bar{Q}_{s,Phx} = \bar{\eta}_{Mad}\ A_{Mad}\ \bar{Q}_{s,Mad}$$

Also note that, for a given $S/\bar{\eta}A$, the storage capacity scales with the product of the monthly efficiency and the array area or inversely with the array insolation, since

$$S_{Phx}/[\bar{\eta}_{Phx} A_{Phx}] = S_{Mad}/[\bar{\eta}_{Mad} A_{Mad}]$$

or

$$S_{Phx}/S_{Mad} = \bar{\eta}_{Phx} A_{Phx}/[\bar{\eta}_{Mad} A_{Mad}] = \bar{Q}_{s,Mad}/\bar{Q}_{s,Phx}$$

The results of Chapter 2 have been used here to conveniently predict system performance, but the simplified procedure outlined in Chapter 4 could be used if other months or other load shapes were to be considered.

CHAPTER 6 REFERENCES

6.1 W.A. Beckman, S.A. Klein, and J.A. Duffie, Solar Heating Design, Wiley Interscience, New York, NY (1977).

6.2 B.Y.H. Liu and R.C. Jordan, ''The Long-Term Average Performance of Flat-Plate Solar-Energy Collectors,'' Solar Energy 2, 53 (1963).

Table 6.1

Example of Manufacturer's Data

Array Size* 0.403 m^2
NOCT (at 0.8 kW/m^2)* 45°C

Reference Condition	Cell* Temp. °C	Insolation* kW/m^2	Max-Power* W (typical)	$\eta^{\dagger}$ (%)
1	28	1.0	40	9.92
2	50	1.0	36.6	9.08
3	45	0.8	29.9	9.15
4	65	0.8	27.4	8.40

* Taken from manufacturer's data

† Calculated from manufacturer's data

DISTRIBUTION:

TID-4500-R66, UC-63a (269)

Division of Distributed Solar Technology
Photovoltaics Branch
U.S. Department of Energy
Washington, DC 20545
Attn: A. S. Clorfeine

D. L. Krenz (2)
Director, Special Programs Division
Albuquerque Operations Office
U.S. Department of Energy
Albuquerque, NM 87115

SERI, Library (2)
1536 Cole Blvd., Bldg. #4
Golden, CO 80401

Jet Propulsion Laboratory (2)
4800 Oak Grove Drive
Pasadena, CA 91107
Attn: R. Forney, W. Callaghan

MIT-Lincoln Laboratory
P.O. Box 73
Lexington, MA 02173
Attn: M. Pope

MIT-Energy Laboratory
E40.172
Cambridge, MA 02139
Attn: R. Tabors

The Aerospace Corporation (2)
P.O. Box 92957
Los Angeles, CA 90009
Attn: S. Leonard, B. Siegel

NASA-Lewis Research Center
21000 Brookpark Rd.
Cleveland, OH 44135
Attn: R. Palmer

4718 K. L. Biringer (15)
8266 E. A. Aas
3141 T. L. Werner (5)
3151 W. L. Garner (3)

For DOE/TIC. (Unlimited Release)

☆U.S. GOVERNMENT PRINTING OFFICE: 1980—677-116/555